Gesellschaft für Reaktorsicherheit (GRS) mbH

SIZEWELL 'B' REACTIVITY FAULT STUDY PHASE B AND C

ANALYSIS OF RCCA BANK WITHDRAWAL WITH THE 3D REACTOR CORE MODEL QUABOX/ CUBBOX-HYCA

GRS - A - 1524 (January 1989)

Work carried out for HM Nuclear Installations Inspectorate under Contract NUC 56/158/1

GRS Order No. 30 901

S. Langenbuch, M. Clemente, E. Kramer

Schwertnergasse 1 · 5000 Köln 1 · Telefon (0221) 2068-0 · Teletex 2214123 grs d

SUMMARY

For the reactor core of Sizewell-'B', PWR, nuclear design calculations and RCCA withdrawal transients have been analyzed by applying the 3D reactor core model QUABOX/CUBBOX-HYCA. The analysis is based on the core configuration as described in the Pre-Construction Safety Report. The basis of these nuclear calculations was a library of nuclear cross-sections that was established within this project. The objective is an independent assessment of reactivity initiated transients by unintended RCCA withdrawal. The results of static and also transient calculations with the fully 3D core model of RCCA withdrawal under various conditions are used to evaluate the assumptions for the spatial power density distribution and its possible changes which are input values in safety analysis for these type of accidents. This work will be supplemented by additional calculations for very fast reactivity insertions as postulated within the rod ejection accident.

TABLE OF CONTENTS

1. INTRODUCTION

The aim of this investigation is the detailed analysis of the power distribution and the reactivity behaviour for the reactor core of Sizewell B as described in the Pre-Construction Safety Report (PCSR) /1/, by static and dynamic calculations with the 3D reactor core model QUABOX/CUBBOX-HYCA /2-6/. The basis of the calculations is the core configuration described in PCSR Chap. 4, and the nuclear data calculated for the fuel assemblies with the nuclear code system RSYST by IKE /7/.

The investigations are executed in different steps. These steps also define the chapters 2 to 6 of this report.

2. Calculation of characteristic cases for which results are also given in PCSR and which can be compared to check the consistency, e.g. radial power distributions and reactivity worths for specified core conditions.

   Additional calculations to quantify the dependence on solution methods, as dependence on the order of polynomials used to approximate the neutron flux and influence of the mesh-size on the accuracy of the solutions.

3. Calculations to determine fundamental aspects of nuclear design, as e.g.

   - radial power distributions for specified core conditions
   - reactivity worths for various RCCA configurations
   - reactivity equivalents for specific changes of core condition, equivalent of Boron change or reactivity coefficients for moderator temperature and fuel temperature respectively
   - reactivity characteristic of specified RCCA banks

4. Static calculations for various core conditions during withdrawal of specified RCCA banks to determine

   - reactivity characteristic
   - radial power distribution
   - axial power profiles

5. Analysis of reactivity transients initiated by RCCA withdrawal

6. Discussion of the results and conclusions.

Based on these results, the axial and radial power distribution assumed for the transient analyses with the plant model ALMOD /8/ are discussed.

2. VERIFICATION OF METHODS FOR ANALYSIS

2.1 Characteristic cases for comparison with results from PCSR

As the nuclear data for the Sizewell B reactor core have been calculated independently, it is useful to make a comparison to results cited in the PCSR /1/ for typical conditions of the reactor core. These comparisons aim to verify the consistency of our calculations.

From the PCSR following information is available

- normalized power density distribution near beginning-of-life (BOL), unrodded core, hot full power
  no Xenon (Fig. 4.3/6)
  equilibrium Xenon (Fig. 4.3/7)

- normalized power density distribution near BOL,
  group D inserted 28%, hot full power,
  equilibrium Xenon (Fig. 4.3/8)

These results for the radial power density distribution are also shown in fig. 2.1 to 2.3.

- The power density distribution is also given for end-of-life conditions (EOL) in fig. 4.3/10 and 4.3/11 of PCSR.

Typical axial power profiles are shown in fig. 4.3/14-17.
Characteristic values of nuclear design parameters are listed in table 4.3-2 of PCSR. Some of these typical values are cited for comparison.

- Reactivity worths at hot zero power, BOL, Xenon free, for various RCCA banks

bank D	640	mN
bank C (+ D inserted)	1230	mN
bank B (+ D + C inserted)	990	mN

A comment was added in the new version of PCSR to clarify that the reactivity worths of RCCA bank C or B have been calculated for conditions with additionally inserted D or D+C bank.

Reactivity worths are specified with absolute values in Niles (10^{-2}) or mN (10^{-5}).

Radial factor F^N_{xy} of power distribution for various RCCA banks inserted from BOL to EOL

unrodded	1.37 to 1.28
bank D	1.50 to 1.45
bank D + C	1.60 to 1.45
bank D + C + B	1.80 to 1.55

- Boron concentration for critical reactor core conditions

hot zero power, unrodded core, at 292°C, 155 bar	1307 ppm
hot full power, no Xenon, unrodded core	1178 ppm
hot full power, equilibrium Xenon, unrodded core	882 ppm

In table 4.3-3 of PCSR is cited the reactivity worth of all RCCA's as 7.54 Niles and the net reactivity worth as 6.46 Niles for all RCCA's but one with highest worth.

These data comprise power density distributions of characteristic core conditions and representative reactivity worths which can be used for a consistency check.

2.2 Consistency check for methods of analysis

To check the methods of analysis and the nuclear data library established by IKE for this analysis a comparison is made with typical parameters of nuclear design parameters as given in PCSR and cited in the preceeding chapter.

Two reactor core states have been chosen for comparison

- near BOL, unrodded core, hot full power, equilibrium Xenon (see fig. 4.3/7 of PCSR)
- near EOL, unrodded core, hot full power, equilibrium Xenon (see fig. 2.10 which corresponds to fig. 4.3/10 of PCSR)

These states are clearly defined and represent realistic core conditions at power. Also both cases were solved as a two-dimensional problem by IKE /7/. The results for BOL condition are shown in fig. 2.4 for the IKE solution and in fig. 2.5 for the QUABOX/CUBBOX solution. In the same manner the results for EOL condition are shown in fig. 2.11 for the IKE solution and in fig. 2.12 for the QUABOX/CUBBOX solution.

A detailed evaluation of the three equivalent solutions for both cases is given in table 2.2-1.

Table 2.2-1

Comparison of radial power density distribution for specified states

	mean BOL	relative deviation standard deviation
IKE vs. PCSR	0.48%	2.53%
QUABOX/CUBBOX vs. PCSR	0.44%	3.53%
QUABOX/CUBBOX vs. IKE	-0.05%	1.86%

The comparison is also shown in fig. 2.6 to 2.9.

EOL

IKE vs. PCSR	0.07%	1.84%
QUABOX/CUBBOX vs. PCSR	-0.13%	1.09%
QUABOX/CUBBOX vs. IKE	-0.18%	2.12%

The comparison is also shown in fig. 2.13 to 2.16.

The comparison is presented in two forms:

The absolute difference between the solution of QUABOX/CUBBOX and PCSR results are given for BOL in fig. 2.6 and for EOL in fig. 2.13 respectively.

The relative deviations in all positions in a quarter core are shown by rows in fig. 2.7-2.9 for BOL and in fig. 2.14-2.15 for EOL respectively. In these figures two lines indicate the relative deviation of $\pm$ 3%. The comparison confirms that in most locations the deviation is smaller than this limit value. Some exceptions exist at fuel assemblies at the reactor core boundary, but there the power density itself is very low, this may partly be influenced by the reflector data. However, the total agreement of the solutions for the power density distributions is very good.

Secondly the reactivity worths for various RCCA configurations and core conditions were compared. In PCSR are given reactivity worths at hot zero power. The reactivity worth of RCCA banks has been calculated by QUABOX/CUBBOX for 2D geometry at hot zero power conditions (see table 3.1-1) and for the C- and D-bank for 3D geometry at hot full power conditions (see tables 4-1 and 4-2).

Table 2.2-2

Comparison of reactivity worths from PCSR and own calculations

	PCSR	QUABOX/CUBBOX	
	HZP	HZP, 2D	relative value
D-bank	640 mN	700 mN	1.09
C-bank (+ D inserted)	1230 mN	1331 mN	1.08
B-Bank (+ D + C inserted)	990 mN	1063 mN	1.07
all rods	7.54 Niles	8.68 Niles	1.15

The values from PCSR and QUABOX/CUBBOX calculations agree very well in the relative worth of different RCCA banks. Generally, all values calculated by QUABOX/CUBBOX are about 10% higher for single RCCA banks. The total reactivity worth of all rods is calculated 15% higher.

The Boron worth compares as follows, for the critical reactor core at hot zero power, no Xenon, the PCSR gives a critical Boron concentration of 1307 ppm. At the same condition with QUABOX/CUBBOX a value of k_{eff} = 0.99988 (chap. 3.3) is calculated. The deviation in reactivity is therefore lower than 12 mN thus the agreement is very good.

From PCSR follows a Boron equivalent of equilibrium Xenon at full power of 296 ppm. The QUABOX/CUBBOX calculations in 3D geometry yield a Boron equivalent of 384 ppm. This difference of about 90 ppm might be reduced by a more detailed representation of Xenon and Boron cross-sections which has been implemented in the computer model recently which fully describes the local dependency of these absorption effects. For reactivity balances it has only the effect of changing the reference value.

With respect to the radial power density distribution a first comparison was included in discussion of the core condition of unrodded core, hot full power, equilibrium Xenon, at the begin of this chapter. For different RCCA configurations values of the radial factor F^N_{xy} are given for BOL. The value F^N_{xy} is defined as the ratio of peak power density to average power density in the horizontal plane of peak local power.
This value can be separated into the contributions $F^N_{xy} = F^N_{Qrad} \cdot F^N_{FA}$.

Where

F^N_{Qrad} is defined as the maximum ratio of the average power density of a fuel assembly to the average power density in the horizontal plane

Comment: Normally, this value is calculated from neutron diffusion equations by coarse mesh methods

F^N_{FA} is defined as the ratio of the peak power density to the average power density of the fuel assembly.

In fig. 4.3/12 of PCSR the value 1.20 is calculated for a typical assembly.

Table 2.2-3

Comparison of nuclear power peaking factors

	PCSR	QUABOX/CUBBOX			
		HZP,2D		HFP,3D	
	F^N_{xy}	F^N_{Qrad}	F^N_{xy}	F^N_{Qrad}	F^N_{xy}
unrodded	1.37	1.30	1.56	1.21	1.45
D-bank	1.50	1.40	1.68	1.31	1.57
D+C-bank	1.60	1.38	1.66		
D+C+B-bank	1.80	1.61	1.93		

The comparison shows that all values at hot zero power condition are higher, because the peaking value will be reduced by feedback effects. The values from 3D calculations at hot full power show that QUABOX/CUBBOX estimates slightly higher values for the radial peaking factors.

3. CALCULATION OF FUNDAMENTAL NUCLEAR DESIGN PARAMETERS

3.1 Radial power distribution and reactivity values of RCCA banks at Hot Zero Power from 2D-calculations

For reactor core conditions at Hot Zero Power, i.e. 292°C at 155 bar, and no Xenon the radial power distribution and the reactivity worth for various RCCA configurations is calculated in 2D geometry. From these results can be determined the reactivity worth of the rod banks under this condition. Also the maximum changes in radial power distribution can be estimated, because no feedback mechanism limits the changes of neutron flux.

The main results are given in the table 3.1-1. The radial power distributions are shown in the figures 3.1 - 3.7.

Table 3.1-1

Reactivity- and F^N_{Qrad} - values for different rod configurations for the state:

HZP, no Xenon, Boron = 1307 ppm, (approximation Mode = 4)

rod position	k_{eff}	$\rho[\times 10^{-3}]$	$\Delta\rho$	F^N_{Qrad}	position
no rods	1.00373	3.706		1.301	(D/4)
B-bank in	0.99634	- 3.673	738 mN	1.528	(H/6)
C-bank in	0.99350	- 6.543	1025 mN	1.647	(D/4)
D-bank in	0.99672	- 3.291	700 mN	1.396	(H/4)
C+D-bank in	0.98367	- 16.601	2.03 N	1.377	(H/4)
B+C+D-bank in	0.97349	- 27.232	3.09 N	1.606	(H/4)
all rods in	0.92329	- 83.083	8.68 N	2.249	(E/5)

3.2 2D-Calculations for Hot Full Power

The reactor core condition at Hot Full Power is defined by following values for

average coolant temperature	309 °C (582.1 K)
average fuel temperature	625 °C (898.1 K)

at a pressure of 155 bar the coolant temperature corresponds to a density of 0.70624 g/cm^3.

In the calculations in 2D geometry these average values are set for all fuel assemblies.

Following cases have been solved

- 2D, unrodded, no Xenon, 1307 ppm Boron, k_{eff} = 0.99430, radial power distribution, fig. 3.8

- 2D, unrodded, eq. Xenon, 1307 ppm Boron, k_{eff} = 0.96920, radial power distribution, fig. 3.9

- 2D, unrodded, eq. Xenon, crit. Boron concentration 973.4 ppm radial power distribution, fig. 3.10

These values together with the unrodded case for zero power conditions give following results

reactivity equivalent for the change from hot zero power to hot full power, without Xenon poisoning and average values for coolant temperature and fuel temperature	944 mN
reactivity worth of equilibrium Xenon	2.60 Niles
Boron equivalent of equilibrium Xenon	333.6 ppm

A comparison of the radial power density distributions from these 2D calculations from fig. 3.8 to 3.9 shows the expected effect that Xenon buildup slightly reduces the radial peaking factors. Otherwise these results confirm that changes in Xenon concentration and changes in Boron concentration have no strong influence on the radial power density distribution.

3.3 3D-Calculations for the change from Hot Zero Power to Hot Full Power

The reactivity equivalents for the change from hot zero power, no Xenon, reactor core condition to the condition hot full power, equilibrium Xenon with critical boron concentration also has been studied by fully 3D calculations. As in the 2D calculations for Hot Full Power the average value of coolant temperature is 309°C resp. of fuel temperature 625°C. In these cases only an uniform feedback for the fuel rod or coolant channel is taken into account as the parallel coolant channel model is not used. Following cases have been calculated

- 3D, Hot Zero Power,
  unrodded, no Xenon, 1307 ppm Boron
  k_{eff} = 0.99988, $\rho = 1.200 \cdot 10^{-4}$, fig. 3.11

- 3D, Hot Full Power,
  unrodded, no Xenon, 1307 ppm Boron
  k_{eff} = 0.99037, $\rho = 9.7236 \cdot 10^{-3}$, fig. 3.12

- 3D, Hot Full Power,
  unrodded, eq. Xenon, 1307 ppm Boron
  k_{eff} = 0.96451, $\rho = 3.6796 \cdot 10^{-2}$, fig. 3.13

- 3D, Hot Full Power,
  unrodded, eq. Xenon, critical Boron concentration 923.1 ppm,
  fig. 3.14.

These values give following result

reactivity equivalent for the change from hot zero power to hot full power, without Xenon buildup and uniform feedback effects	960 mN
reactivity worth of equilibrium Xenon	2.71 Niles
Boron equivalent of equilibrium Xenon	383.9 ppm

A comparison of the reactivity equivalents from 2D and 3D calculations is shown in the following table 3.3-1. These differences in reactivity worth of about $1.0 \cdot 10^{-3}$ or Boron changes of about 50 ppm have to be taken into account if only 2D solutions are available. The higher value for the Xenon reactivity worth in 3D geometry follows from the axial profile of the Xenon concentration.

Table 3.3-1

Comparison of reactivity worths and Boron concentration from 2D and 3D calculations

	2D	3D
reactivity equivalent of 100% power change (only representative value as uniform feedback is assumed)	944 mN	960 mN
reactivity worth of equilibrium Xenon	2.60 Niles	2.71 Niles
Boron equivalent of equilibrium Xenon	333.6 ppm	383.9 ppm

A comparison of the radial power density distributions from 3D calculations, which are presented in fig. 3.11-3.13, confirms the result of 2D solutions related to the weak influence of Xenon and Boron changes. Additionally, the comparison supports that the radial power density distribution for axially homogeneous core conditions is well represented by 2D solutions.

In addition to these representative calculations with uniform feedback the core condition of Hot Full Power, unrodded, equilibrium Xenon, 900 ppm Boron concentration including the locally feedback effects from the parallel coolant channel model has been calculated and this modelling has been used for all following calculations. This calculation gives a value k_{eff} = 0.99612. Using the reactivity coefficient of Boron 70.59 mN/ppm, a critical Boron concentration of 845 ppm for this core condition can be estimated.

In table 4.3-2 of PCSR is given for this core condition a critical Boron concentration of 882 ppm. Thus the agreement of the critical Boron concentrations is good.

4. CHARACTERISTIC VALUES FOR C- AND D-BANK

The results discussed now are based on fully 3D static calculations including the parallel coolant channel model to describe the local feedback effects. Two cases have been chosen for analysis because of following considerations.

The total reactivity worth of various RCCA banks has been analyzed in chapter 3.1. The results show, that the C-bank has the highest reactivity worth, therefore this group should be analyzed in more detail in view of a worst core condition for an inadvertent withdrawal of a RCCA bank. However, during normal power operation only the D-bank is used for power control. That means, it can be assumed that an inadvertent withdrawal occurs most probably by this group.

For both cases, the reactivity insertion characteristic has been calculated. The initial condition was chosen as hot full power, unrodded, equilibrium Xenon, 900 ppm Boron concentration. From this initial state the D-bank resp. C-bank was inserted to specified positions keeping the total reactor power and the Xenon concentration constant.

The results are given in table 4-1 and table 4-2.

Table 4-1

Reactivity characteristic and power peaking factors for D-bank

relative bank insertion	reactivity worth		power peaking factor	
	abs. (mN)	rel.	total	radial
0.00	0.0	0.000	1.665	1.212
0.20	88.8	0.114	1.709	1.194
0.33	205.0	0.264	1.765	1.209
0.66	553.3	0.713	1.724	1.261
0.80	696.6	0.898	1.724	1.287
1.00	775.9	1.000	1.750	1.306

The radial power density distributions in the reactor core are shown in fig. 4.1-4.6 for different positions of D-bank. These distributions are representative for nominal power operation.

Table 4-2

Reactivity characteristic and power peaking factors for C-bank

relative bank insertion	reactivity worth		power peaking factor	
			total	radial
	abs. (mN)	rel.		
0.00	0.0	0.000	1.665	1.212
0.20	131.2	0.109	1.823	1.233
0.33	308.3	0.256	1.836	1.258
0.66	853.8	0.709	1.950	1.350
0.80	1075.7	0.893	1.907	1.398
1.00	1203.5	1.000	1.935	1.431

The results can be evaluated with respect to the changes of the power density distribution or with respect to the maximum possible reactivity insertion rate.

Discussing first the changes of power density distribution:
The results given in the tables for the total power peaking factor do not include the local power peaking factor F^N_{FA} (1.20) of the fuel assembly. Therefore it follows that the nuclear power peaking factor F^N_{xyz} reaches 2.12 (1.765·1.20) for the D-bank and 2.34 (1.950·1.20) for the C-bank movement. The design value of the core is specified as 2.32. It includes a factor 1.05 of conservatism and 1.03 as an engineering uncertainty contribution as described in the PCSR, chap. 4.3.3.3.6.
Including these additional factors of uncertainty the value for the D-bank of 2.12 corresponds to 2.29. thus the change of power density distribution for the RCCA bank, which is normally used for reactivity control, yields a value below the specified limiting value.

In view of the disturbance by a C-bank movement the limiting value will be reached without taking into account additional uncertainty contributions. However, as mentioned before, this RCCA-bank will not be inserted into the core during normal operation.

In both cases of RCCA bank movement the axial location of the maximum power density is changing with the bank position.

The evaluation related to maximum reactivity insertion rate gives following results:
The total reactivity worth of D- or C-bank respectively is 776 mN or 1204 mN. Assuming a linear reactivity insertion characteristic over the core height of 366 cm and a velocity of 1 cm/s of RCCA movement these values correspond to reactivity rates of 2.12 mN or 3.28 mN per second. The S-shaped reactivity insertion characteristic can be estimated from tables 4-1 and 4-2. It follows an increase of slope by a factor 1.40. The maximum possible reactivity insertion rate from D- or C-bank movement is therefore 2.97 mN/s or 4.59 mN/s.

If the reactivity worth of all RCCA„ calculated as 3.7 Nike is used to estimate the maximum reactivity insertion rate in the same way„ it follows a rate of 33 mN/s

In the analysis of reactivity initiated transients the range from 1.0 to 100.0 mN/s of insertion rates has been investigated. Therefore„ the results confirm that the chosen range includes all possible values of reactivity insertion rates due to single RCCA or RCCA-bank withdrawal.

5. ANALYSIS OF REACTIVITY TRANSIENTS INITIATED BY RCCA WITHDRAWAL

In the preceding chapter the characteristic parameters of the C- and D-bank have been discussed. If the postulated RCCA bank withdrawal is slow, the local power density distribution can be analyzed by static calculations or by really time-dependent calculations. The effects can be best understood, when the results of both types of calculations are compared. Therefore, the results of static solutions are described next, afterwards the result of transient solutions are given and finally the comparison is discussed.

5.1 Static calculations for a slow withdrawal of C- or D-bank

For these analyses it is postulated that the C-bank or the D-bank is 2/3 of its length inserted, the Boron concentration is adjusted in such a way that the reactor core is critical at nominal power. For this condition also Xenon equilibrium is assumed. The thermohydraulic boundary condition with respect to coolant flow rate, inlet enthalpy and pressure are also assumed to be at nominal values. From this initial state it is postulated that the RCCA bank is slowly removed. The reactivity addition from RCCA withdrawal will be compensated by the negative feedback reactivity contributions due to the initiated power increase. A new steady state condition is possible if criticality is gained again. This new value of reactor power is calculated assuming that the thermohydraulic inlet condition including Boron and Xenon concentrations are kept constant.

These boundary conditions follow from the assumption that no additional actions are taken during the time-period of RCCA withdrawal and that also the increased power generation in the core has no effect on the coolant conditions at the core inlet. If an increase of coolant temperature at core inlet is really taken into account, the resulting reactor power would be lower due to the additional negative reactivity feedback effects.

The results for the two banks of control rods are given in table 5.1-1 and 5.1-2.

Table 5.1-1

Mean power values and power peaking factors for D-bank from 3D static solutions

relative bank insertion	mean power		power peaking factor	
			total	radial
	abs. (W/cm^3)	rel.		
0.66	104.48	1.000	1.724	1.262
0.50	114.22	1.093	1.795	1.233
0.33	123.29	1.180	1.758	1.209
0.20	130.18	1.246	1.696	1.196

Table 5.1-2

Mean power values and power peaking factors for C-bank from 3D static solutions

relative bank insertion	mean power		power peaking factor	
			total	radial
	abs. (W/cm^3)	rel.		
0.66	104.48	1.000	1.910	1.339
0.50	119.19	1.141	1.900	1.275
0.33	133.31	1.276	1.790	1.223

These results show that the slow withdrawal over 1/3 of the core height of the C- or D-bank leads to a power increase of 27.6% or 18.0% respectively. After this power increase the positive reactivity insertion due to the rod withdrawal has been compensated by the negative feedback reactivities from fuel temperature and moderator temperature increase.

The dependence of the results from both tables is graphically presented in fig. 5.1 to 5.4 for the D-bank and in fig. 5.5 to 5.8 for the C-bank.

If the results from table 4-1 and 5.1-1 as well as from table 4-2 and 5.1-2 are combined, a power coefficient for this type of events can be estimated.

Table 5.1-3

Relation of reactivity insertion and critical power for the D- and C-bank.

rel. bank insertion	reactivity (10^{-3})		reactivity equivalent (10^{-3})		relative power increase	
	D-bank	C-bank	D-bank	C-bank	D-bank	C-bank
0.66	5.533	8.538	0.000	0.000	1.000	1.000
0.50					1.093	1.141
0.33	2.050	3.083	3.483	5.455	1.180	1.276
0.20	0.888	1.312	4.645	7.226	1.246	

A power coefficient $\Gamma_p = \Delta\rho/\Delta P\%$ can be defined as ratio of reactivity change and corresponding percentage of power change. From the calculations following values are determined

for C-bank $\Gamma_p = 1.976 \cdot 10^{-4}$ (bank moved from 0.66 to 0.33)

for D-bank $\Gamma_p = 1.935 \cdot 10^{-4}$ (0.66 to 0.33)
$\Gamma_p = 1.761 \cdot 10^{-4}$ (0.33 to 0.20)

This coefficient allows to calculate the power increase related to a certain amount of inserted reactivity from the equation $\Delta P\% = \Gamma_p^{-1} \Delta\rho$. By this relation it is possible to extrapolate the results that were calculated for a specified bank configuration to other reactivity changes of the reactor core. These specific power coefficients for core conditions including relatively deep inserted RCCA banks have higher values than the usually defined total power coefficient for unrodded core conditions.

An overview of the spatial power density distribution and its changes due to bank withdrawal is given in a sequence of figures 5.9-5.23.

For the various cases of bank position for C- or D-bank:

Case A	RCCA bank	242.0	cm	or	0.66,
Case B		182.9	cm	or	0.50,
Case C		121.0	cm	or	0.33,
Case D		73.2	cm	or	0.20 inserted,

the radial power density distribution in different planes is shown. The 4 planes are regularly chosen with a distance of 75 cm and are numbered from the bottom to the top of the reactor core. They correspond to a distance from the top or a relative core length (in comparison to the insertion depth) as following

plane 6	295.4	cm	or	0.808
plane 9	220.4	cm	or	0.603
plane 12	145.4	cm	or	0.397
plane 15	70.4	cm	or	0.192

These fig. 5.9-5.23 shall be illustrative of the power density redistribution as consequence of the stepwise withdrawal of the RCCA banks.

5.2 Transient calculations for a RCCA withdrawal

As an example for the fully space- and time-dependent behaviour of the reactor core, a withdrawal of the C-bank is analyzed.

This bank has the highest reactivity worth. The following case is postulated. The same initial condition as for the static solutions is assumed, i.e., the group is 2/3 of its length inserted. Otherwise the reactor core conditions are chosen as nominal values. The transient is initiated by a bank withdrawal over 1/3 of the core length, because in this part of the reactor core the reactivity insertion characteristic reaches its highest value.

The total reactivity worth of 545.5 mN for this bank movement corresponds to different reactivity insertion rates dependent on the speed of withdrawal. For a speed of 1 cm/s the withdrawal ends after about 120 s and the reactivity insertion rate would be 4.5 mN/s.

For the calculation a relatively high speed of 40 cm/s for bank withdrawal is chosen, under this condition the rod motion ends after about 3 s and the reactivity insertion rate corresponds to 180 mN/s.

For the reactivity fault transients in the PCSR and the own transient calculations with the ALMOD-code a spectrum of reactivity insertion rates from +3 mN/s up to +80 mN/s was analyzed. Thus, the space-time dependent calculations are representative for a high reactivity insertion rate.

The time-dependent behaviour in the mean is given in table 5.3-1, which describes the time history of neutron flux.

Table 5.3-1

Time history of mean neutron flux

time (s)	rel. neutron flux
0.0	1.000
1.0	1.041
2.0	1.141
3.0	1.292
4.0	1.438
5.0	1.524

The reactor trip from "high neutron flux" would be initiated at 2.3 s, when the limit value 1.18 is passed.

The changes in the radial and axial power density distributions are evaluated in a series of figures.

These results can be summarized in the following way

- During the RCCA withdrawal a strong redistribution of local power density is occuring.

- The local increases are starting and reach their highest values at the tip of the moving RCCA. But it should be noted that at this location the absolut value of power density is low.

- The maximum nuclear power peaking factor nearly remains unchanged during the transient.

- Though the withdrawal velocity was chosen very high, the local power density is at all locations within the limits of static power density distributions to corresponding axial RCCA positions.

The presentation and the evaluation of results are structured as follows.

The time-dependent changes of axial power density profiles during the rod withdrawal transient are shown in series 1 and 2. For comparison in series 3 are given axial power density profiles from static calculations to specified positions of the C-bank during the withdrawal. The time-functions at selected positions in the reactor core are presented in the following figures.

Series 1:

Fig. 5.24 to 5.32 show the axial power profile in a selected number of radial positions during the transient at time-points of 0.0 s, 2.0 s, 3.0 s, and 5.0 s. The radial positions named by their channel number are chosen in the following way, the channel 1 is located in the core center (H/8), the following channels are located on the diagonal directed to the outer fuel assembly (C/3), so channel 18 and 34 correspond to (G/7), channel 50 and 66 to (F/6), channel 82 and 98 to (E/5) and channel 114 and 128 to (D/4).

The location of the RCCA's belonging to the C-bank is (F/6), that is channel 50 and 66, and (H/2) respectively (B/8). Therefore in these radial positions the greatest changes of axial power profile occur.

To illustrate the notation a picture of the core from fig. 2 or 3 should be used.

Series 2:

The fig. 5.33 to 5.34 show the axial power profile in three representative positions: the core center (channel 1), the position where the C-bank is moving (channel 50 and 66) and the position of maximum power density (channel 114 and 128) for the initial state and during the transient at 5.0 s. At this time the RCCA is no longer moved, as it has reached the final position of 121.0 cm already within 3s, but the profiles show that the power density redistribution is still continuing. This can be better seen by comparing these profiles with the next figures.

Series 3:

The fig. 5.35 to 5.37 present the axial profiles from corresponding static solutions to three different values, 66%, 50% and 33% of insertion depth at the same positions as described before. These results are taken from the calculations described in chapter 5.1, where the power was increased to get criticality again. Thus these static profiles can be directly compared to the transient changes of the power profiles, no additional power normalization is necessary. The comparison of these static figures with the result of figures in serie 2 shows that the transient power density distribution is still approaching the shape from the steady state conditions. The static solutions give a limiting power density distribution for the RCCA withdrawal transient.

In addition to these axial power density profiles are shown in fig. 5.38 to 5.40 the time-functions at selected radial positions for a number of neighboured axial nodes, i.e. from axial plane 5 (insertion length 320 cm) in equal distancies of 25 cm to axial plane 12 (insertion length 145.4 cm).

In channel 50 the motion of the RCCA occurs. The withdrawal can be followed directly. The rod tip at 242.0 cm corresponds to node 8. The local power increase starts for node 7 and 8. During the time of rod withdrawal with a certain time delay the local power density increases in the following nodes 9, 10, 11, and 12, when the rod tip passes through these nodes. The withdrawal of the RCCA ends in plane 13. The following figures show the time-function in the channels on the diagonal to the

outer direction. Channel 98 is directly neighboured to the moving rod, the next on diagonal is channel 98 which again is neighboured to channel 114, where normally in this reactor core design the maximum power density occurs. For this radial position (channel 114) is shown the normalized power density distribution in fig. 5.41. Comparing the increase of maximum local power density of about 13% after 5s with the increase of mean power density given in table 5.1-3 of about 27% from static calculations, it follows again that these static distributions are limiting power density distributions.

5.3 Discussion of results obtained by 3D methods

The investigations for the RCCA withdrawal based on static and transient 3D reactor core calculations can be summarized in the following way. Although for the time-dependent analysis a fast RCCA withdrawal was postulated, equivalent to a reactivity insertion rate of about 180 mN/s, the local neutron flux and correspondingly the local power density behaviour showed no peculiar overshooting effects, because the inserted reactivity itself is sufficiently below prompt critical values. Therefore, for comparison a set of static solutions were analyzed, where the power was increased together with the removed RCCA-bank to get again critical core conditions. The evaluation shows that these static power density distributions are envelopes for the possible changes of local power density. That will be the case even more, if the bank withdrawal occurs with slower speed. Therefore, the results for the radial and axial power density distributions from the detailed analysis of C- or D-bank withdrawal can be taken as representative for the further discussion of reactivity initiated transients.

5.4 Discussion of results in view of the hot channel analysis to determine the minimum DNB-Ratio

The safety analysis of transients, where the overall plant behaviour is studied, is completed by a hot channel analysis. As discussed in detail with the ALMOD calculations /8/, the most important parameters for this analysis are the hot channel factors and the specific assumptions upon the axial power density distribution.

In the hot channel approach has been used a total heat flux hot channel factor F_Q=2.32 and normalized axial power density distributions for begin of cycle and end of cycle conditions as shown in fig. 5.42 respectively, both distributions have been taken from PCSR. These values and power distributions should be confirmed by own 3D calculations. Results for BOC have been already discussed, to complete the analysis a fully three-dimensional burnup calculation has been performed with the reactor core model HYCA. The calculated axial power density distribution at EOC conditions is shown in fig. 5.43 together with the axial profile at BOC. A comparison of axial power density profiles from PCSR and own calculations is given in fig. 5.44. The result shows a very good agreement for BOC conditions and also the differences for EOC conditions are sufficiently low. The axial power peaking factor from PCSR which has been used in ALMOD calculations is 1.35 for BOC and 1.13 for EOC respectively. The corresponding values from HYCA calculations are 1.34 for BOC and 1.17 for EOC conditions.

The relation of typical core conditions with respect to the total heat flux factor 2.32 has been given in chapter 4, where it was discussed that for the unrodded core and all conditions of D-bank insertion the maximum local power density or heat flux including uncertainty factors is below the specified limiting value.

For calculating DNB-ratios the worst conditions are defined, when the power density or heat flux density is high near the top of the reactor core. At these positions the quality of coolant reaches the highest values and consequently the critical heat flux reaches the lowest values.

The axial power profile for end-of-cycle conditions bounds the BOC distributions. An additional disturbance may be due to Xenon nonequilibrium conditions. But from calculations analyzing this effect it can be concluded, that the possible changes to BOC profiles in the upper core region will not reach the values of the EOC profile. However, these effects have to be taken into account also at EOC core conditions.

In the ALMOD calculations it was assumed that the total heat flux hot channel factor of 2.32 is reached together with the axial power density profile at EOC conditions. The realistic calculations give a reduction of the axial power peaking factor from 1.34 to 1.17. This result should be included into the evaluation if for certain cases the DNB-limit was reached, when the EOC axial power profile was used.

6. DISCUSSION OF RESULTS AND CONCLUSIONS

The reactivity fault study has the aim to analyze the reactor core behaviour for events due to failures in the RCCA system.

The different fault sequences

- single RCCA withdrawal
- RCCA bank withdrawal
- RCCA ejection

are analyzed in detail by following steps.

As for the safety cases with RCCA withdrawal the whole plant behaviour must be simulated, the transient analysis code ALMOD was used. The results obtained are documented in /8/. This analysis is based on several specific model features. The reactor core behaviour is described by pointkinetics. Consequently, the reactivity insertion rate from RCCA movements is described by reactivity function tables and the power density distribution and its changes are included into the hot channel analysis, which makes assumptions about the axial power profile and the power peaking factors.

To check the main input parameters of this analysis, it was decided to perform independent calculations based on fully 3D simulations of the reactor core.

The results of these calculations have been described in this report. They are assigned to the different aspects of the nuclear core design and the RCCA withdrawal transients as follows

1. Consistency check of the nuclear data and the reactor core model

2. Check of input parameters used in ALMOD calculations with respect to

   - correlation between reactivity insertion rate and RCCA movements

- change of power density distribution due to single RCCA movement or RCCA bank withdrawal
- representative axial power density profiles for BOL and EOL conditions respectively

3. Calculation of RCCA withdrawal by fully 3D methods.

In a first step the nuclear data, which have been independently calculated, have been verified by comparison to basic nuclear parameters given in the PCSR of Sizewell B. The evaluation of representative power density distributions at BOL and EOL shows good agreement with deviations below 3%. Also the reactivity worths and critical Boron concentrations agree well. As an example the critical Boron concentration of Hot Zero Power at BOL, unrodded, 1307 ppm, is determined with a reactivity deviation of 12 mN which corresponds to about 2 ppm. The critical Boron concentration of Hot Full Power at BOL, unrodded, equilibrium Xenon is calculated with 30 to 40 ppm difference. From the various comparisons can be concluded that the own calculations based on independently calculated nuclear data and the reactor core model QUABOX/CUBBOX-HYCA give consistent results for the reactor core of Sizewell B.

The results of 3D calculations of reactor core conditions related to the input parameters of the reactivity transient analyses by the plant model ALMOD confirmed

1. that the rates of reactivity insertion taken into account in the ALMOD and PCSR are greater than the predicted values by the QUABOX/CUBBOX analysis and

2. that the hot channel factors and the axial power profiles used in the safety analysis are limiting values.

The representative calculation of a RCCA withdrawal using the fully 3D reactor core model including the local feedback effects from a parallel coolant channel model gives no indication that locally higher power density values are reached, though a relatively high reactivity insertion rate was analyzed.

The analysis of fast rod ejection transients will be analyzed in the next step of this project.

REFERENCES

/1/ CEGB/NNC:
Sizewell 'B' Pre-Construction Safety Report (PCSR)
April 1982 and November 1987

/2/ S. Langenbuch
QUABOX/CUBBOX-HYCA, Ein dreidimensionales Kernmodell mit parallelen Kühlkanälen für Leichtwasserreaktoren
GRS-A-926 (Januar 1984)

/3/ S. Langenbuch, W. Maurer
CUBBOX-HYCA-Ø2, Ein dreidimensionales Kernmodell mit parallelen Kühlkanälen für Leichtwasserreaktoren
GRS-A-672 (Februar 1982)

/4/ S. Langenbuch
Das dreidimensionale LWR-Kernmodell QUABOX/CUBBOX-HYCA mit parallelen Kühlkanälen
Reaktortagung Hannover, 15.-18. April 1978

/5/ S. Langenbuch, W. Maurer, W. Werner
Coarse-Mesh Flux-Expansion Method for the Analysis of Space-Time-Effects in large LWR Cores
Nuclear Science and Engineering, 63, 437-456 (1977)

/6/ S. Langenbuch, W. Maurer, W. Werner
High-Order Schemes for Neutron Kinetics Calculations, based on a local Polynomial Approximation
Nuclear Science and Engineering, 64, 508-516 (1977)

/7/ D. Lutz
Cross-section library for the Sizewell 'B' Reactor
IKE Stuttgart, 6-FB-33 (Februar 1986)

/8/ S. Langenbuch, J.P. Weber
Sizewell 'B' - Reactivity Fault Study, Phase A:
Calculation of RCCA Bank withdrawal with the Plant Model ALMOD4
GRS-A-1387 (November 1987)

FIGURES

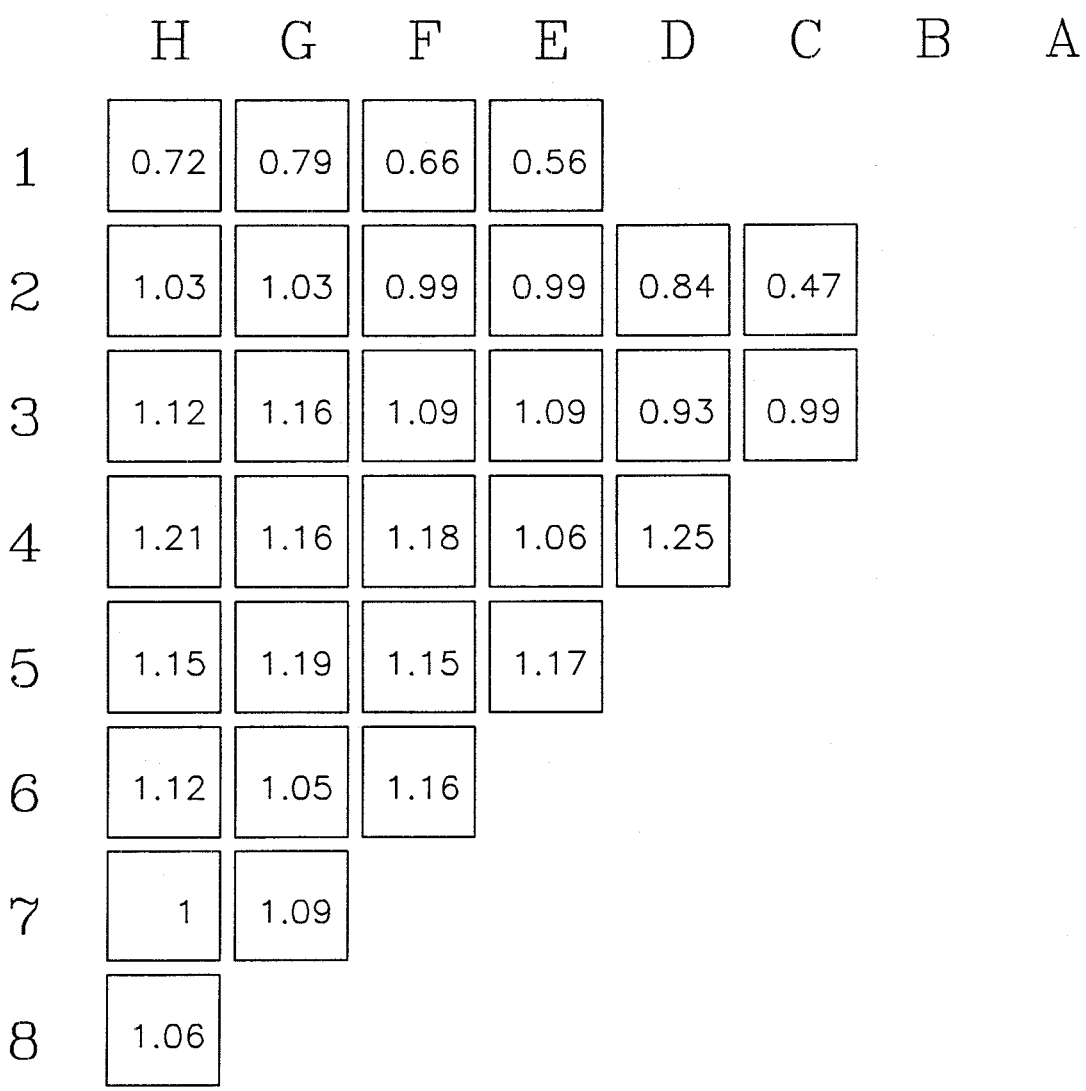

State: near BOL, unrodded Core,
Hot Full Power, no Xenon
from PCSR fig 4.3/6

Fig. 2.1 Radial Power Distribution

JF1

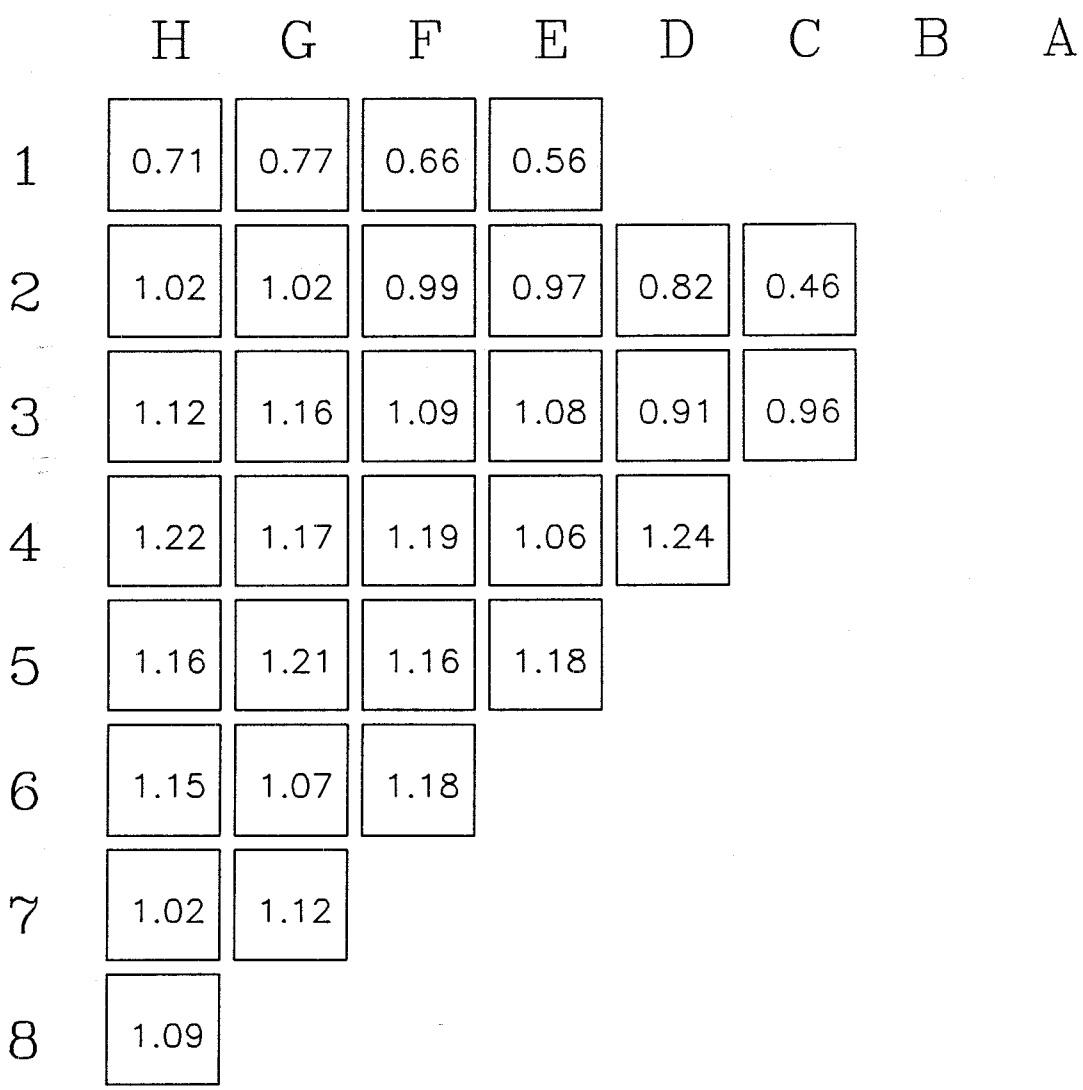

State: near BOL, unrodded Core,
Hot Full Power, Eq. Xenon
from PCSR fig 4.3/7

Fig. 2.2 Radial Power Distribution

JF1A

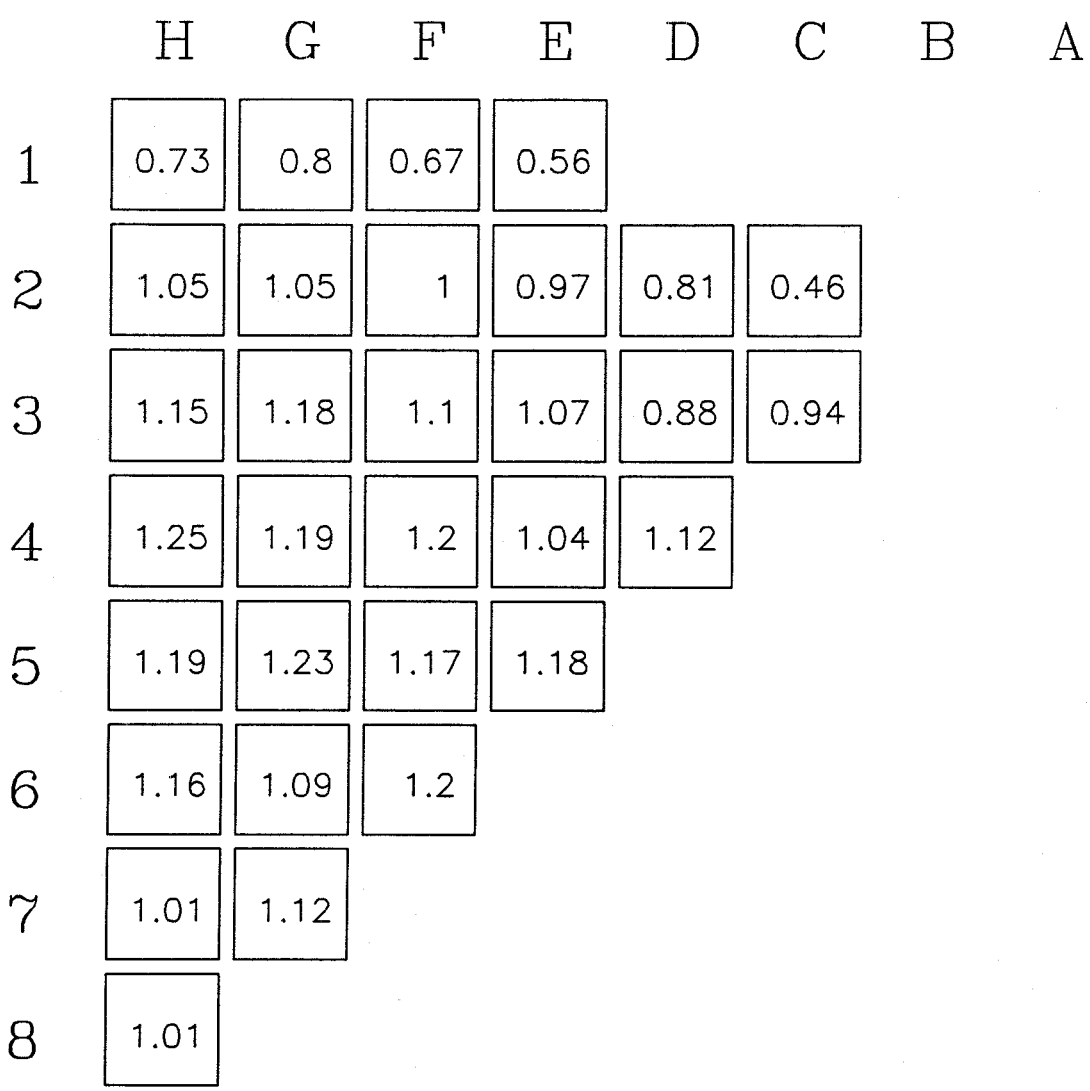

State: near BOL, D—bank 28% in,
Hot Full Power, Eq. Xenon
from PCSR fig 4.3/8

Fig. 2.3 Radial Power Distribution

JF1B

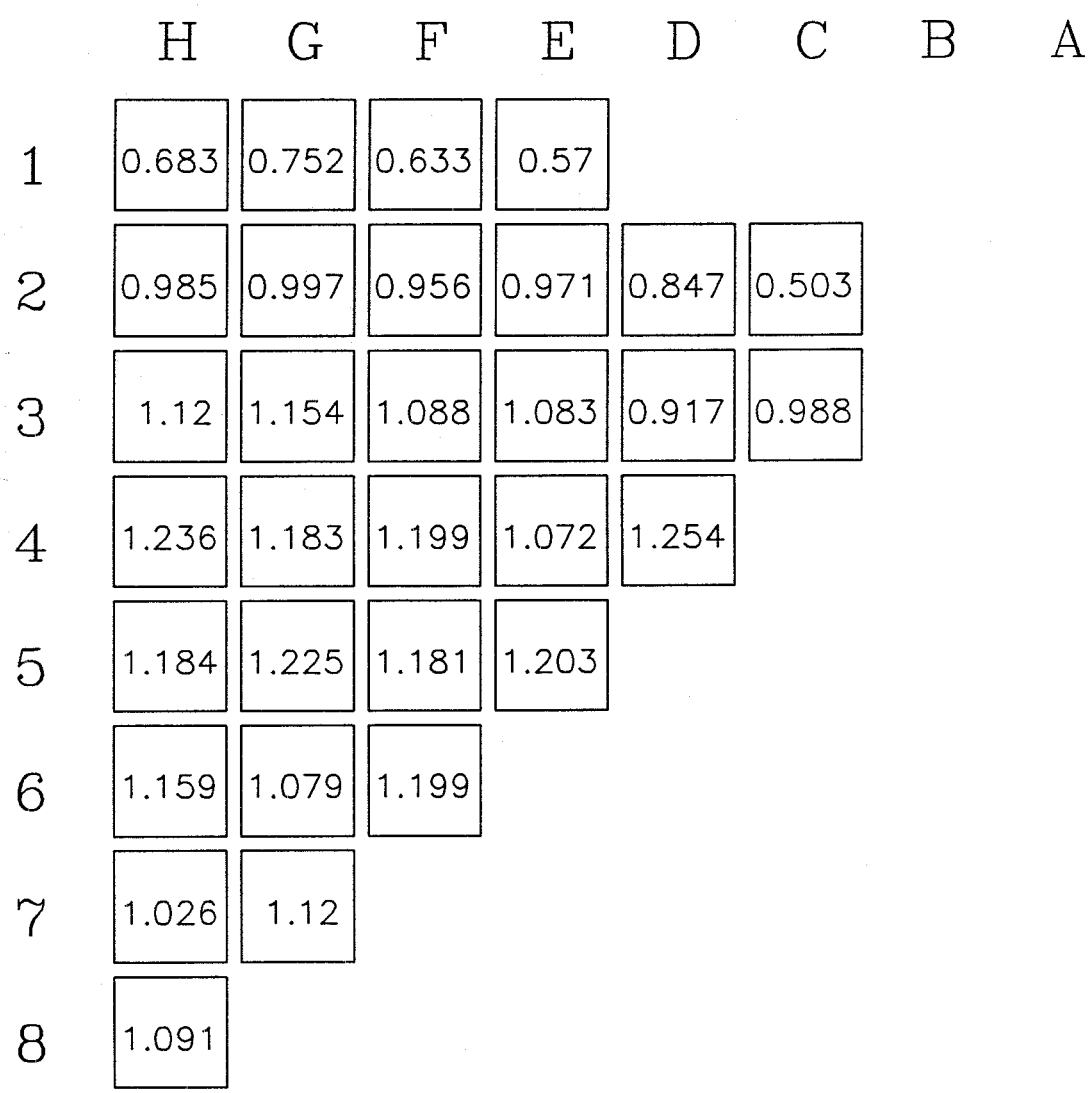

State: near BOL, unrodded Core,
Hot Full Power, Eq. Xenon
IKE Calculation

Fig. 2.4 Radial Power Distribution

JF2

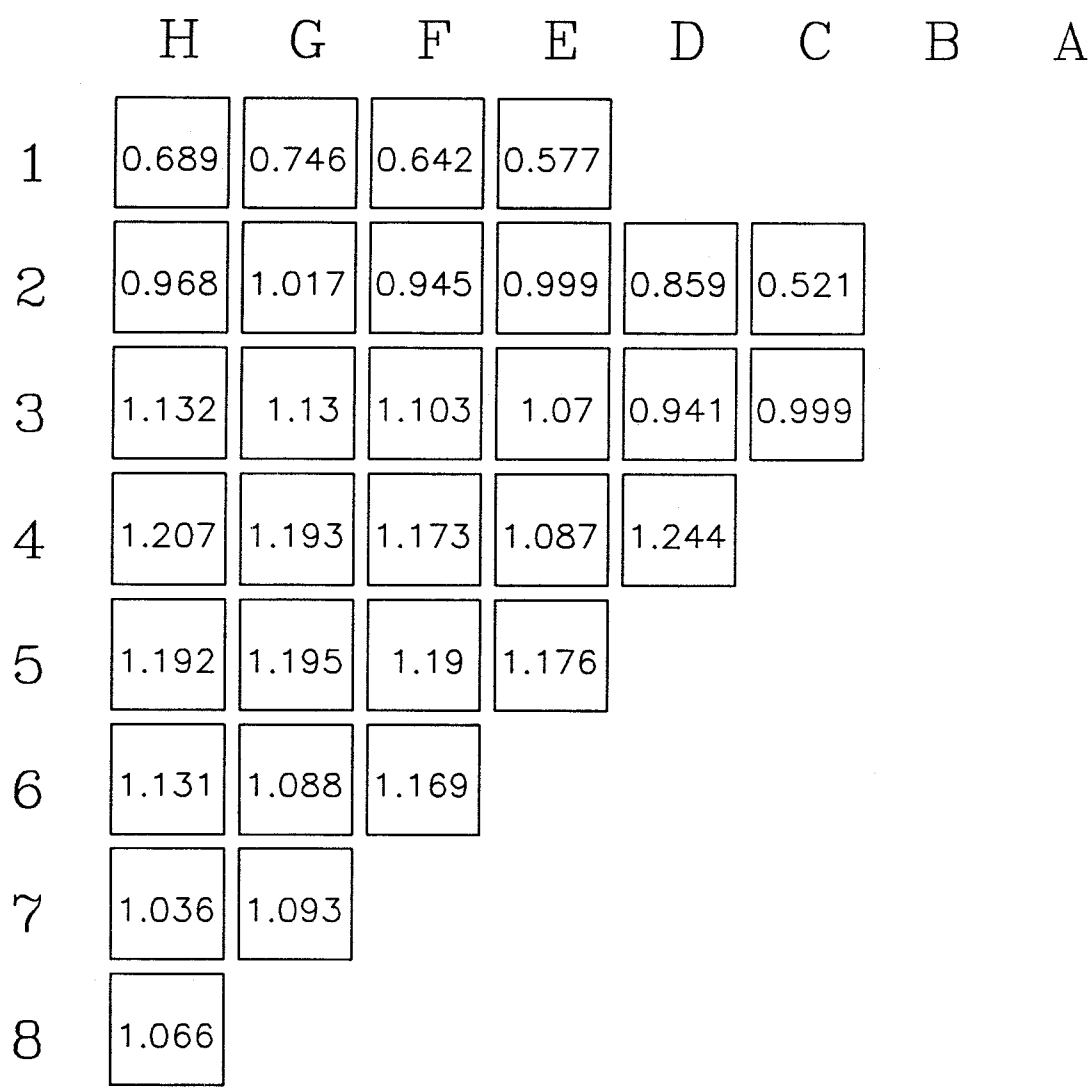

State: BOL, unrodded Core,
Hot Full Power, Eq. Xenon, crit. Boron
QUABOX/CUBBOX,Mode=4

Fig. 2.5 Radial Power Distribution

JF6

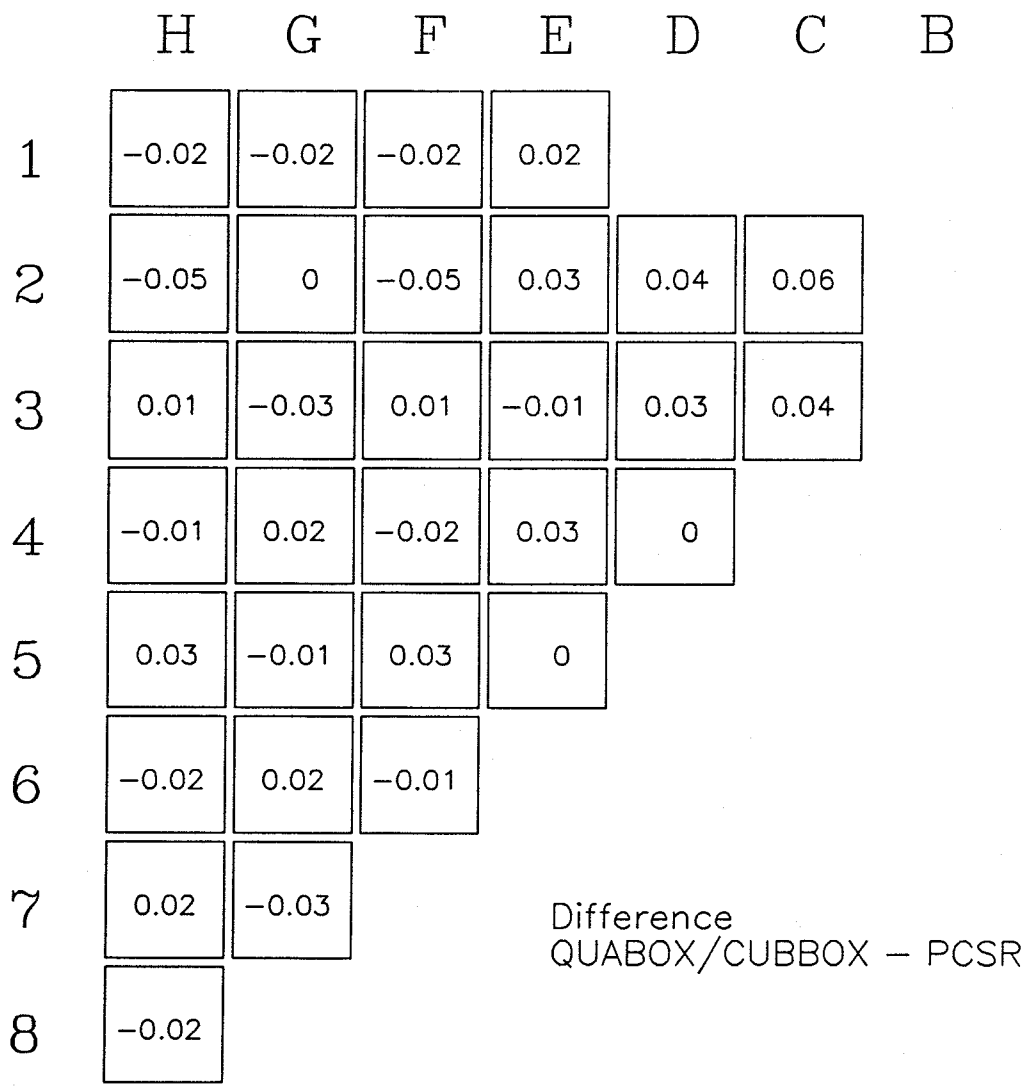

State: near BOL, unrodded Core,

Hot Full Power, Eq. Xenon

Fig. 2.6 Comparison of Radial Power Distribution

QUABOX/CUBBOX vs. PCSR

Fig. 2.7 Comparison of radial power distributions at BOC
IKE–Calculation vs. PCSR

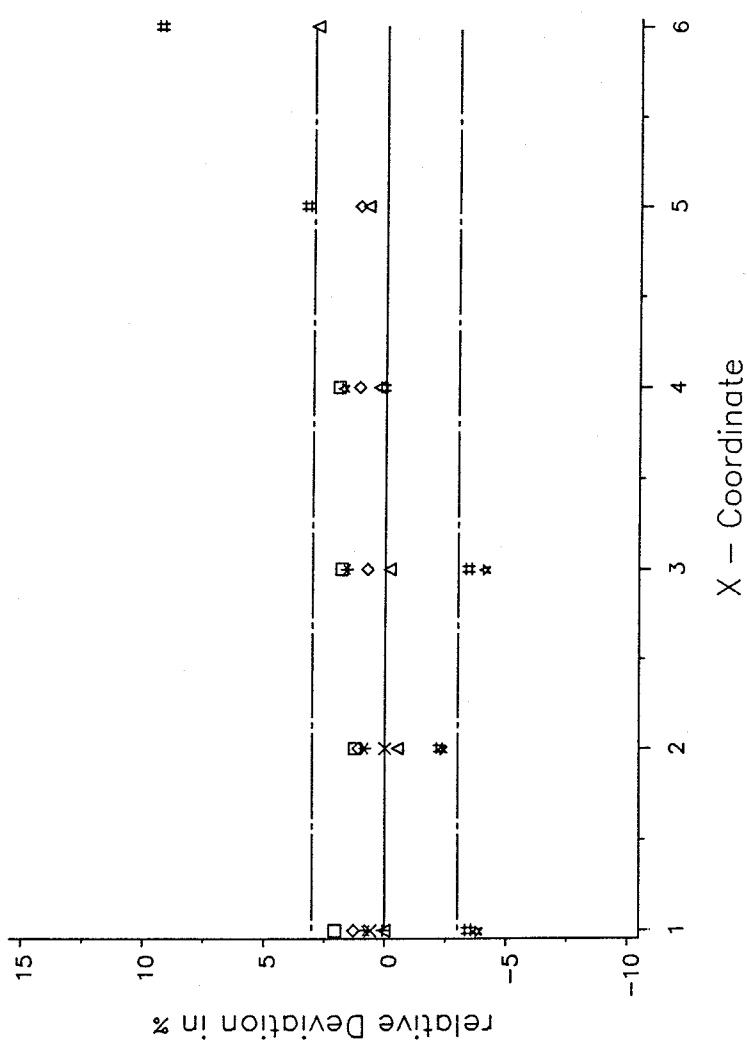

Fig. 2.8 Comparison of radial power distributions at BOC
QUABOX/CUBBOX vs. PCSR

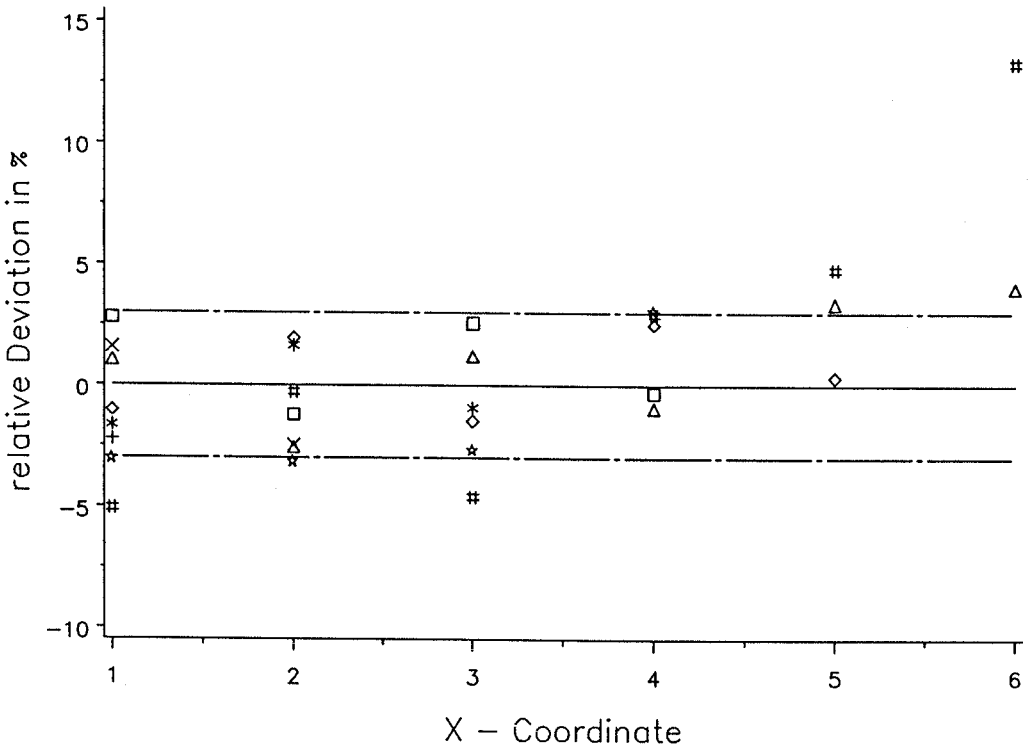

Fig. 2.9 Comparison of radial power distributions at BOC
QUABOX/CUBBOX vs. IKE–Calculation

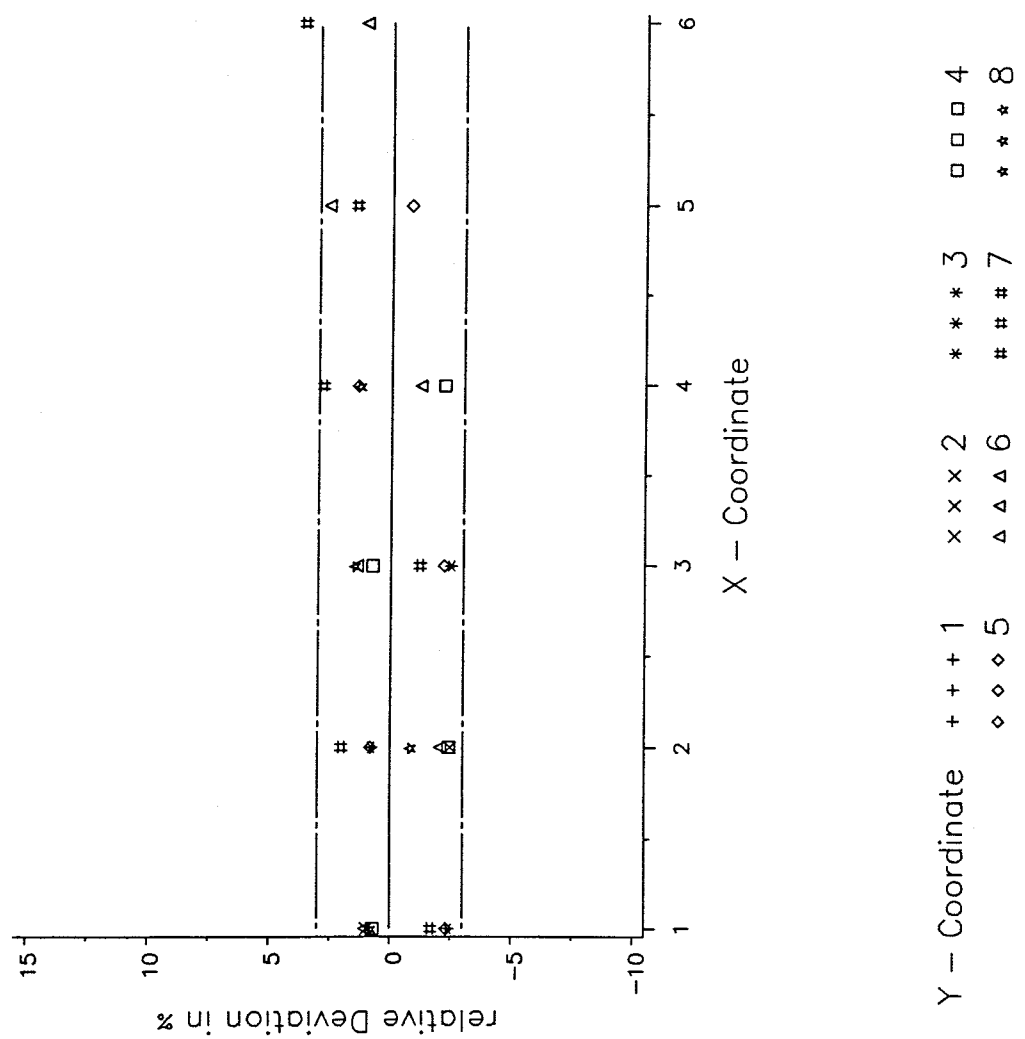

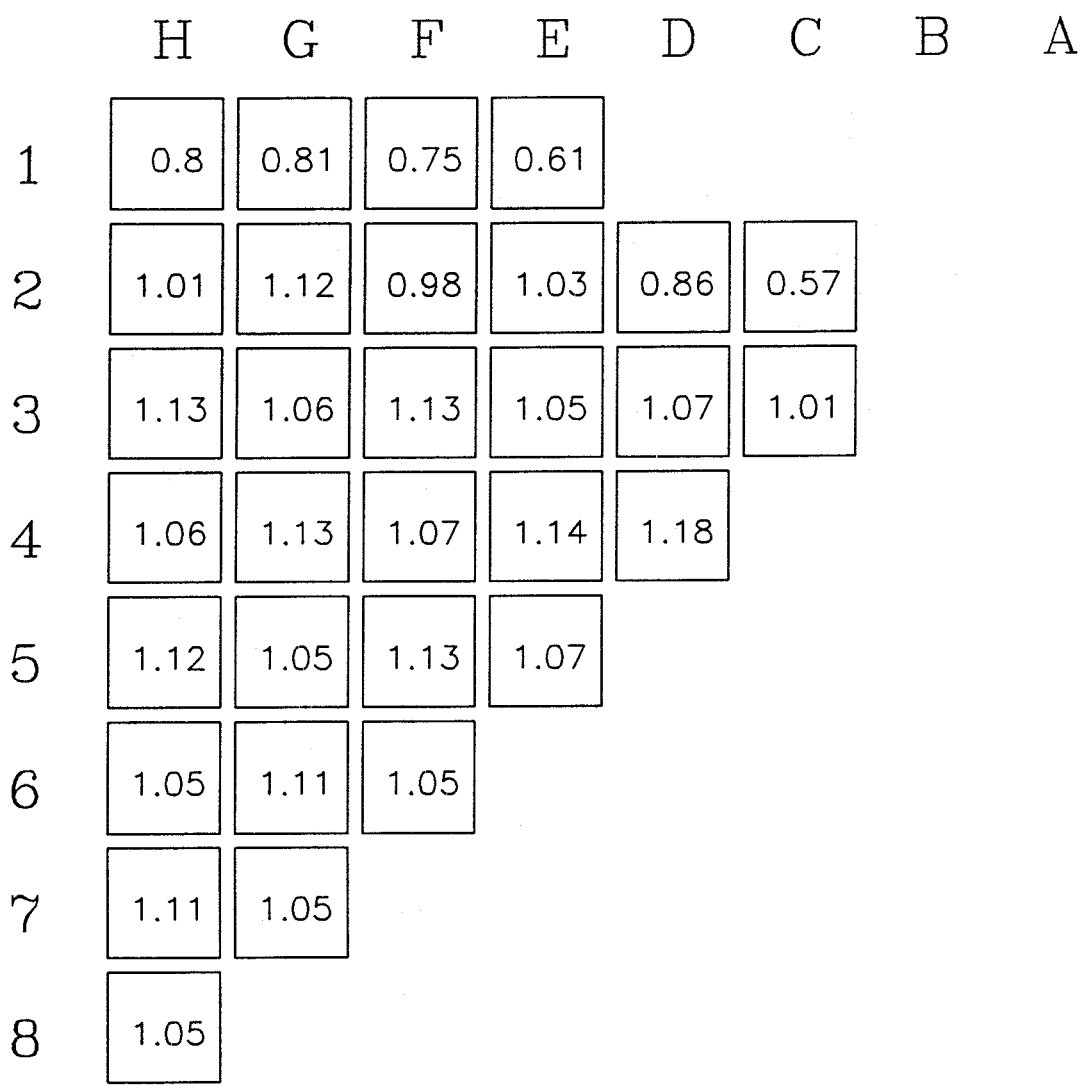

State: near EOL, unrodded Core,
Hot Full Power, Eq. Xenon
from PCSR fig 4.3/10

Fig. 2.10 Radial Power Distribution

JF1AE

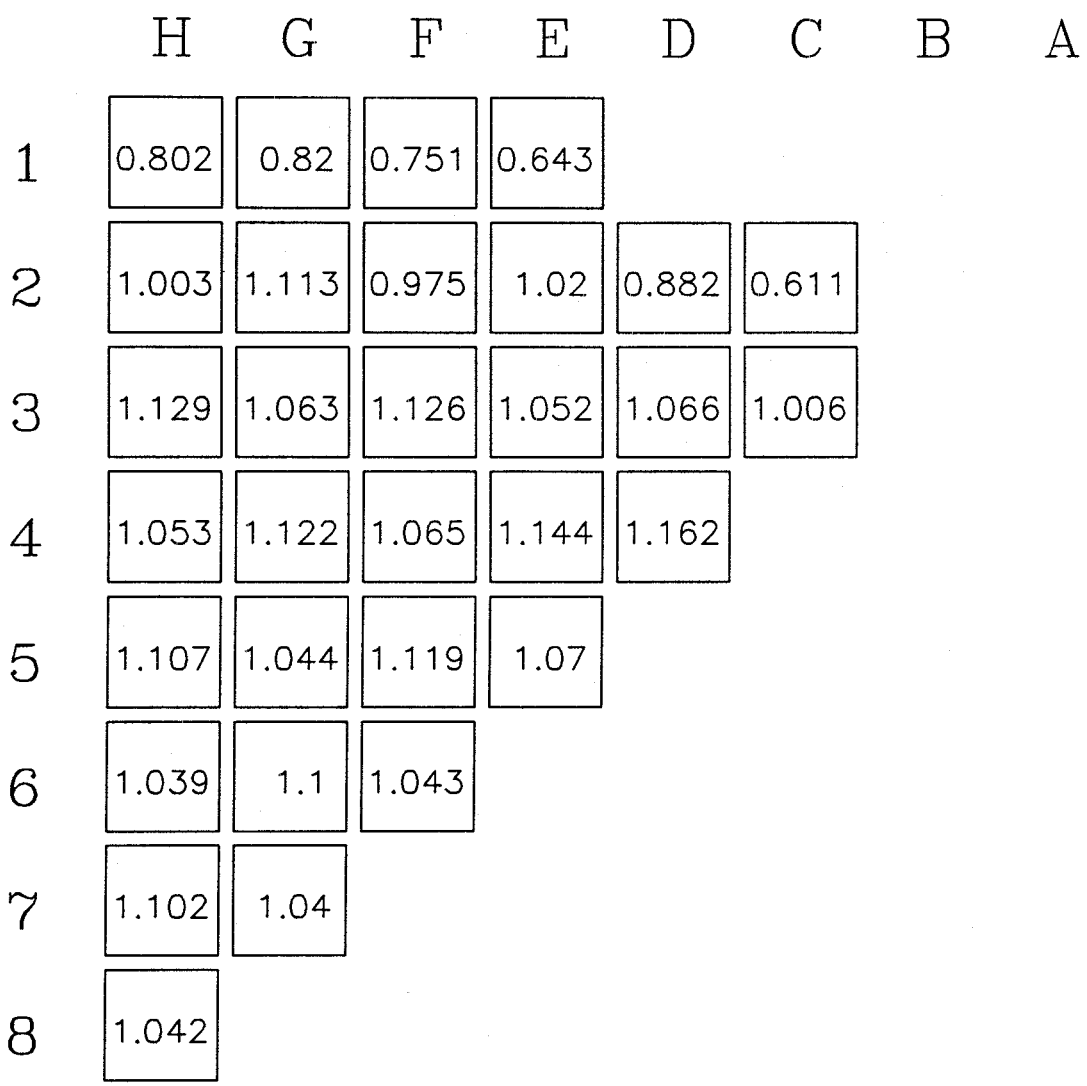

State: near EOL, unrodded Core,
Hot Full Power, Eq. Xenon
IKE Calculation

Fig. 2.11 Radial Power Distribution

JF2E

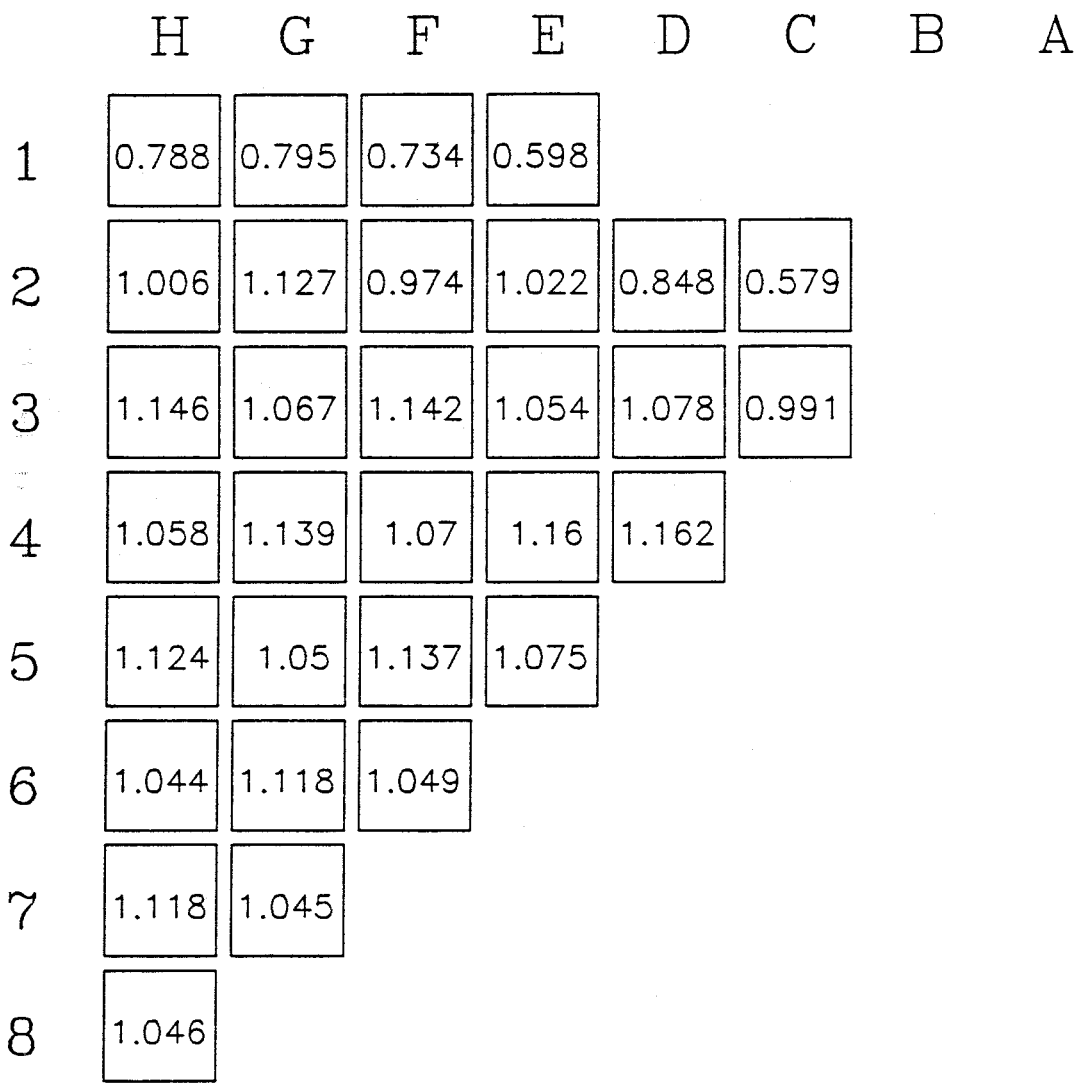

State: near EOL, unrodded Core,
Hot Full Power, Eq. Xenon
QUABOX/CUBBOX,Mode=4

Fig. 2.12 Radial Power Distribution

JF6E

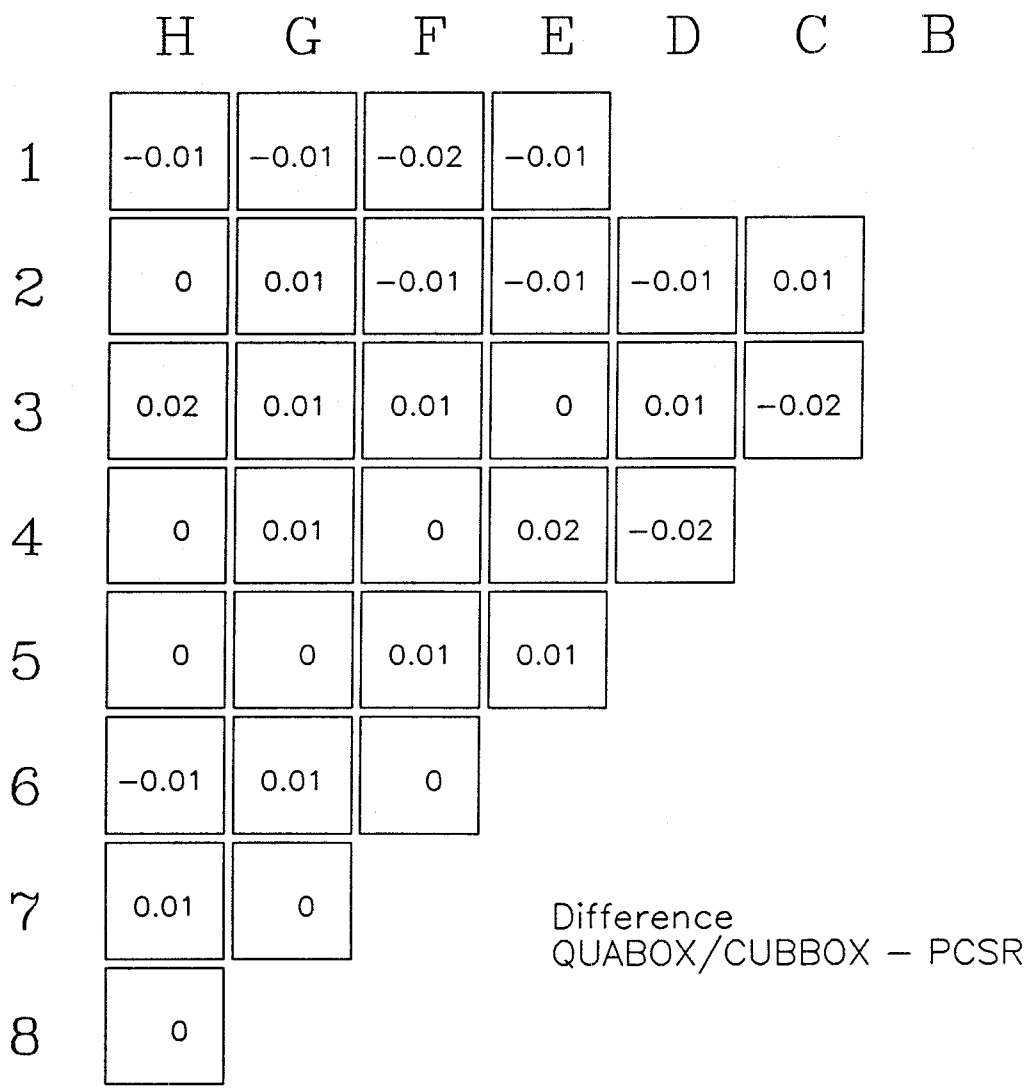

State: near EOL, unrodded Core,

Hot Full Power, Eq. Xenon

Fig. 2.13 Comparison of Radial Power Distribution

QUABOX/CUBBOX vs. PCSR

Fig. 2.14 Comparison of radial power distributions at EOL
IKE–Calculation vs. PCSR

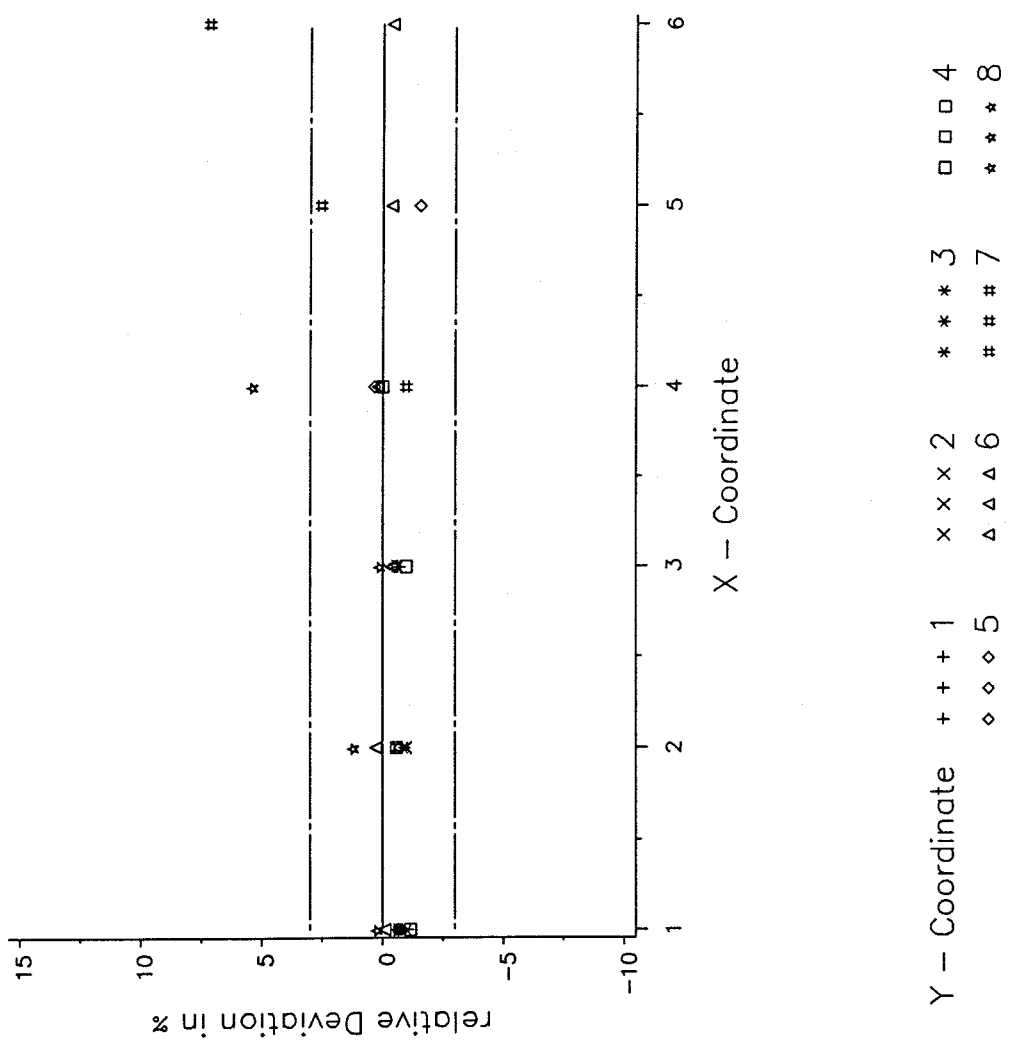

Fig. 2.15 Comparison of radial power distributions at EOL
QUABOX/CUBBOX vs. PCSR

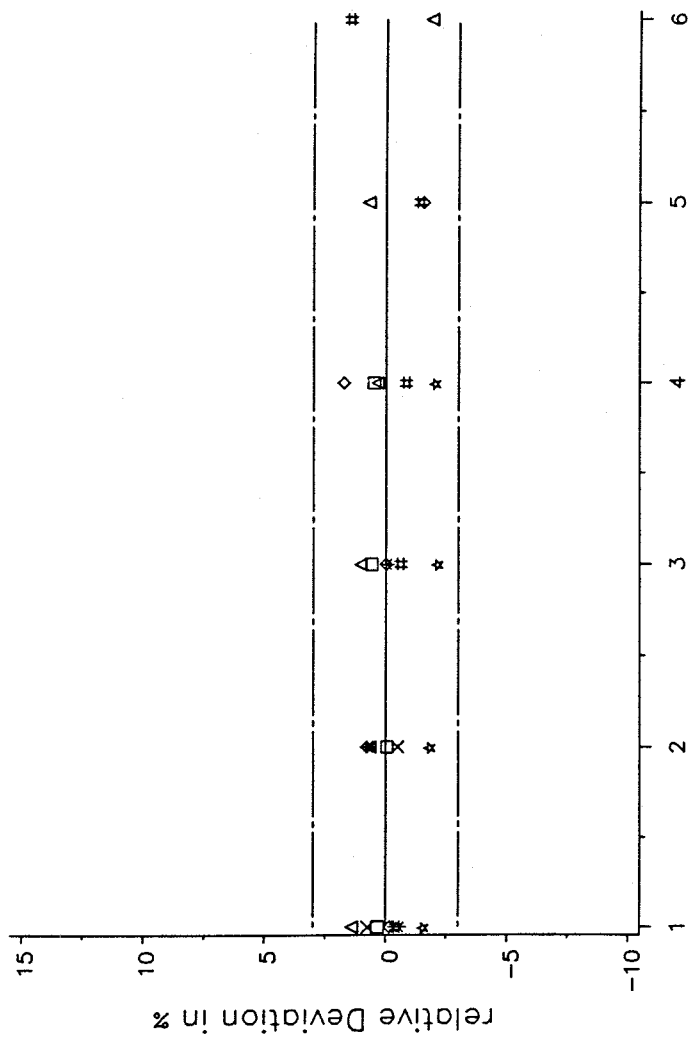

Fig. 2.16 Comparison of radial power distributions at EOL
QUABOX/CUBBOX vs. IKE–Calculation

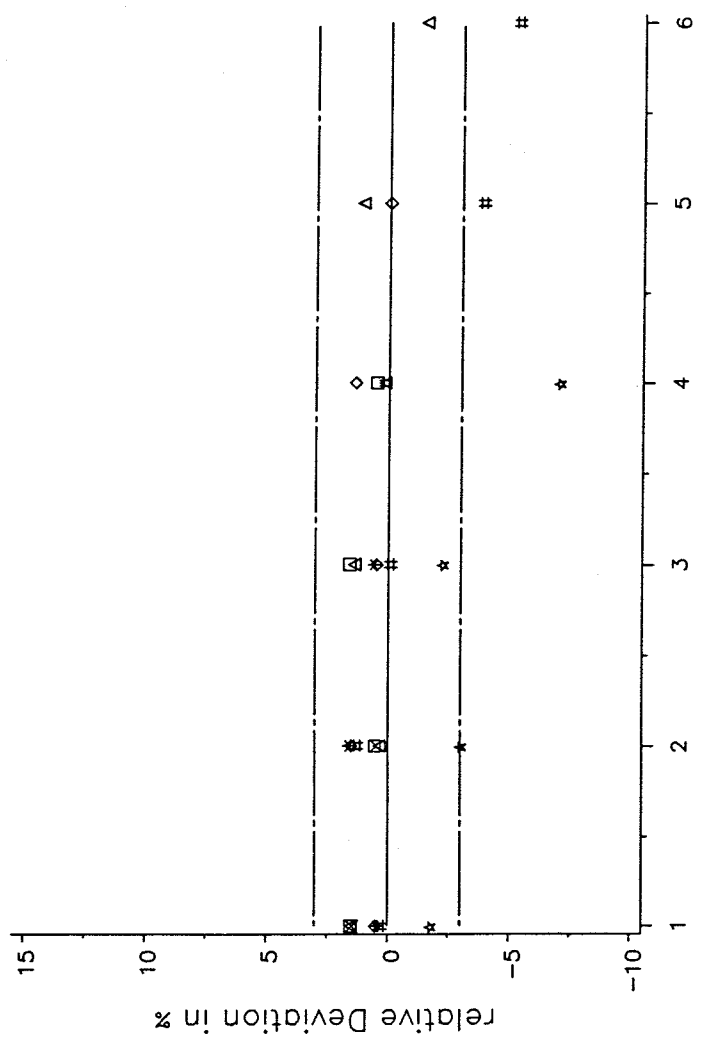

FIGURES

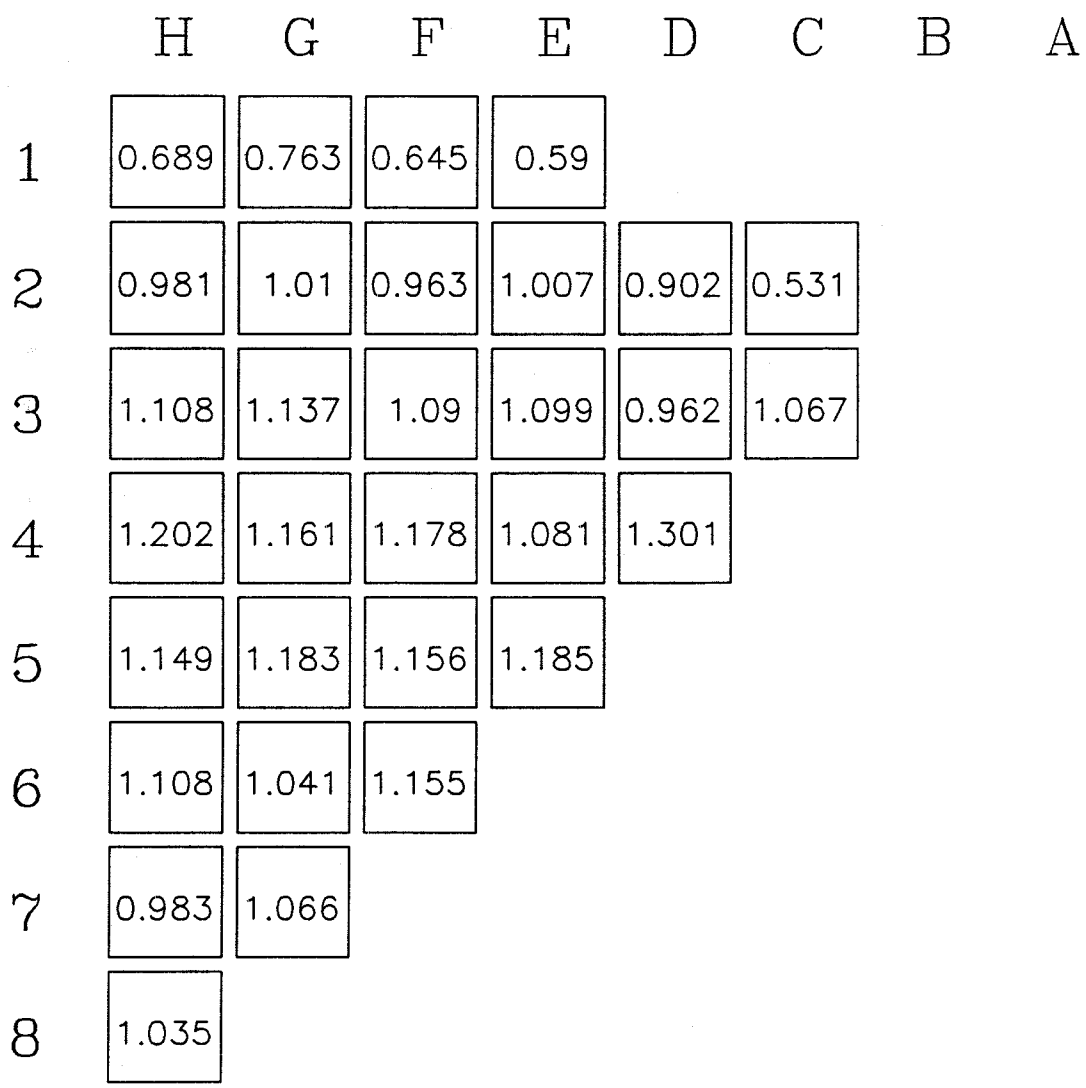

State: BOL, unrodded Core,
Hot Zero Power, no Xenon
QUABOX/CUBBOX, 2D

Fig. 3.1 Radial Power Distribution

JF8

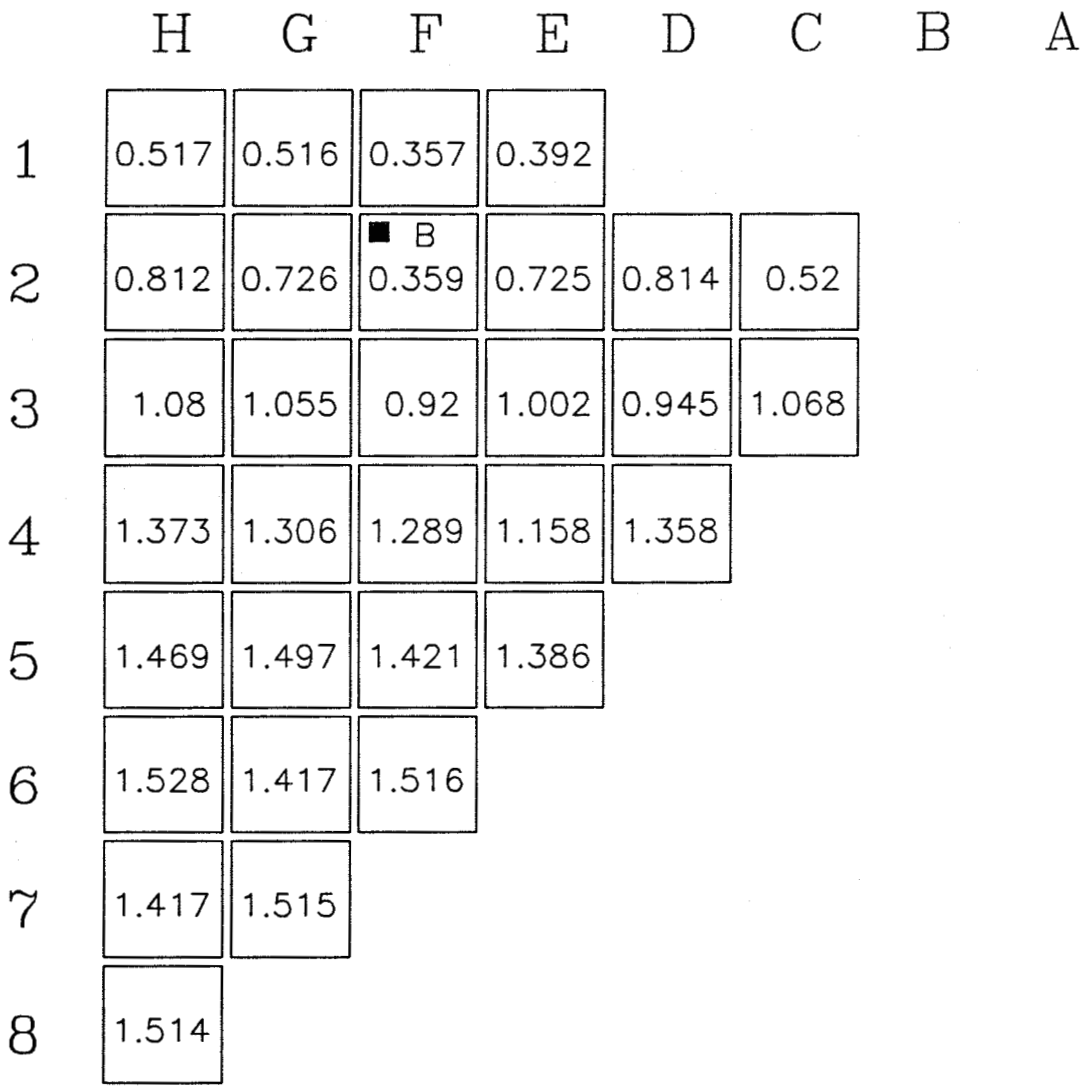

State: BOL, B–Bank inserted,

Hot Zero Power, no Xenon

QUABOX/CUBBOX, 2D

Fig. 3.2 Radial Power Distribution

JF8A

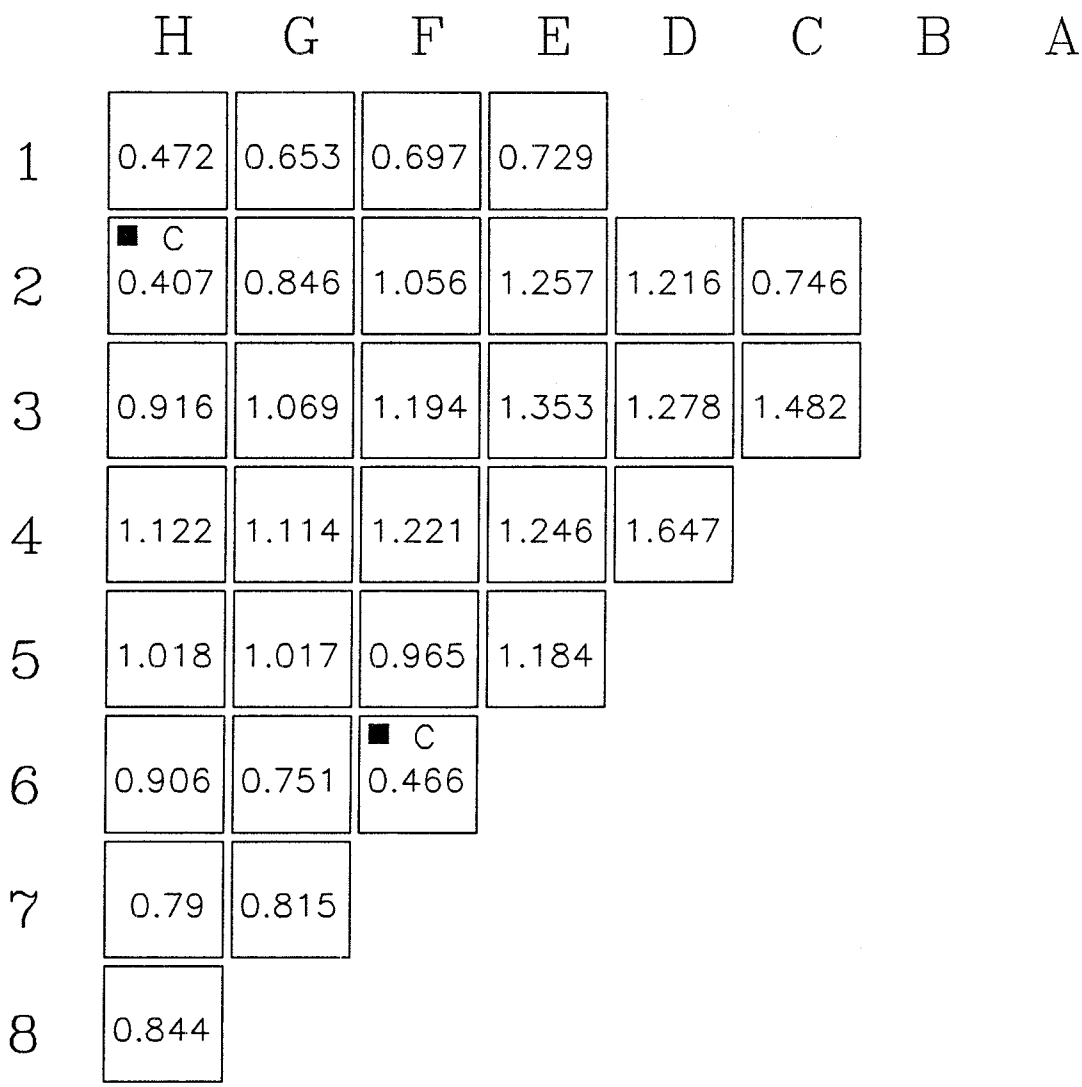

State: BOL, C-Bank inserted,

Hot Zero Power, no Xenon

QUABOX/CUBBOX, 2D

Fig. 3.3 Radial Power Distribution

JF8B

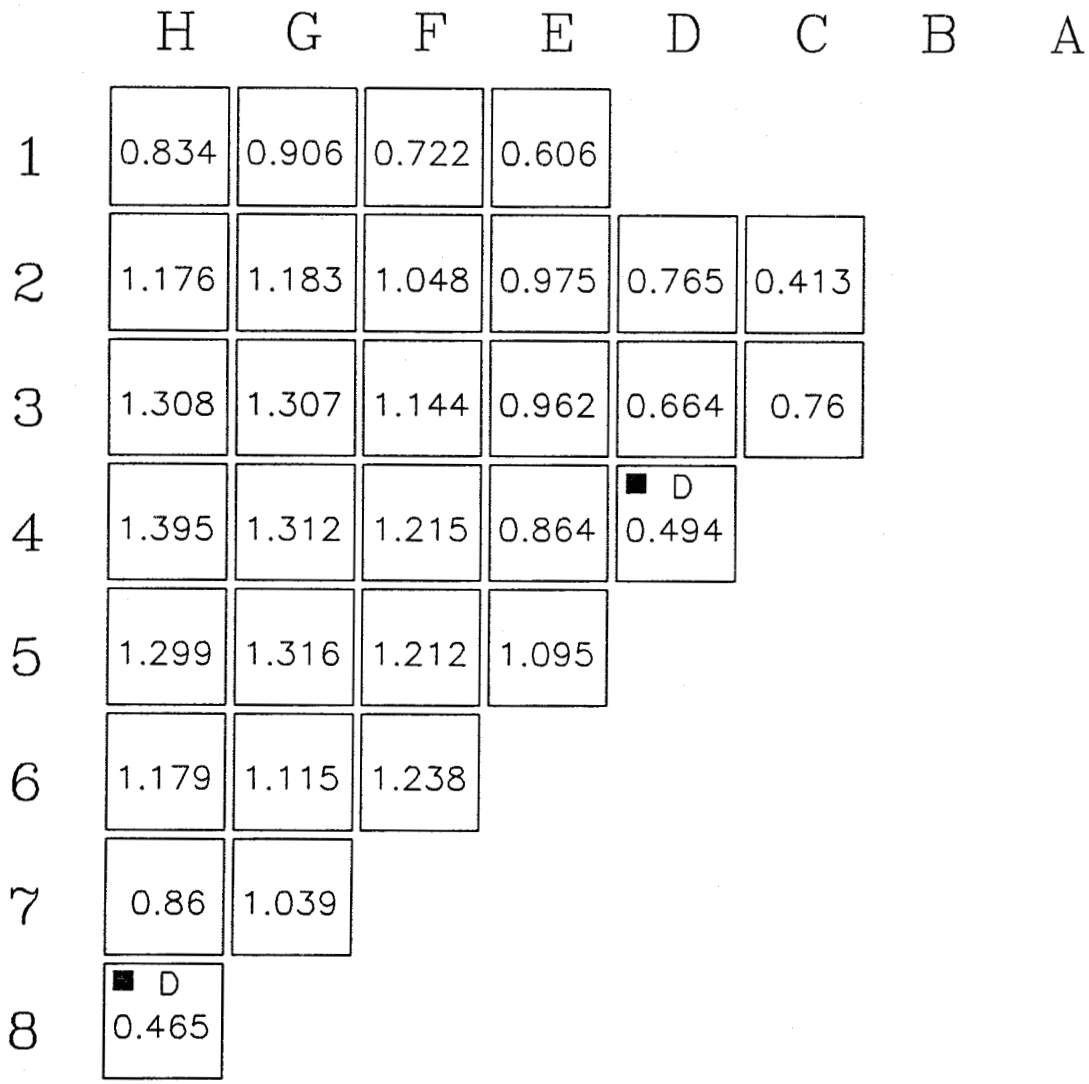

State: BOL, D-Bank inserted,

Hot Zero Power, no Xenon

QUABOX/CUBBOX, 2D

Fig. 3.4 Radial Power Distribution

JF8C

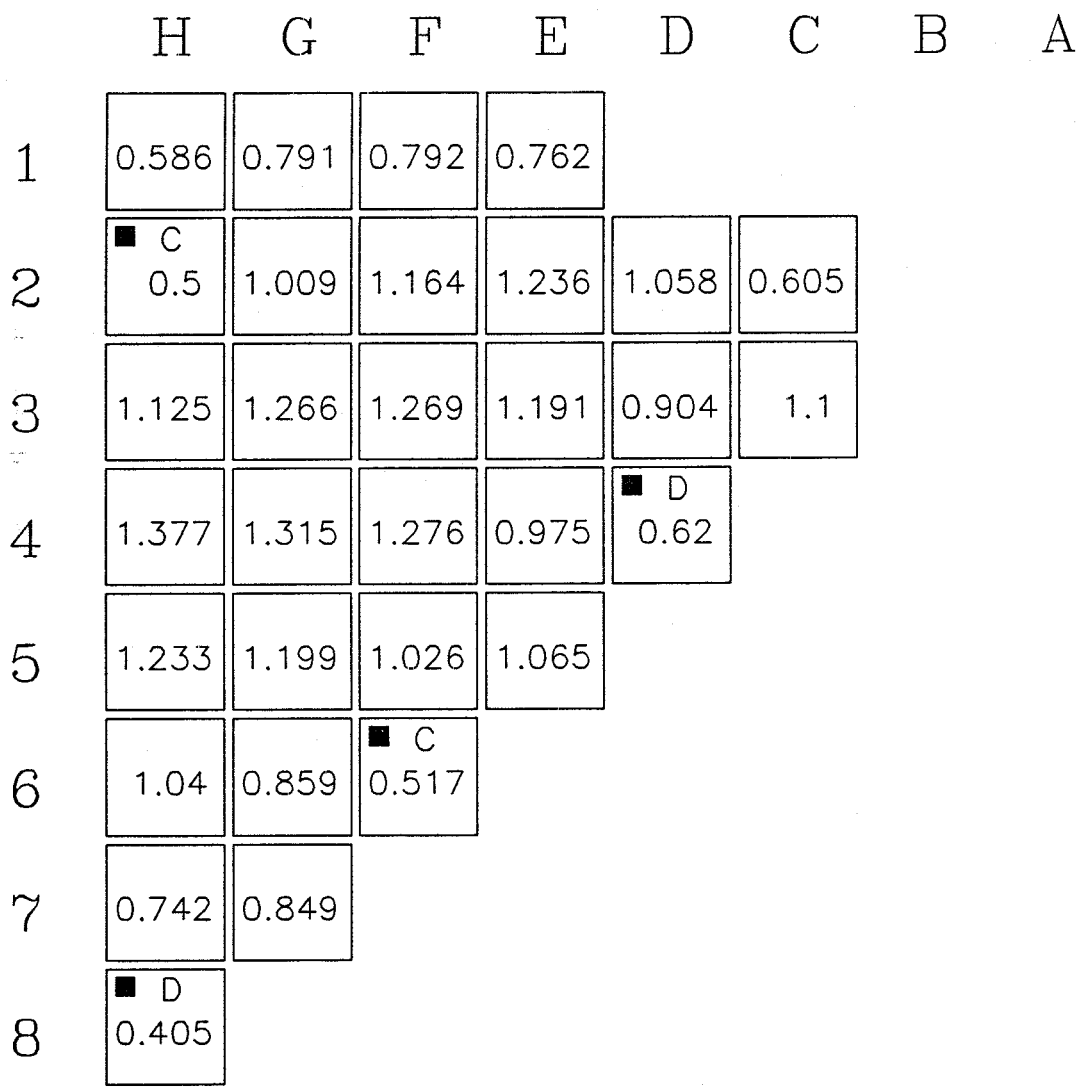

State: BOL, C+D–Bank inserted,

Hot Zero Power, no Xenon

QUABOX/CUBBOX, 2D

Fig. 3.5 Radial Power Distribution

JF8D

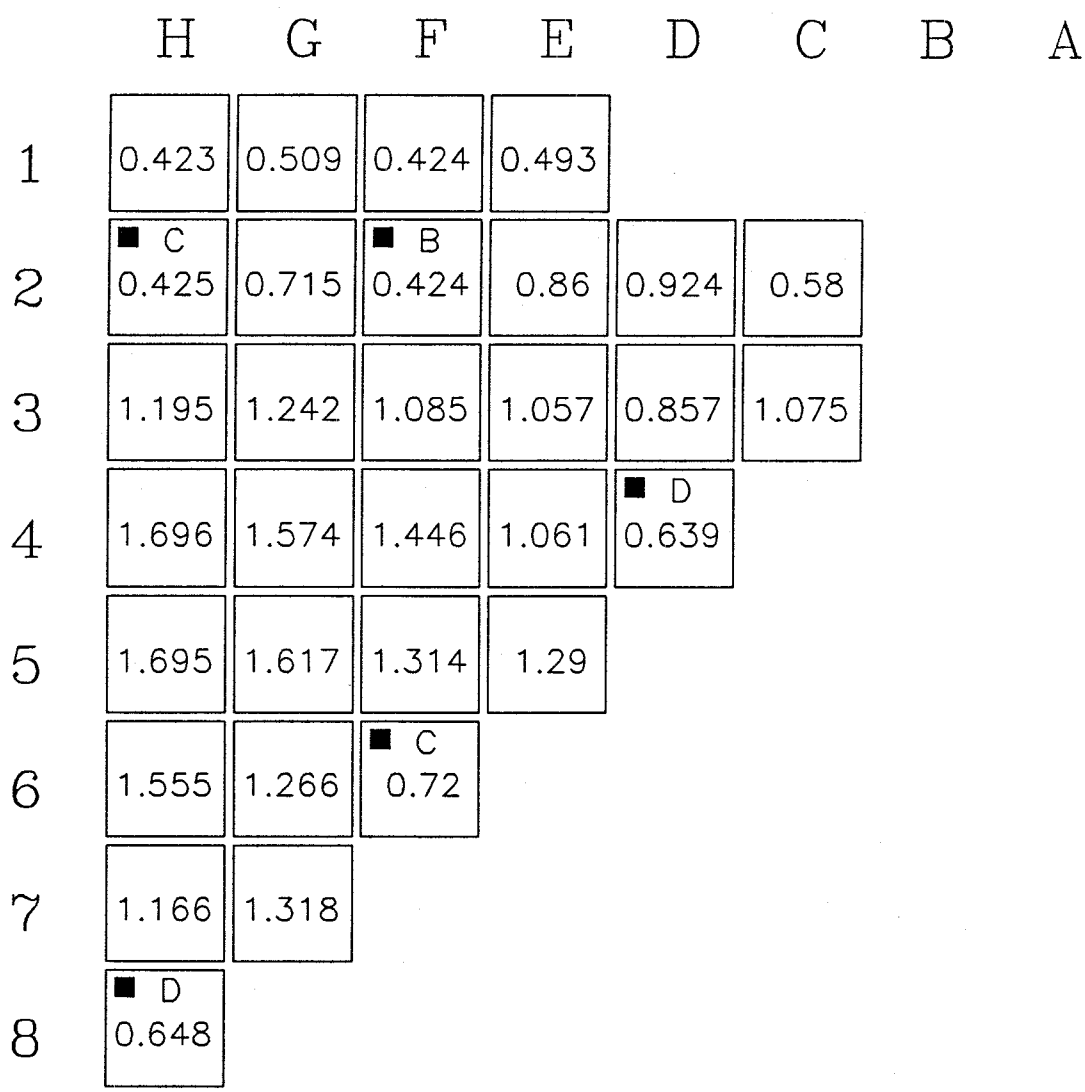

State: BOL,B+C+D—Bank inserted,

Hot Zero Power, no Xenon

QUABOX/CUBBOX, 2D

Fig. 3.6 Radial Power Distribution

JF8E

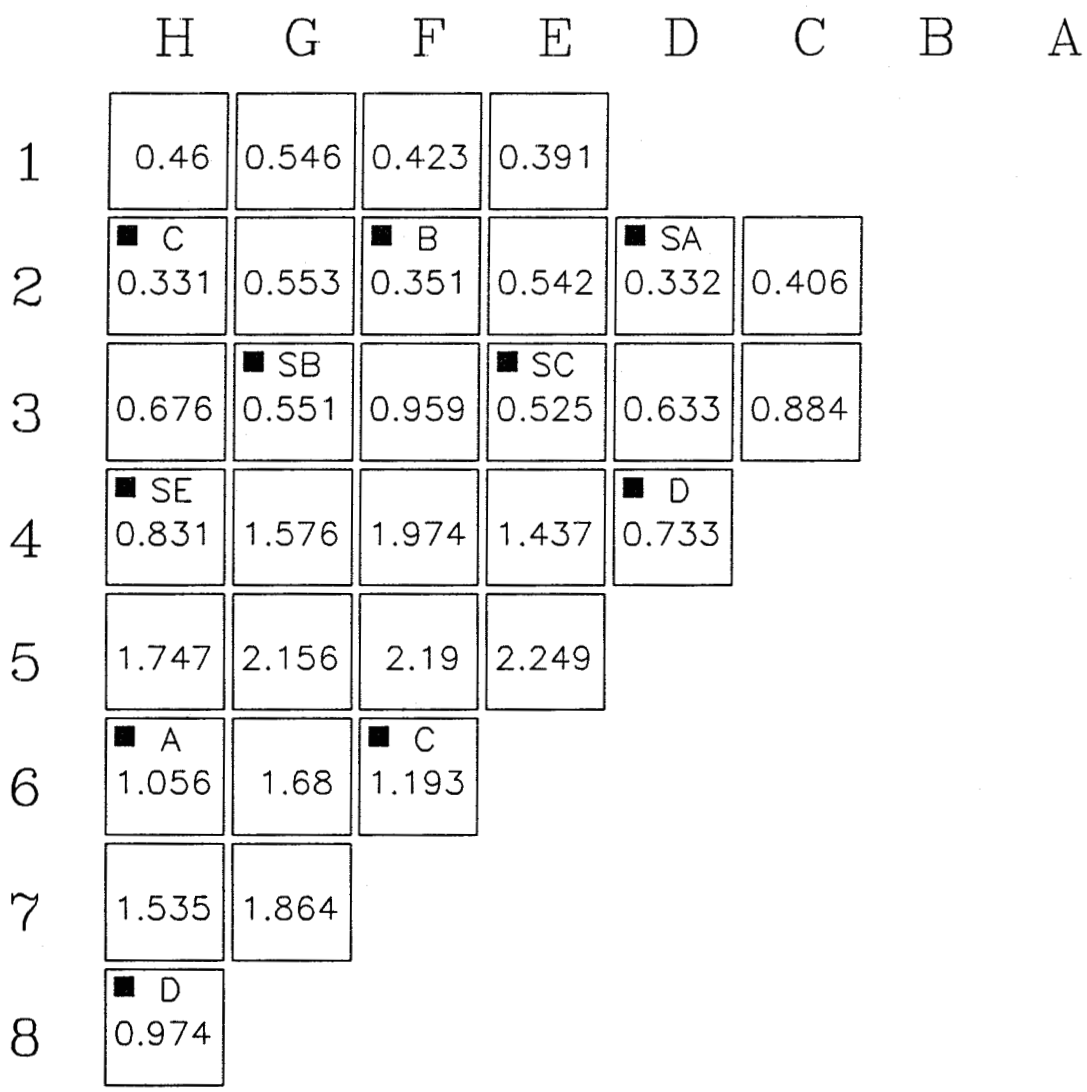

State: BOL, all rods inserted,

Hot Zero Power, no Xenon

QUABOX/CUBBOX, 2D

Fig. 3.7 Radial Power Distribution

JF8F

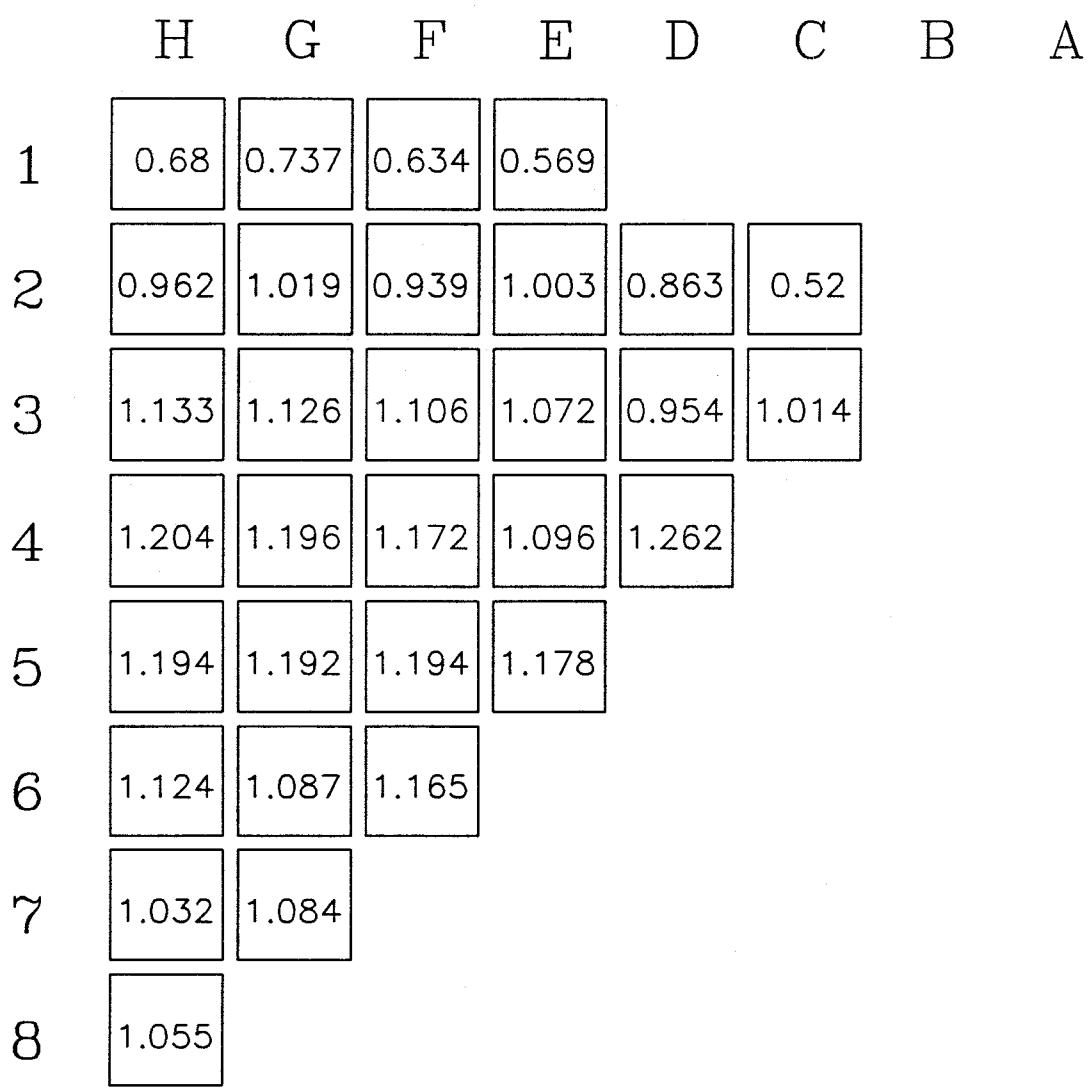

State: BOL, unrodded Core, 1307ppm
Hot Full Power, no Xenon
QUABOX/CUBBOX

Fig. 3.8 Radial Power Distribution

JF9

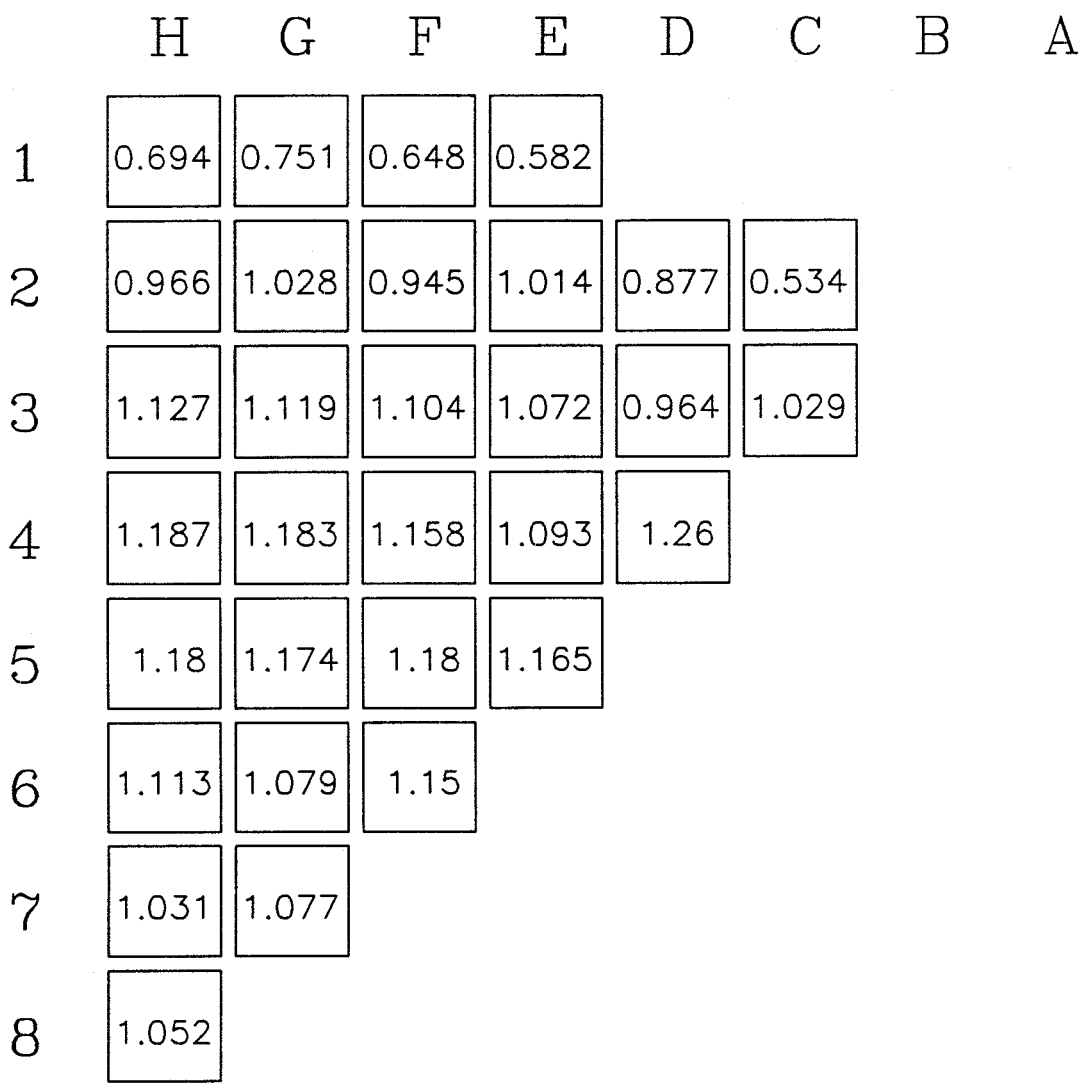

State: BOL, unrodded Core, 1307ppm
Hot Full Power, Eq. Xenon
QUABOX/CUBBOX

Fig. 3.9 Radial Power Distribution

JF9A

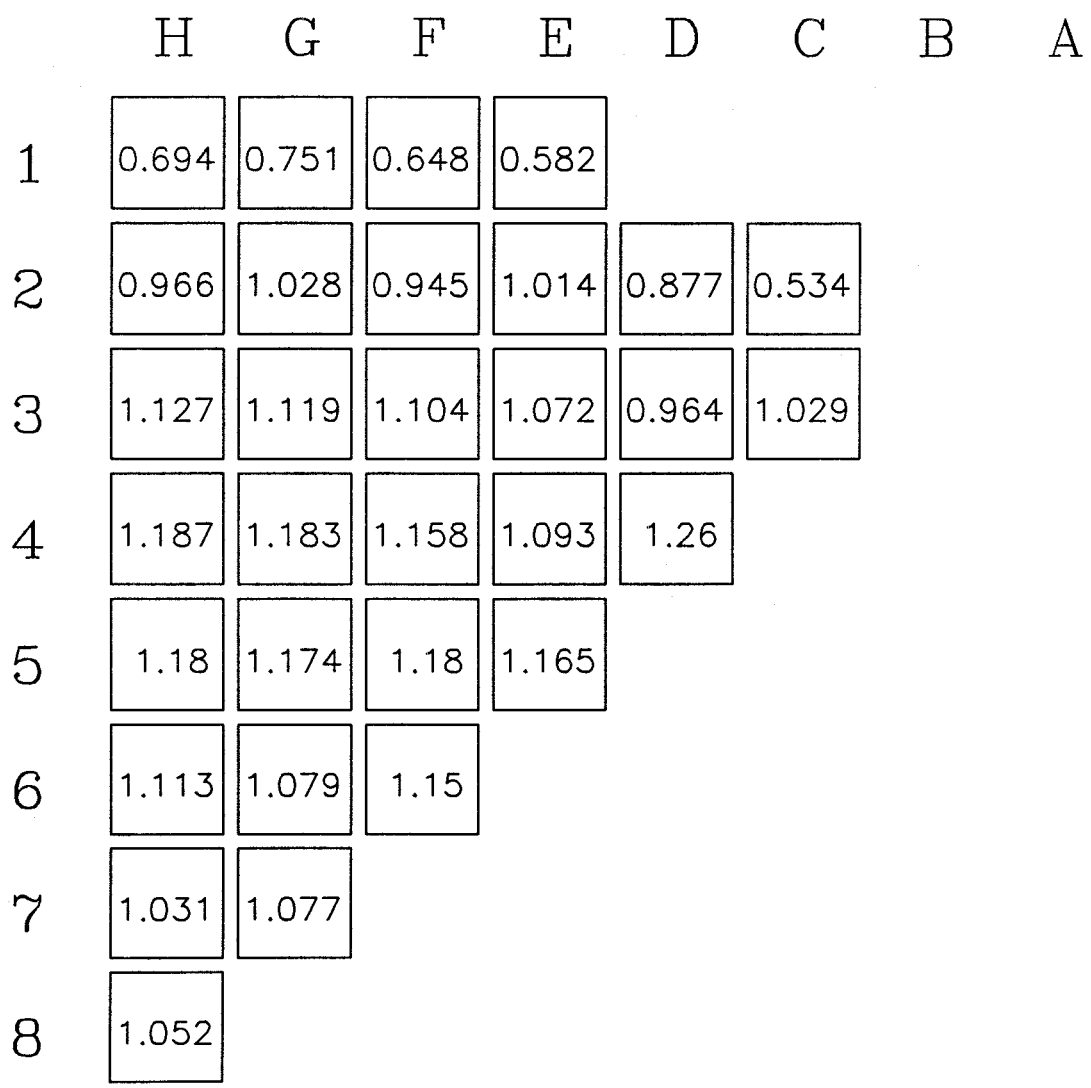

State: BOL, unrodded Core, crit.Boron
Hot Full Power, Eq. Xenon
QUABOX/CUBBOX

Fig. 3.10 Radial Power Distribution

JF9B

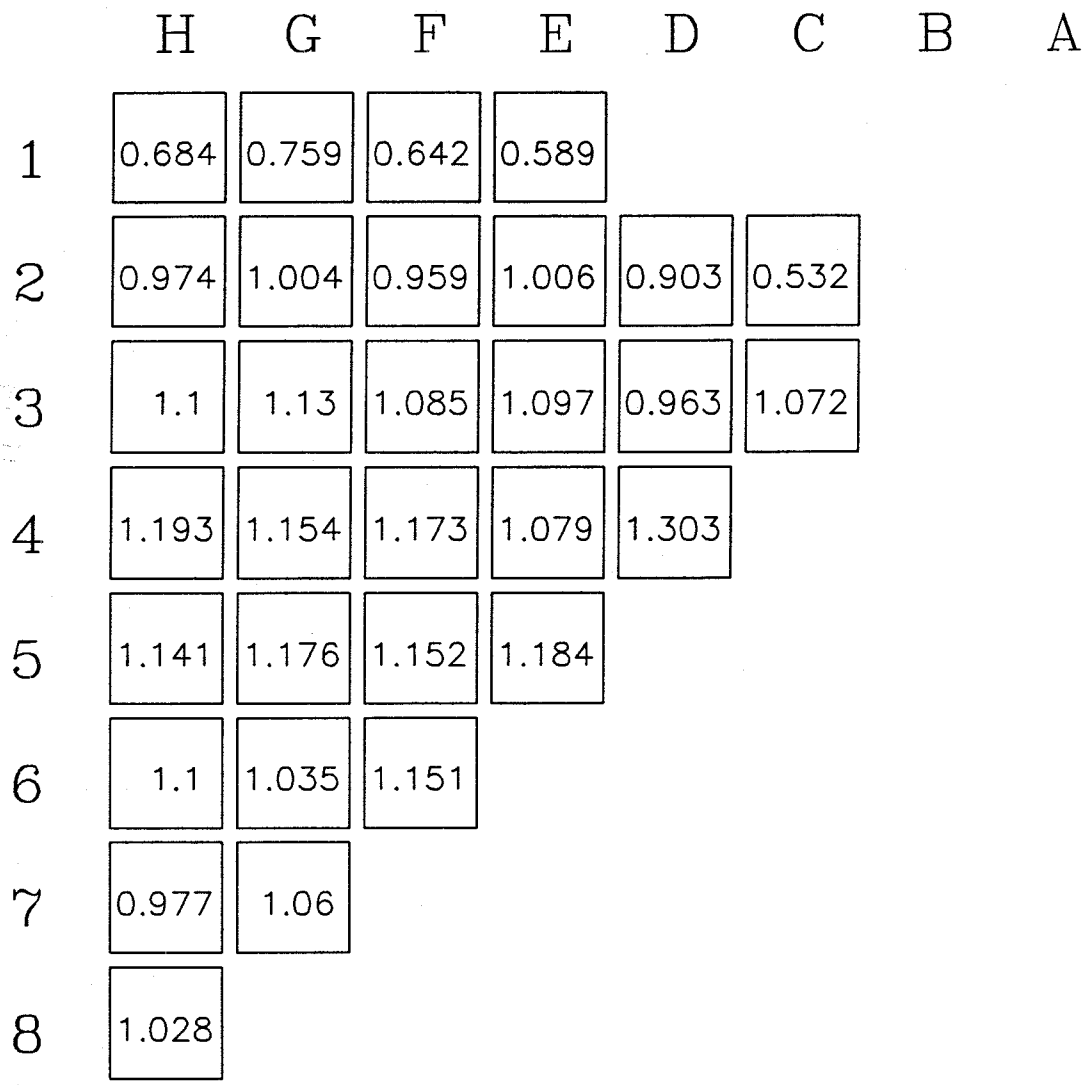

State: BOL, unrodded Core, 1307ppm
Hot Zero Power, no Xenon
QUABOX/CUBBOX, 3D

Fig. 3.11 Radial Power Distribution

JFA1

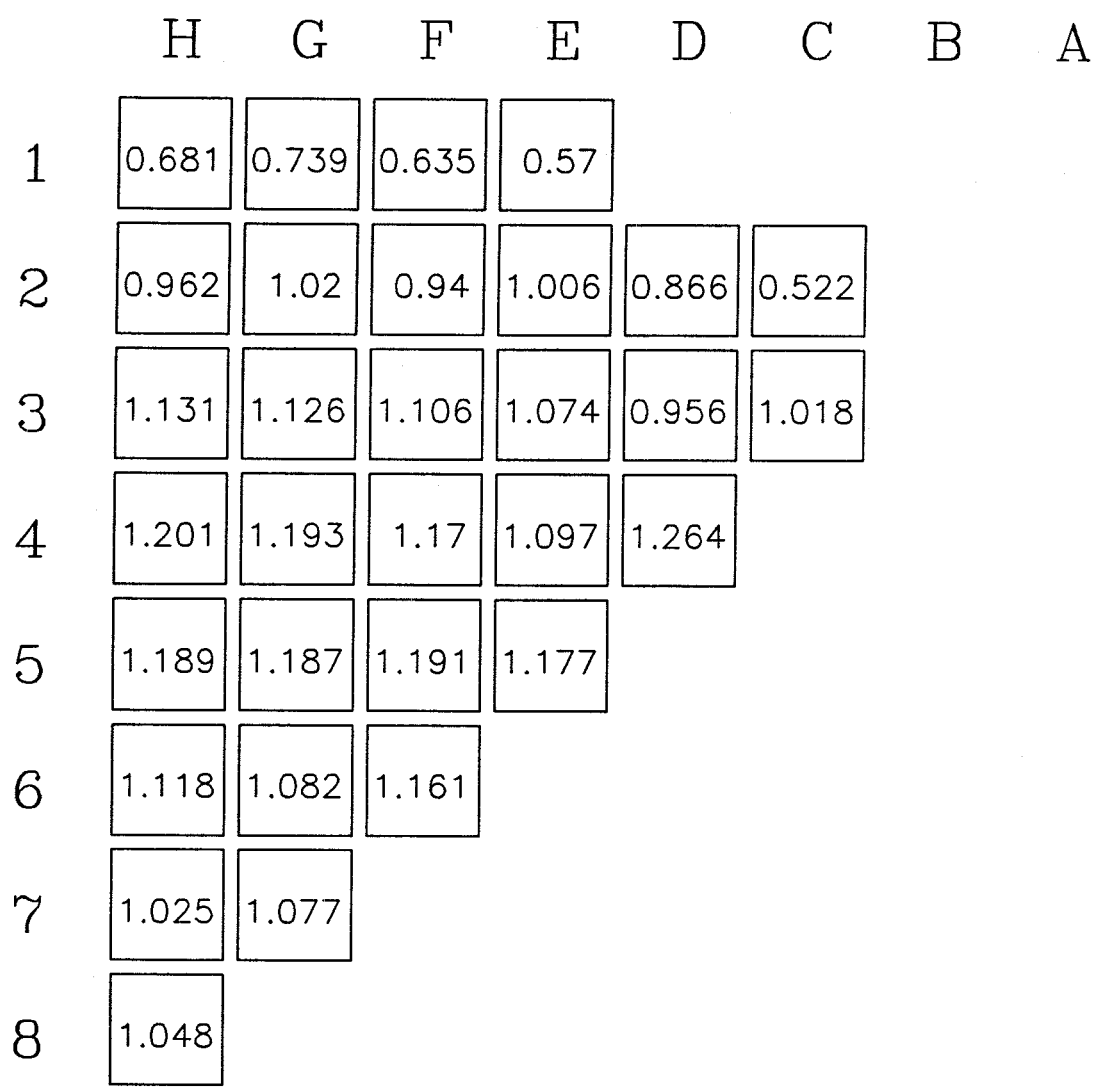

State: BOL, unrodded Core, 1307ppm
Hot Full Power, no Xenon
QUABOX/CUBBOX, 3D

Fig. 3.12 Radial Power Distribution

JFA2

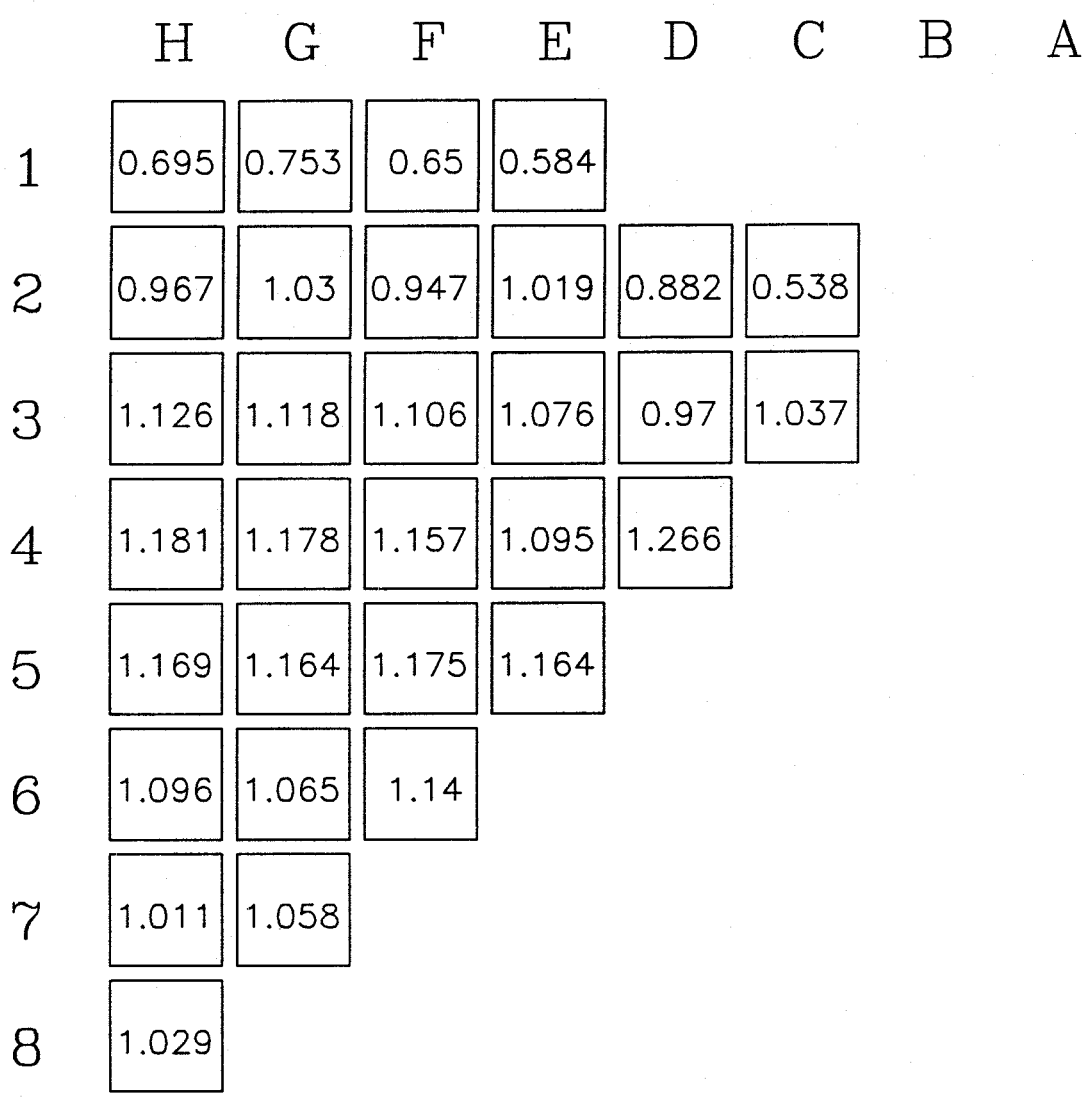

State: BOL, unrodded Core, 1307ppm
Hot Full Power, Eq. Xenon
QUABOX/CUBBOX, 3D

Fig. 3.13 Radial Power Distribution

JFA3

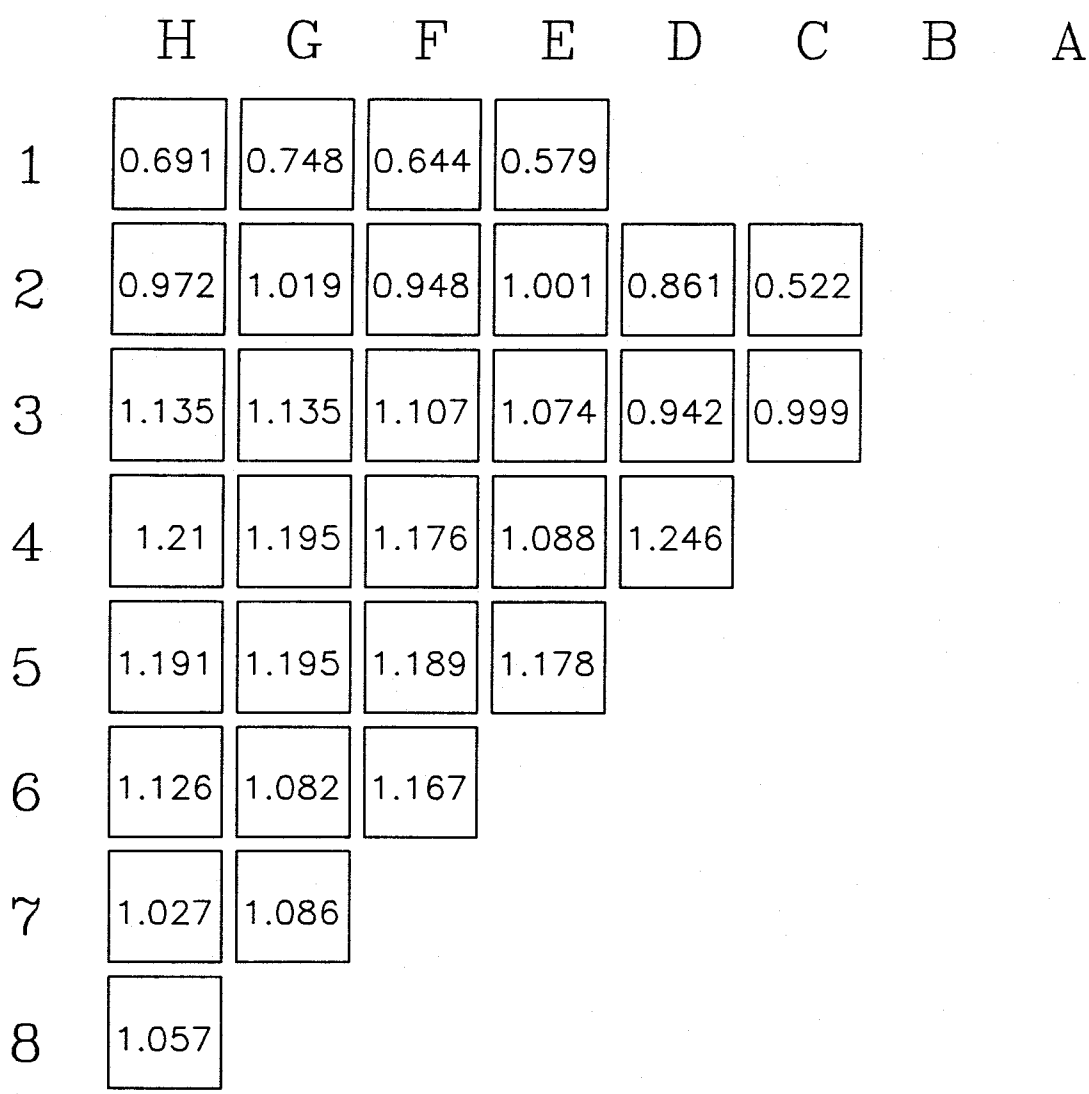

State: BOL, unrodded Core, crit. Boron
Hot Full Power, Eq. Xenon
QUABOX/CUBBOX, 3D

Fig. 3.14 Radial Power Distribution

JFA4

FIGURES

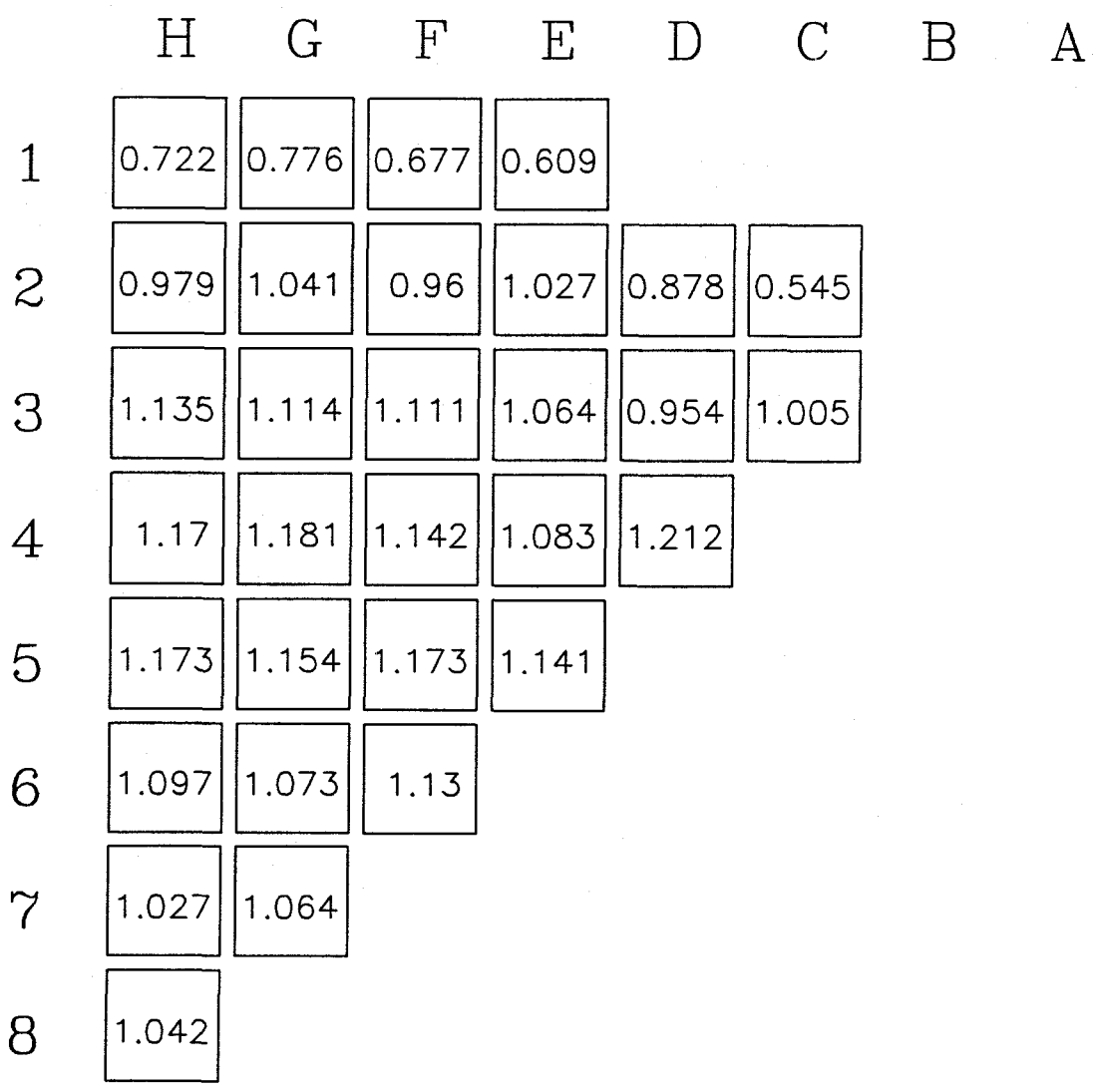

State: BOL, D–bank characteristic
Hot Full Power, Eq. Xenon
D–bank 0 % inserted

Fig. 4.1 Radial Power Distribution

JFB1

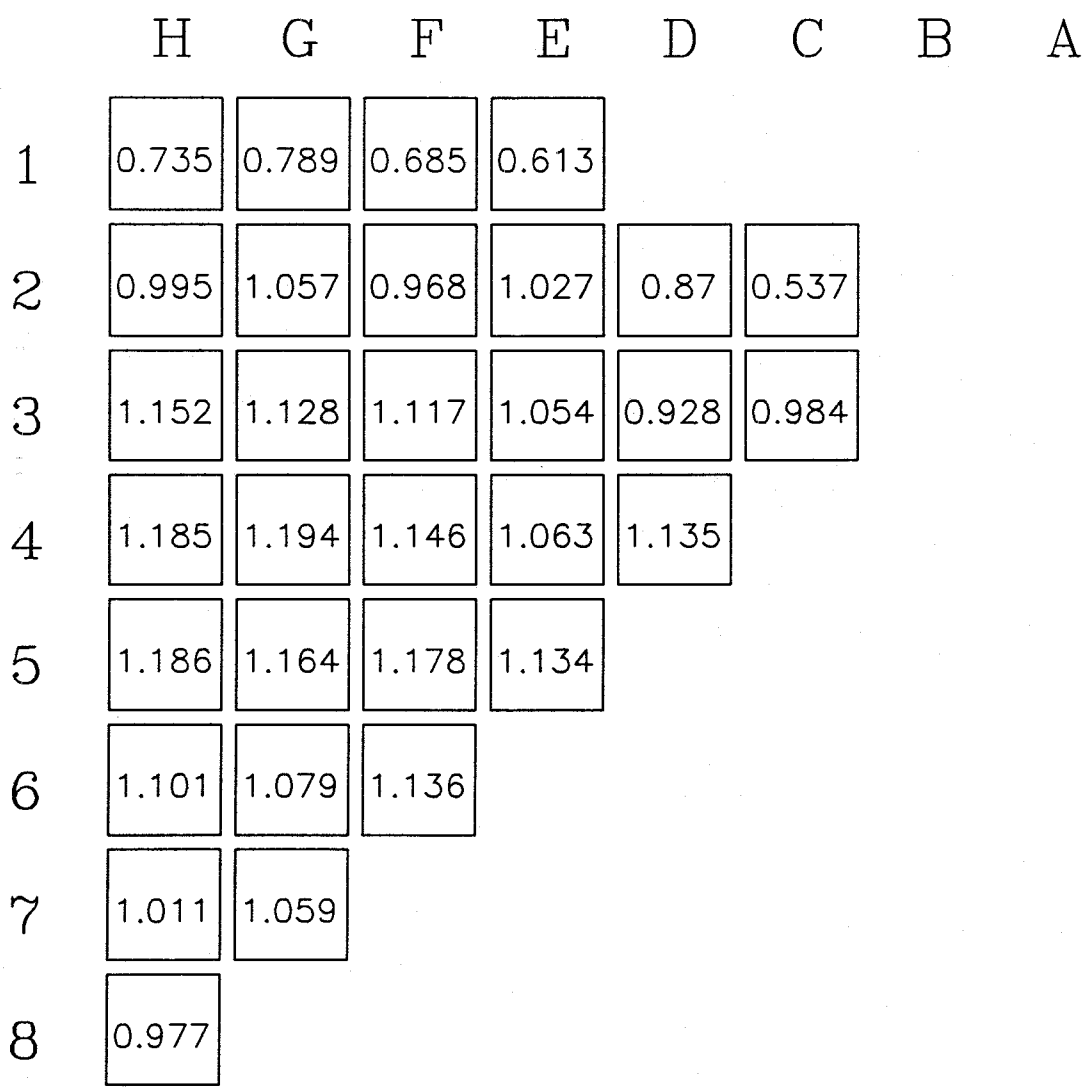

State: BOL, D–bank characteristic
Hot Full Power, Eq. Xenon
D–bank 20 % inserted

Fig. 4.2 Radial Power Distribution

JFB2

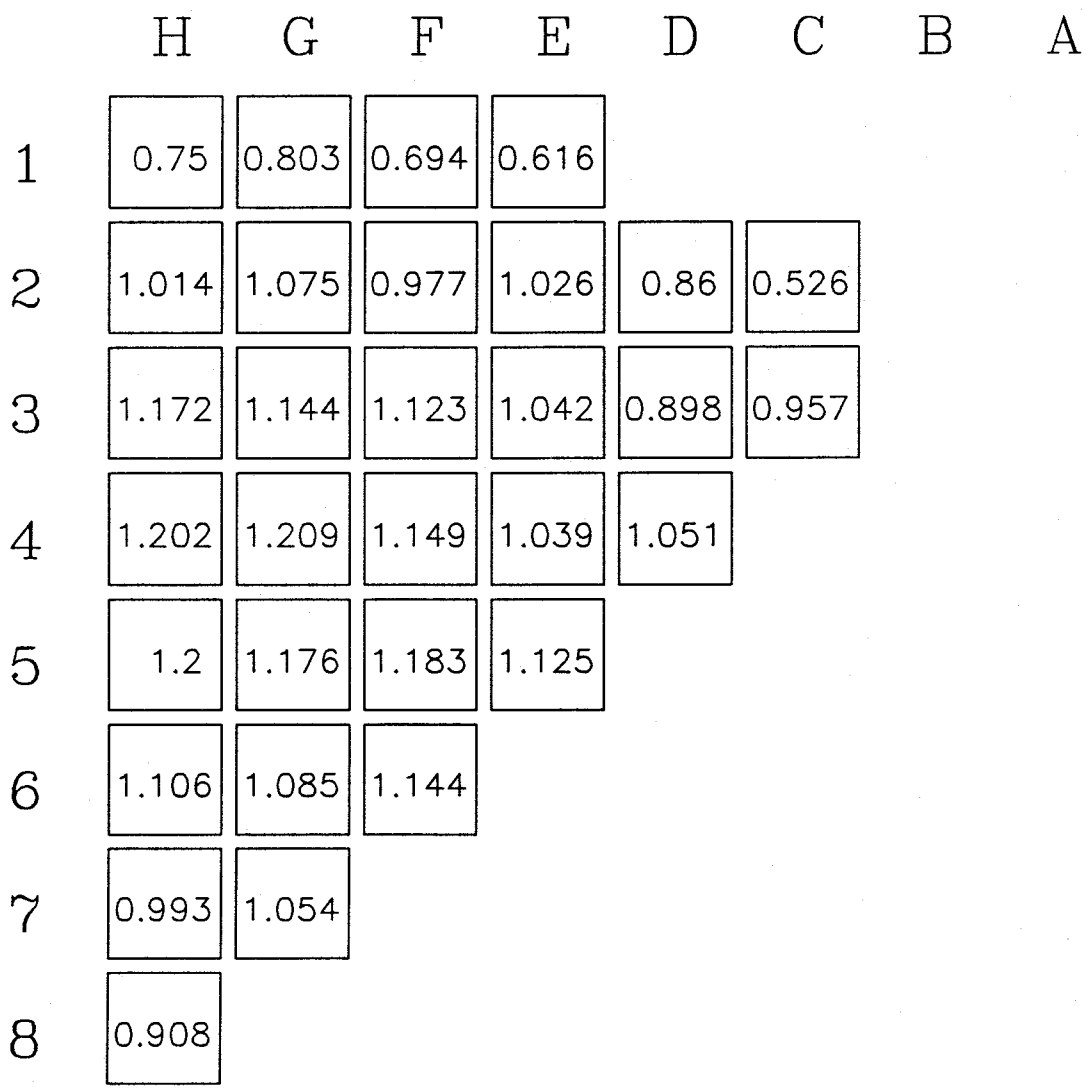

State: BOL, D–bank characteristic
Hot Full Power, Eq. Xenon
D–bank 33 % inserted

Fig. 4.3 Radial Power Distribution

JFB3

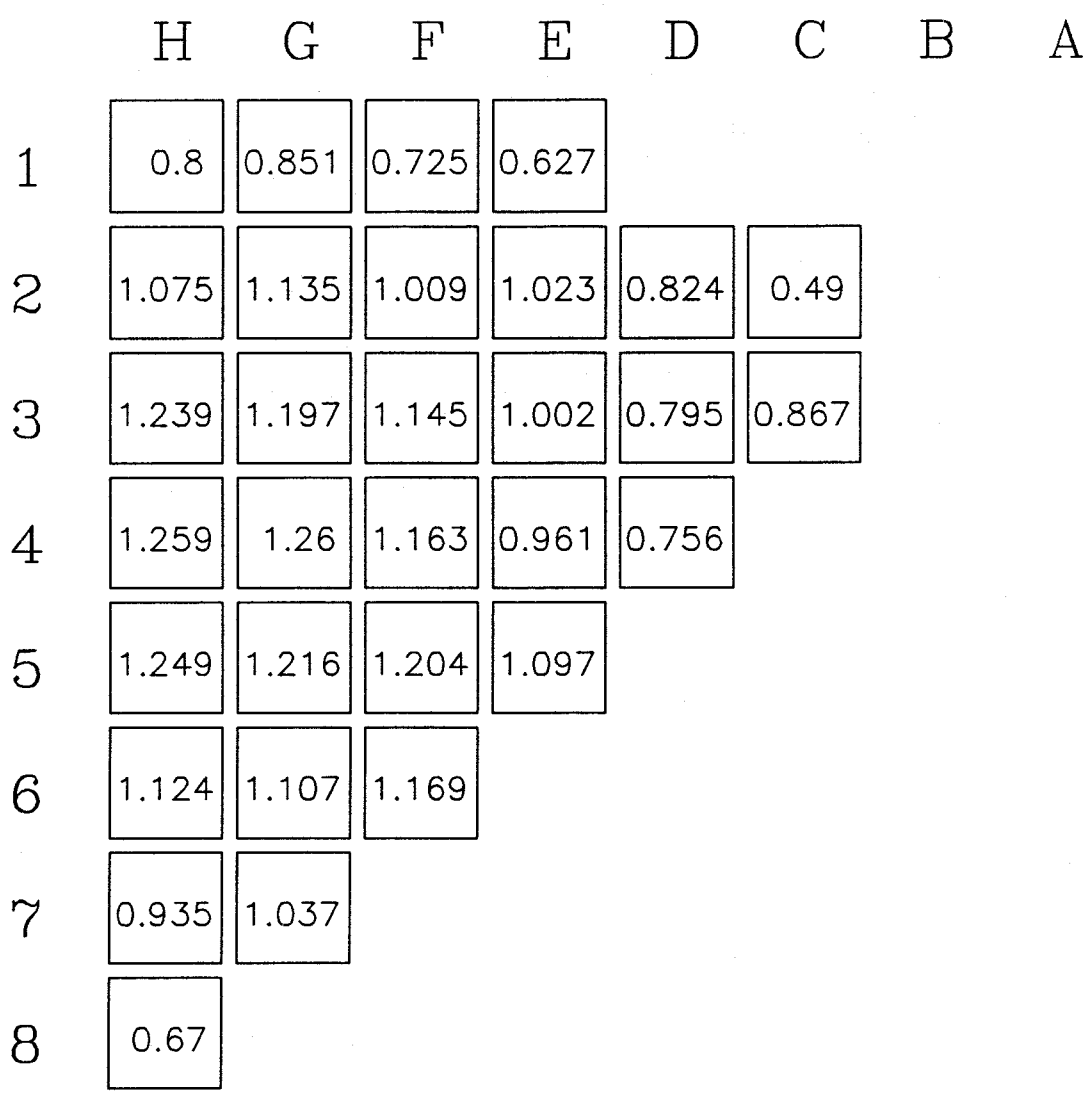

State: BOL, D–bank characteristic
Hot Full Power, Eq. Xenon
D–bank 66 % inserted

Fig. 4.4 Radial Power Distribution

JFB4

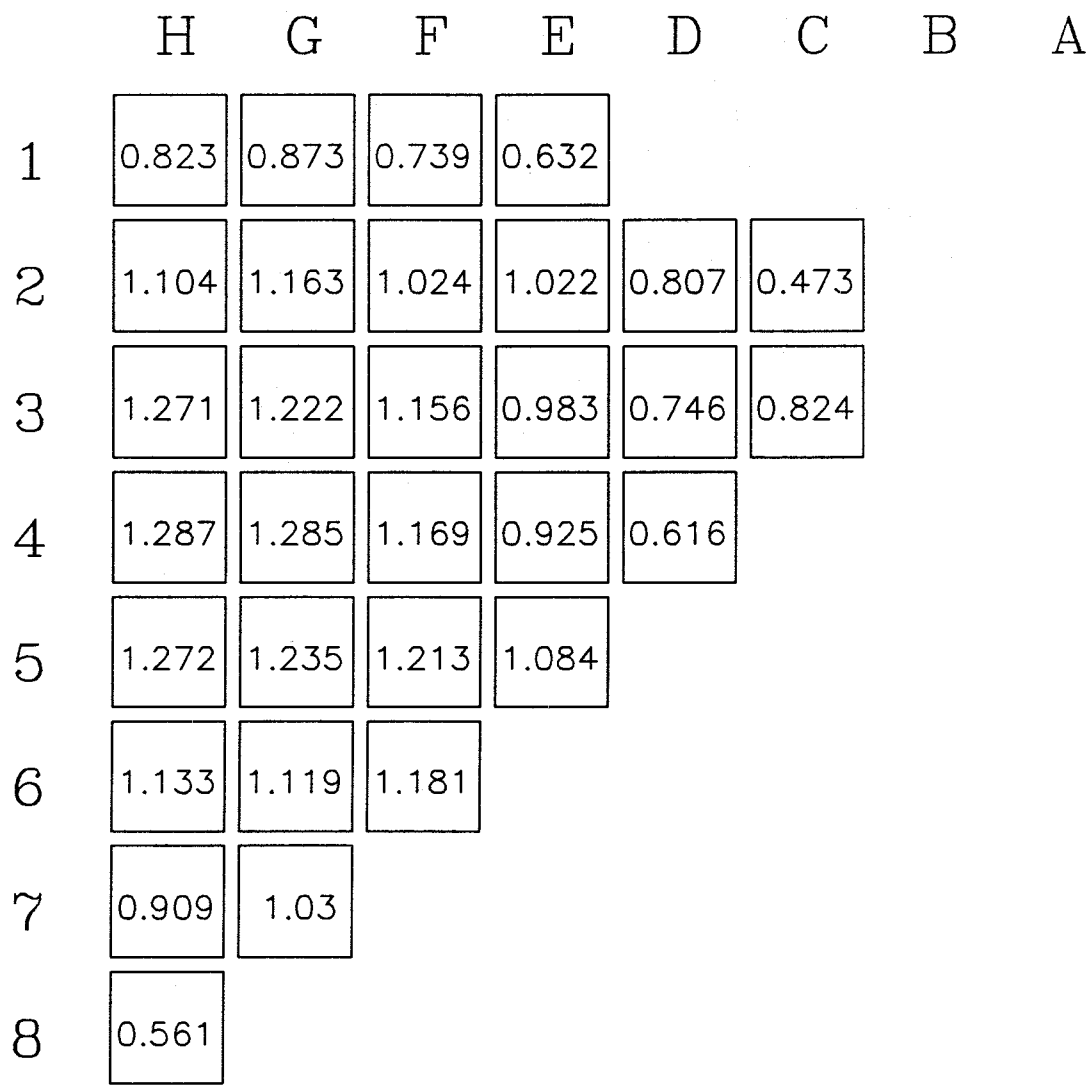

State: BOL, D–bank characteristic
Hot Full Power, Eq. Xenon
D–bank 80 % inserted

Fig. 4.5 Radial Power Distribution

JFB5

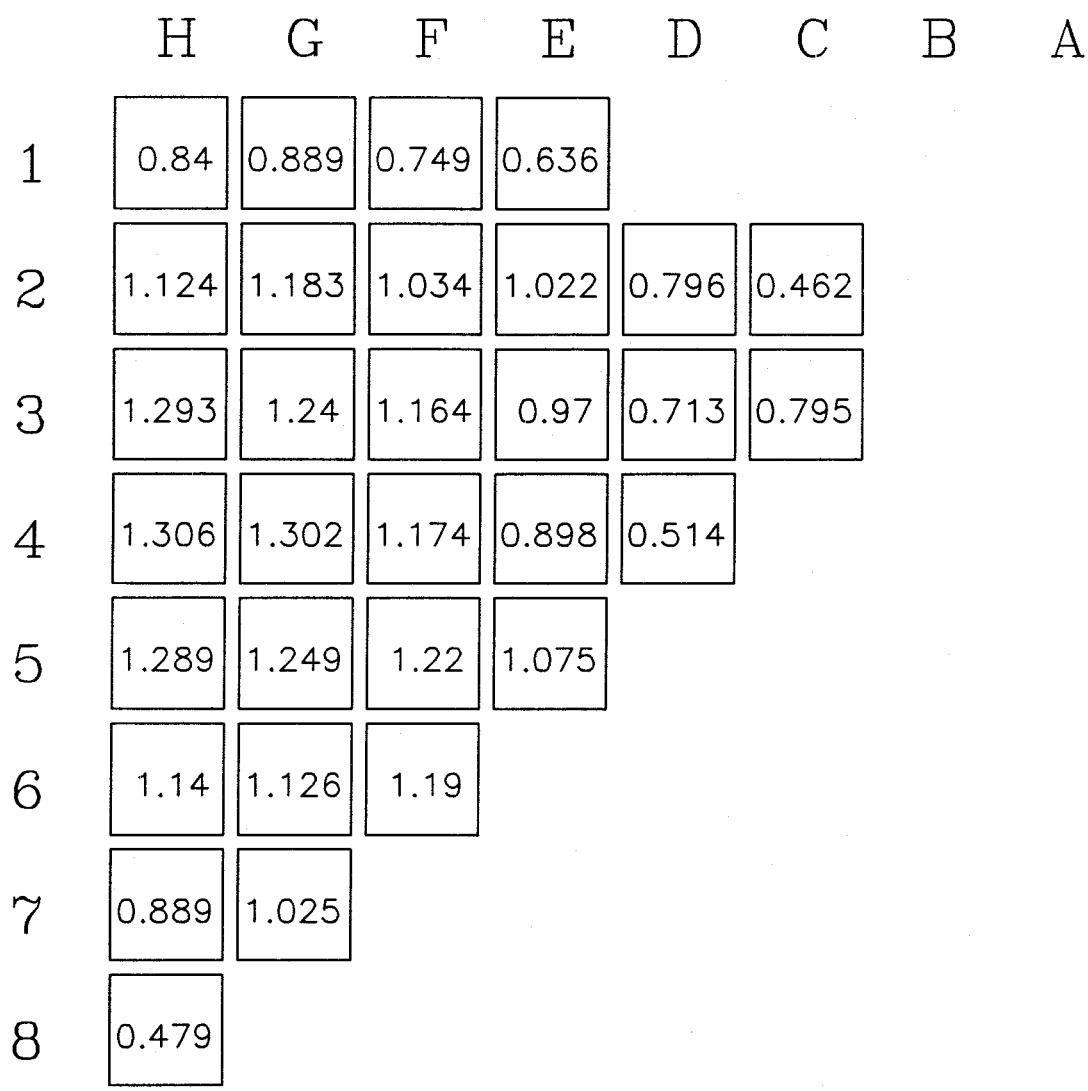

State: BOL, D–bank characteristic
Hot Full Power, Eq. Xenon
D–bank 100 % inserted

Fig. 4.6 Radial Power Distribution

JFB6

FIGURES

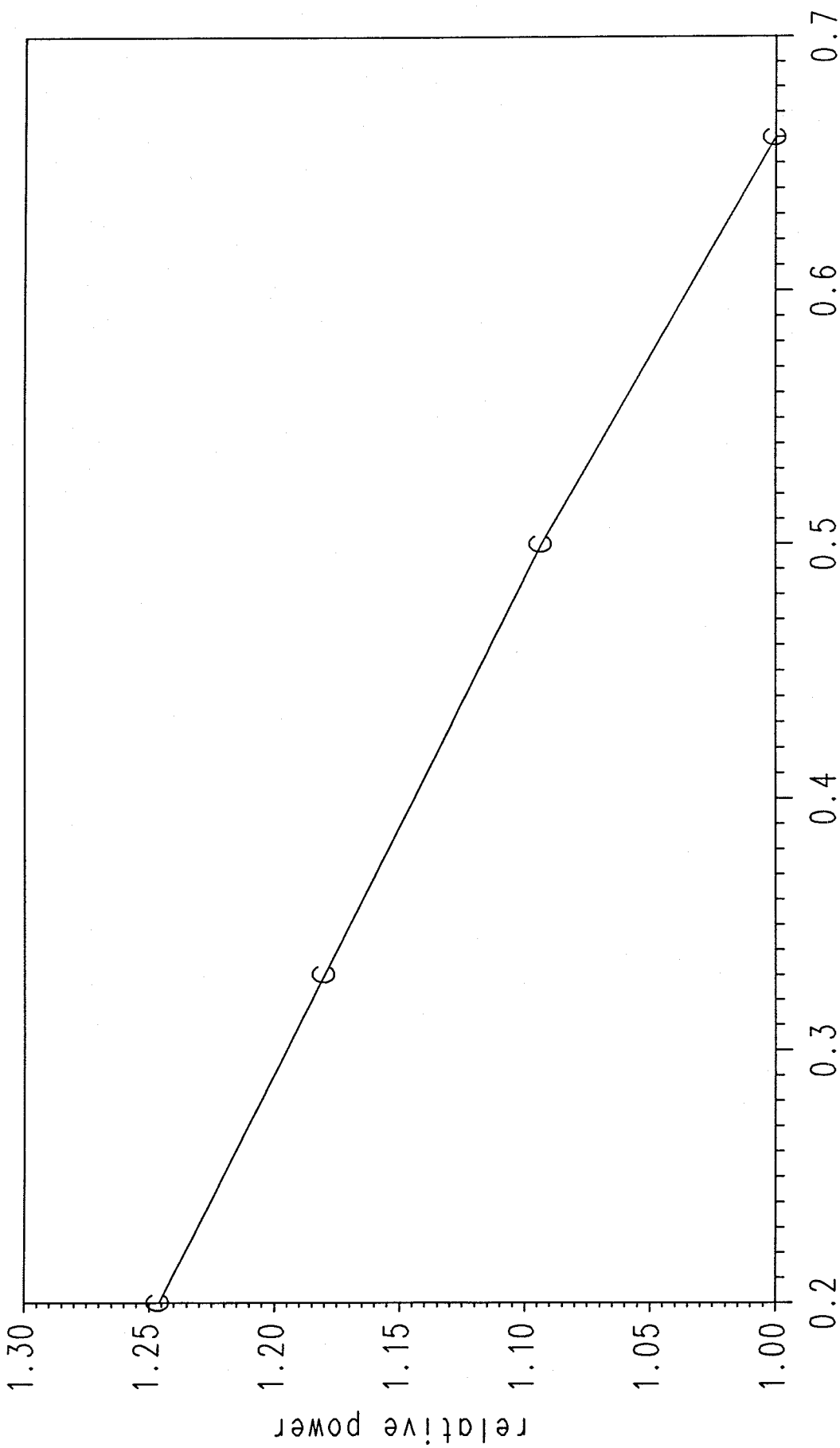

Fig. 5.1 D-bank withdrawal static calculations

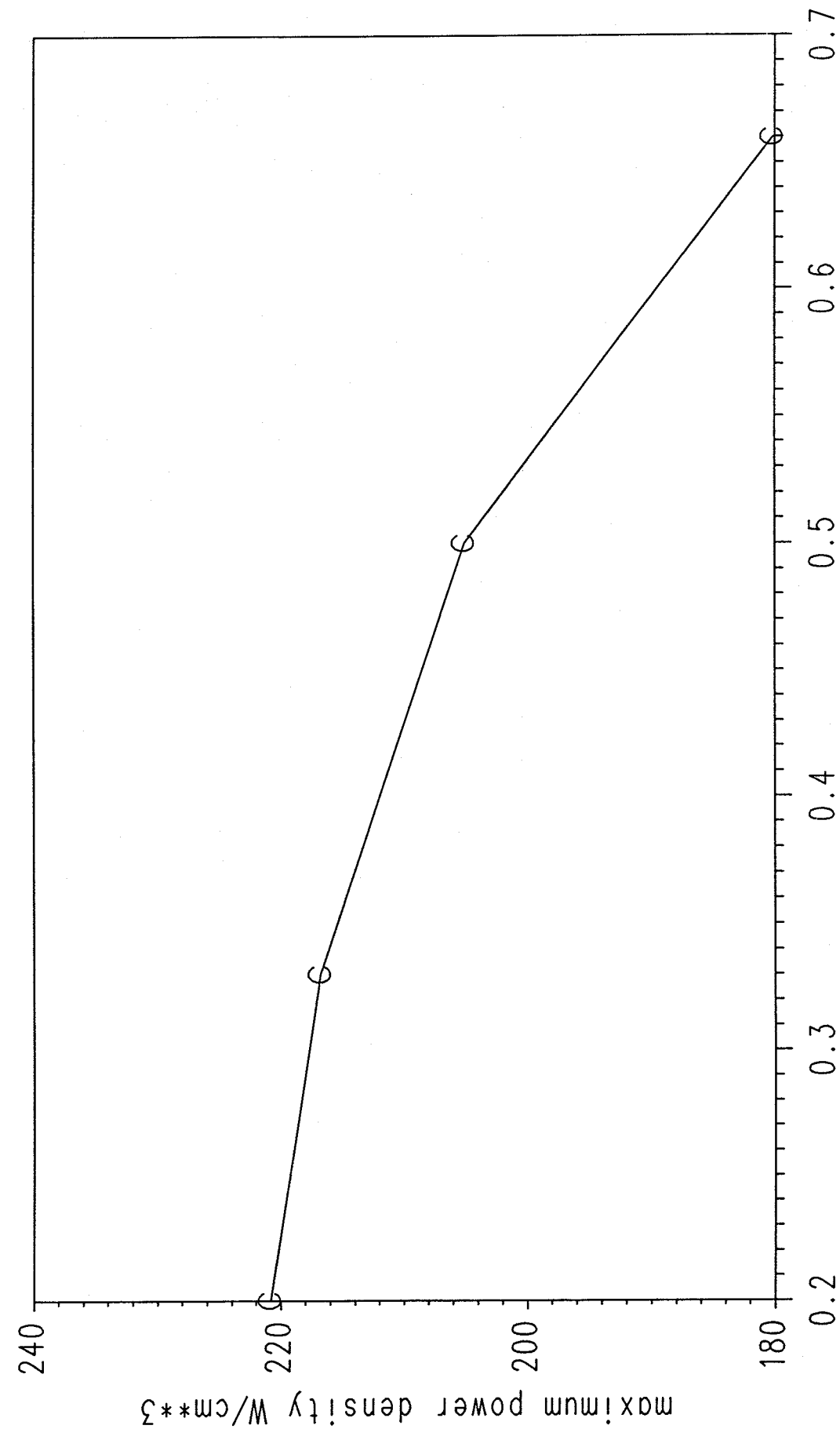

Fig. 5.2 D-bank withdrawal
static calculations

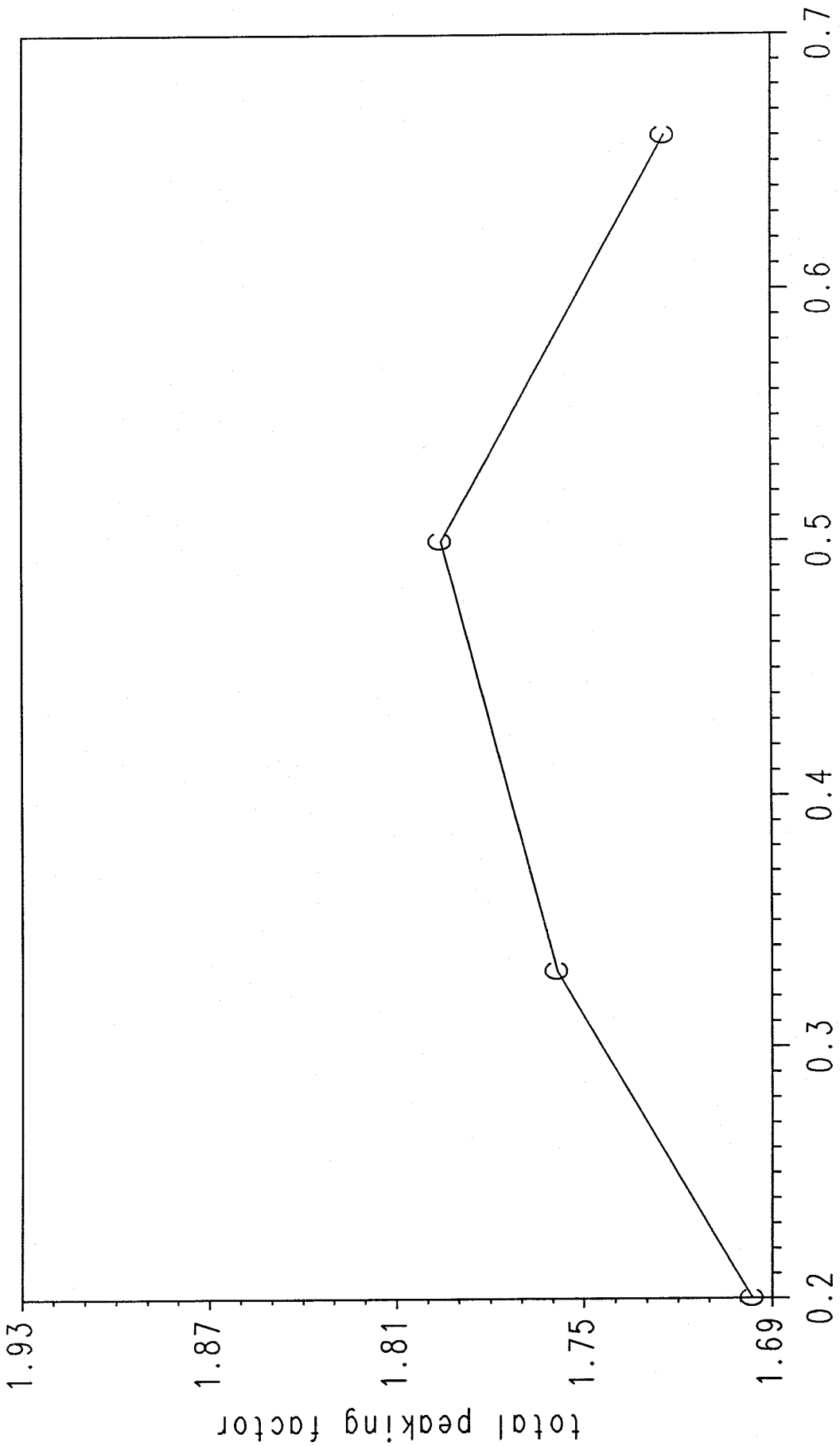

Fig. 5.3 D-bank withdrawal
static calculations

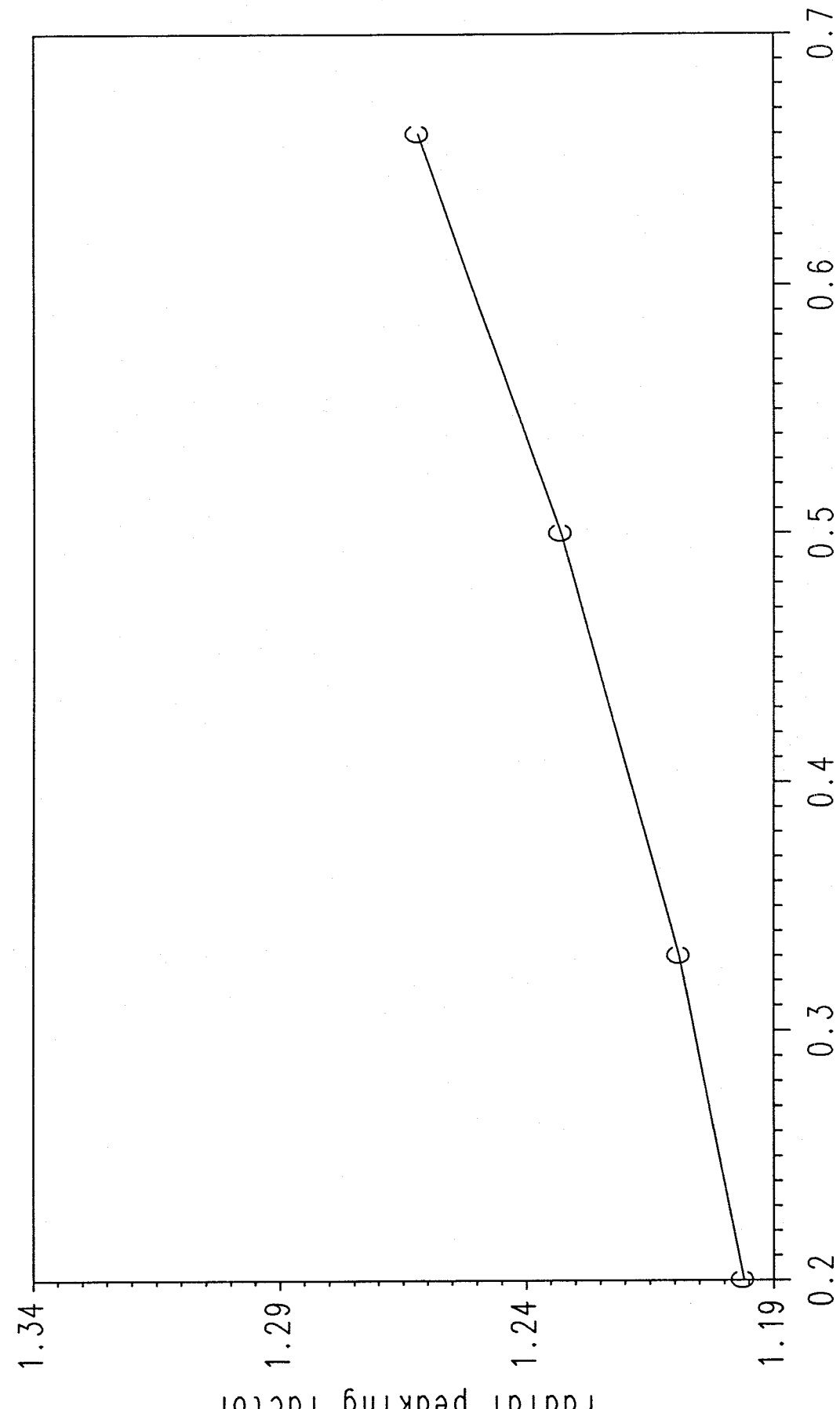

Fig. 5.4 D-bank withdrawal
static calculations

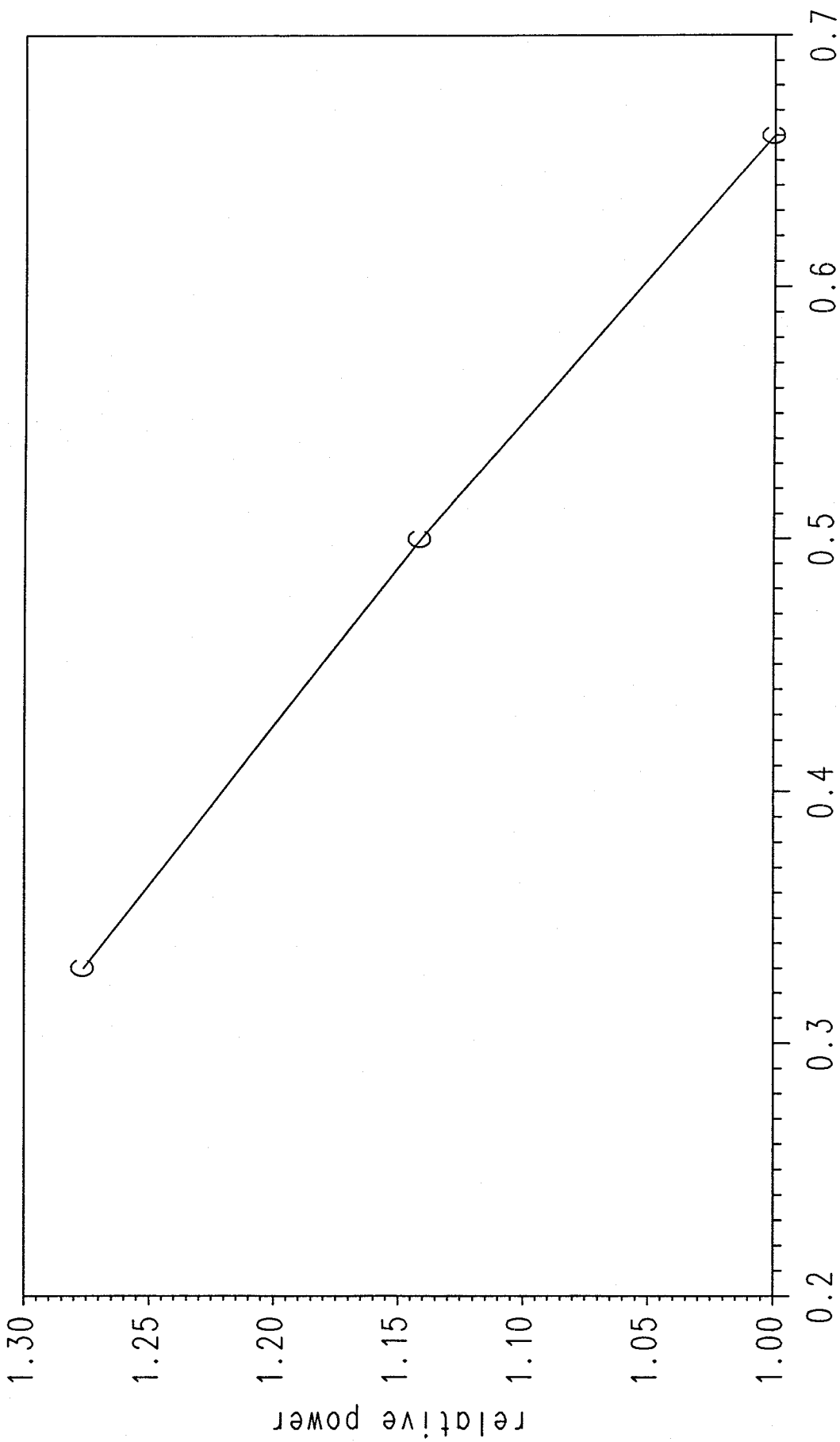

Fig. 5.5 C-bank withdrawal
static calculations

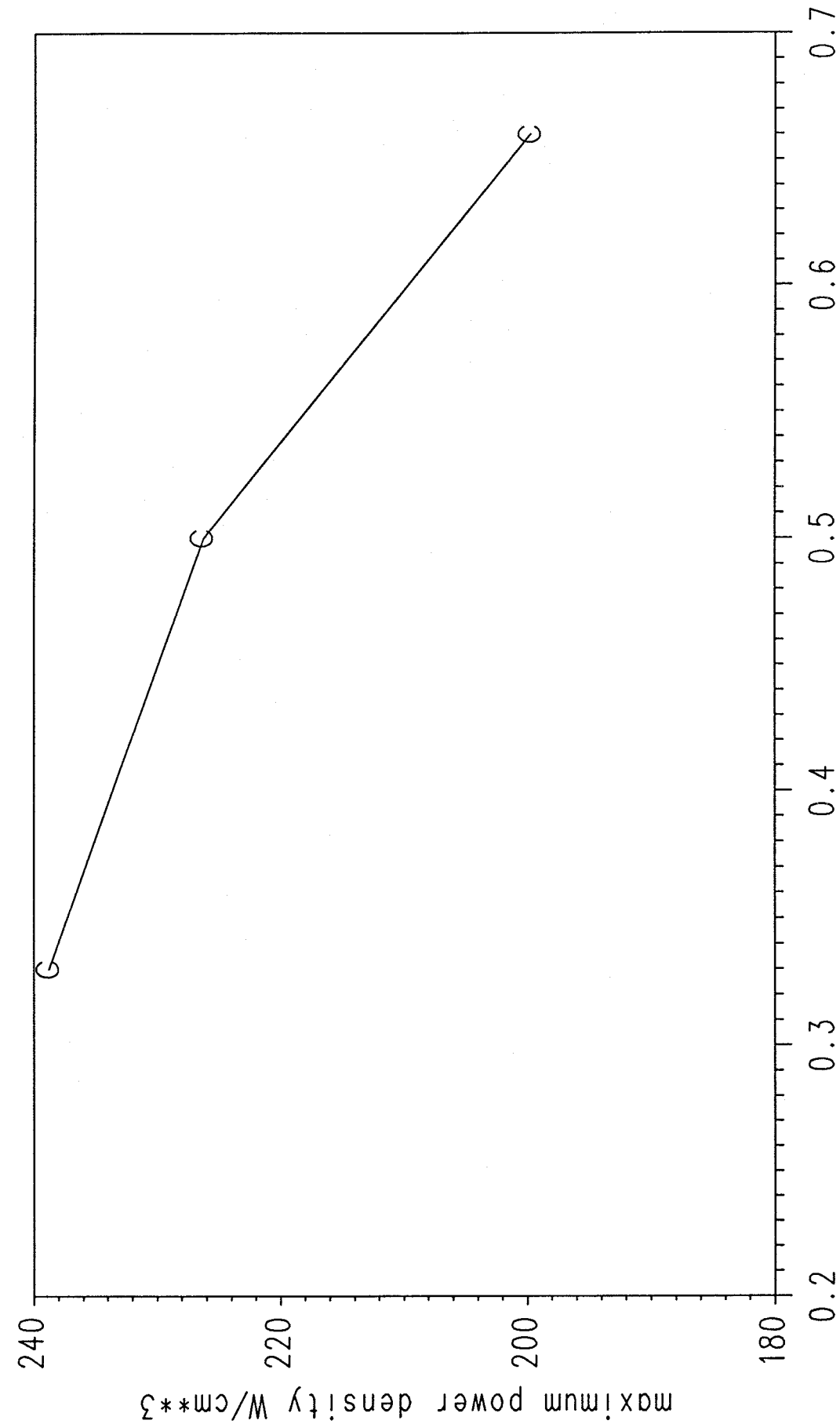

Fig. 5.6 C–bank withdrawal
static calculations

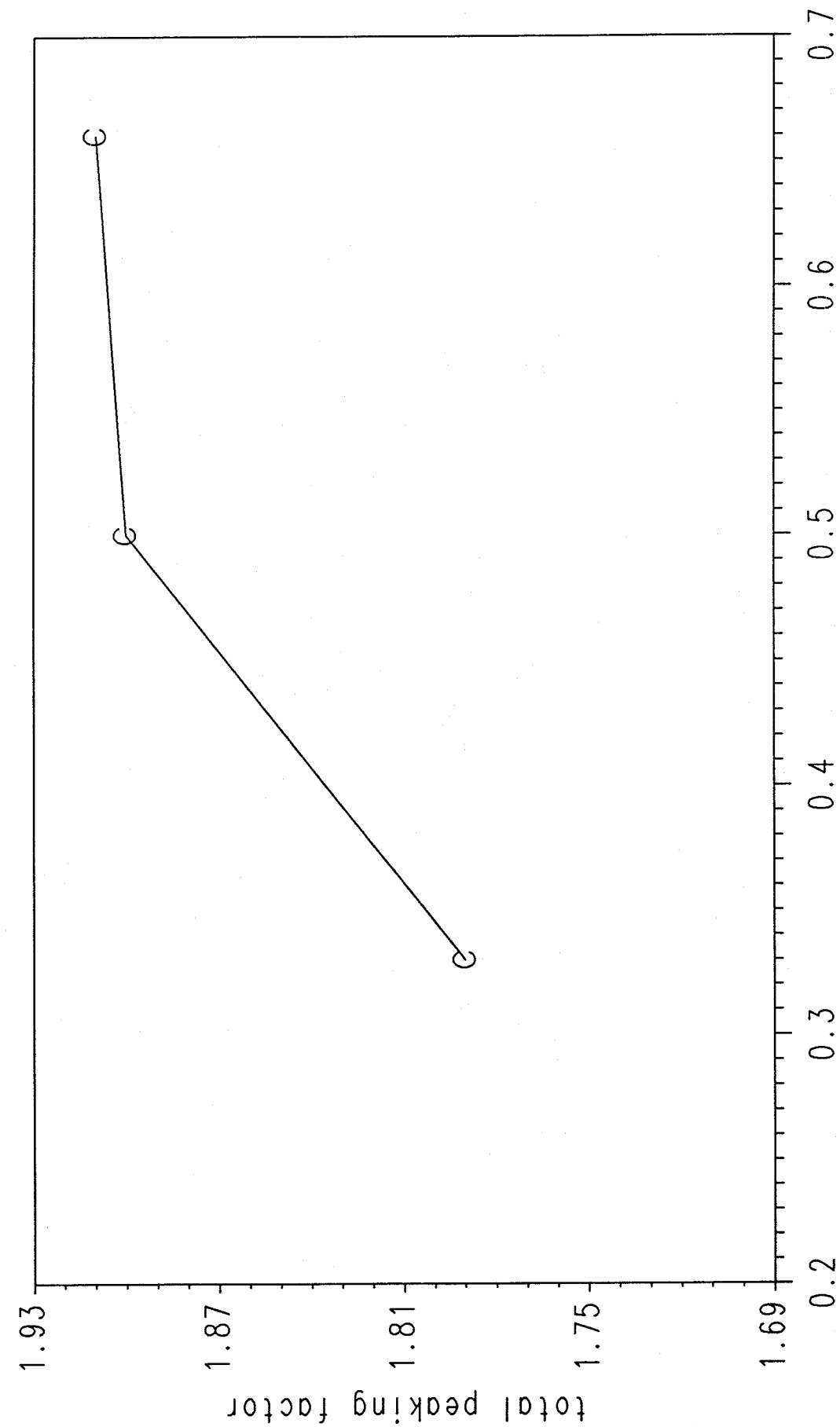

Fig. 5.7 C-bank withdrawal
static calculations

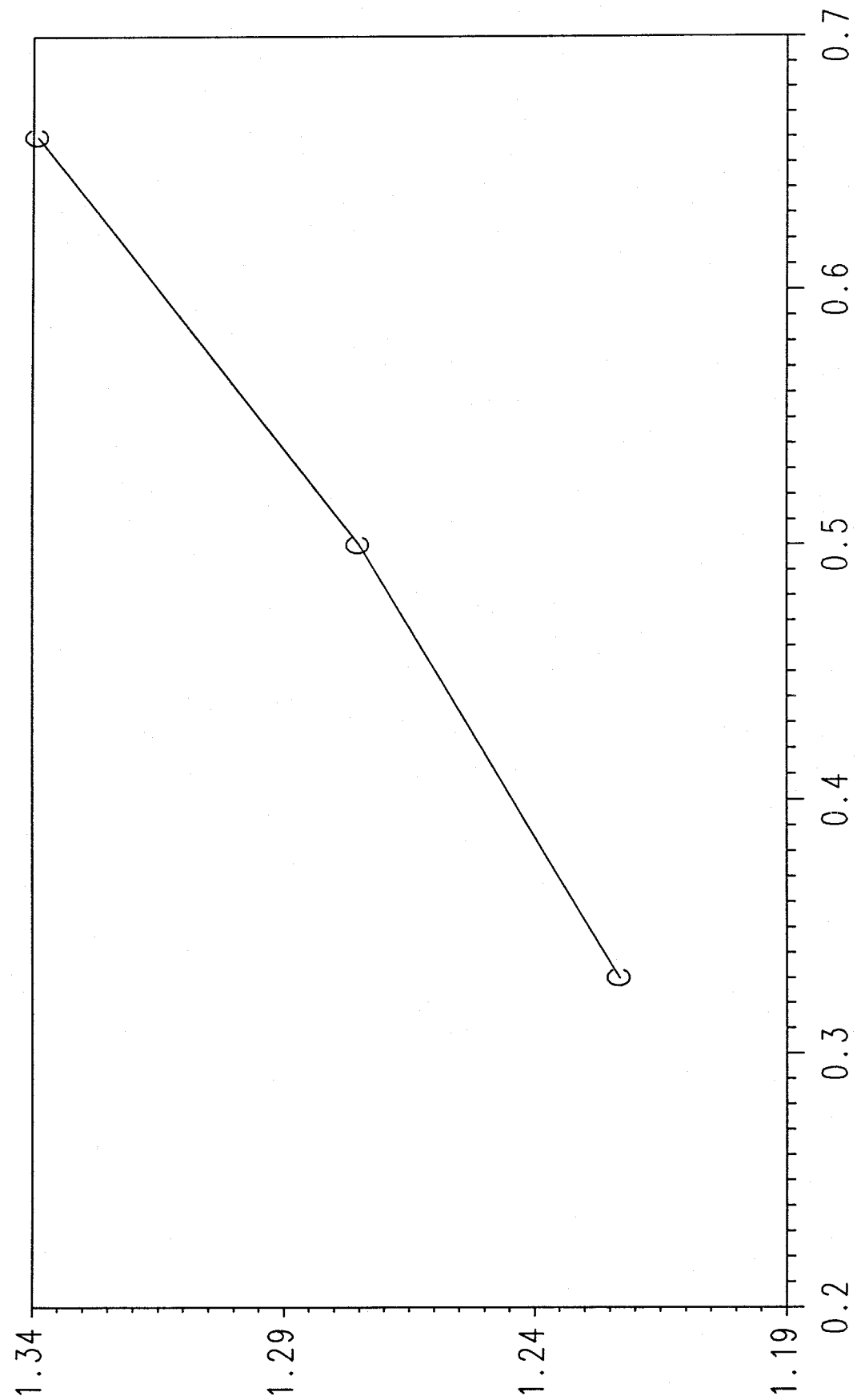

Fig. 5.8 C-bank withdrawal
static calculations

FIGURES

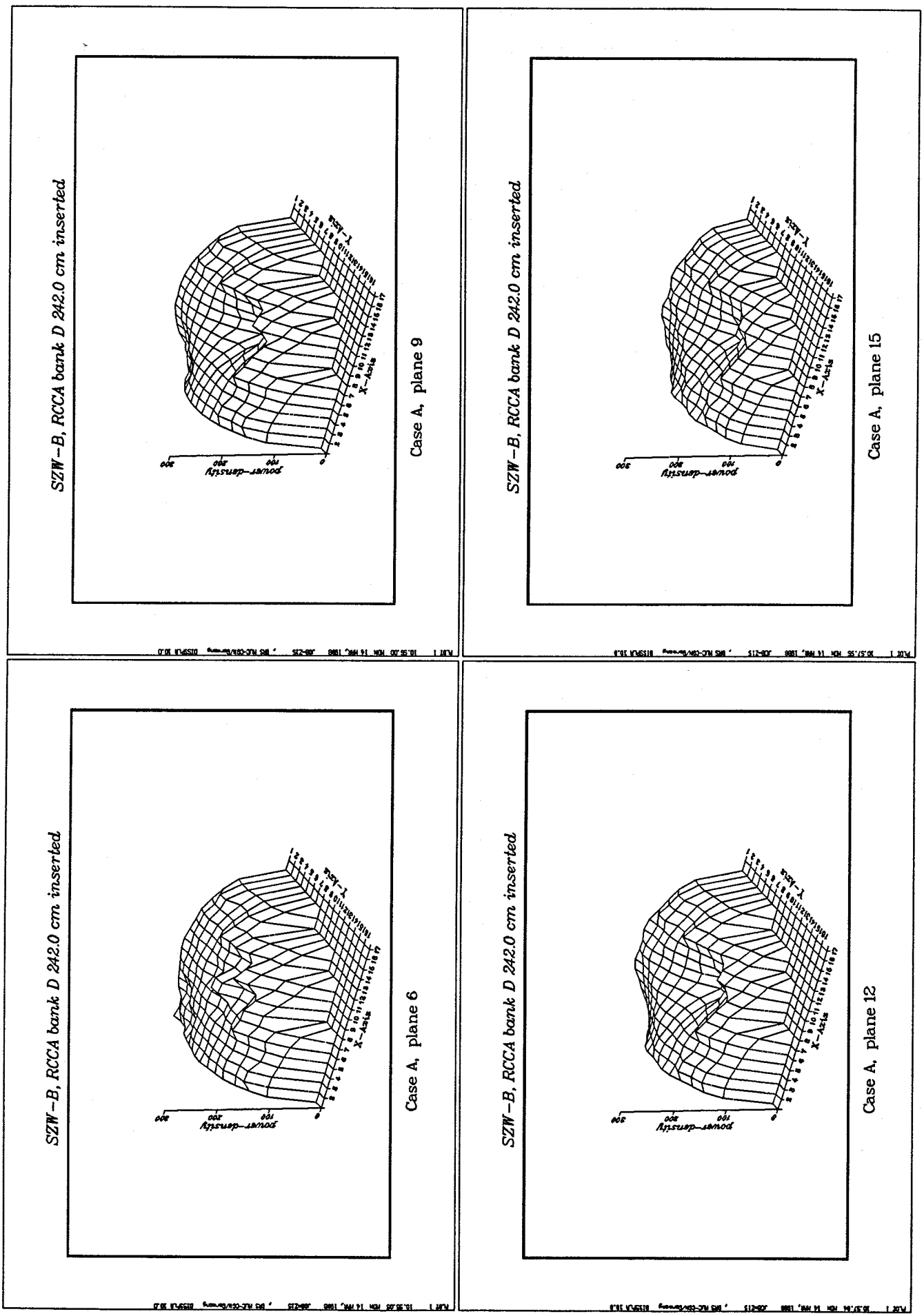

Fig. 5.9 Power density distribution for D-bank insertion

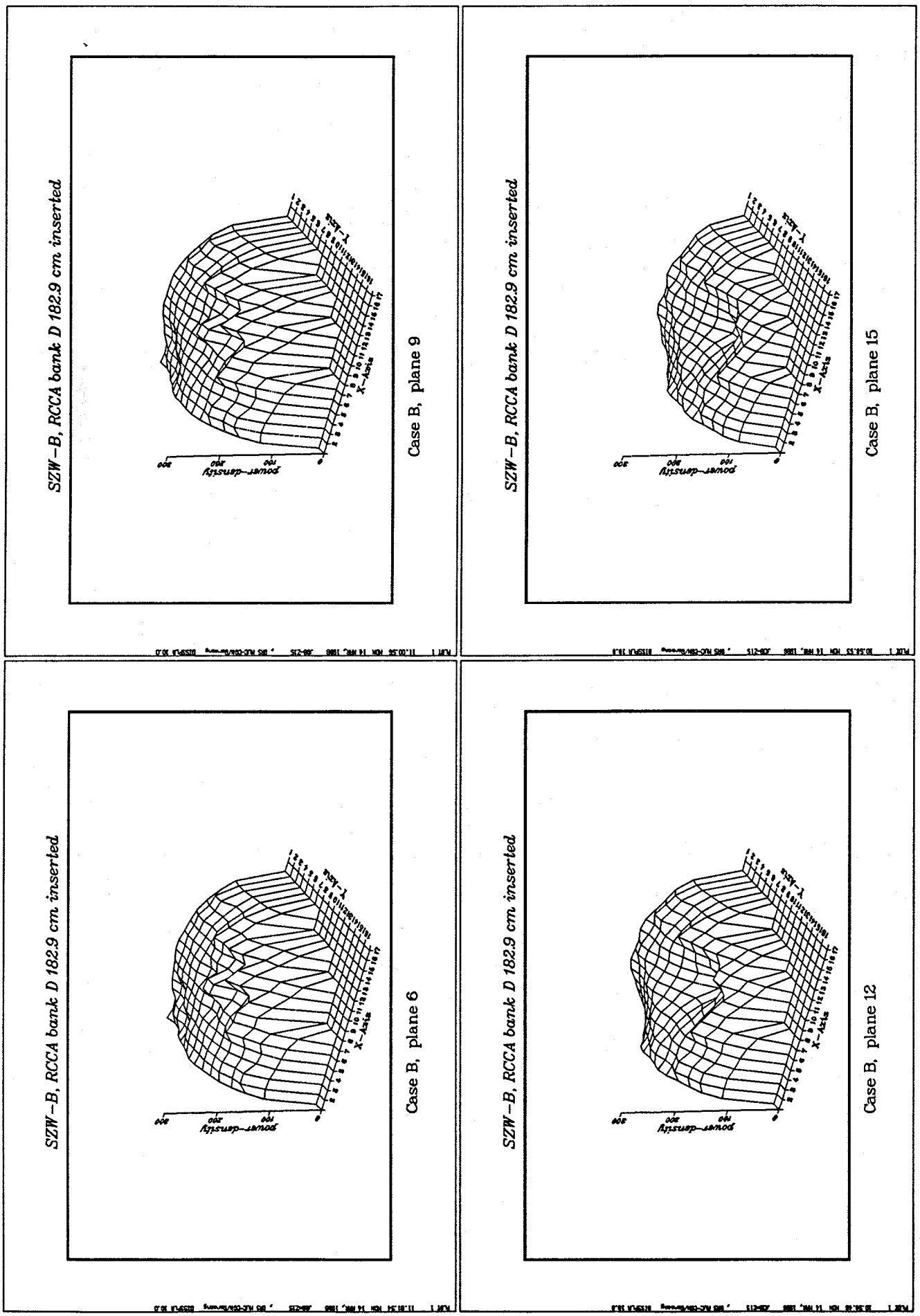

Fig. 5.10 Power density distribution for D-bank insertion

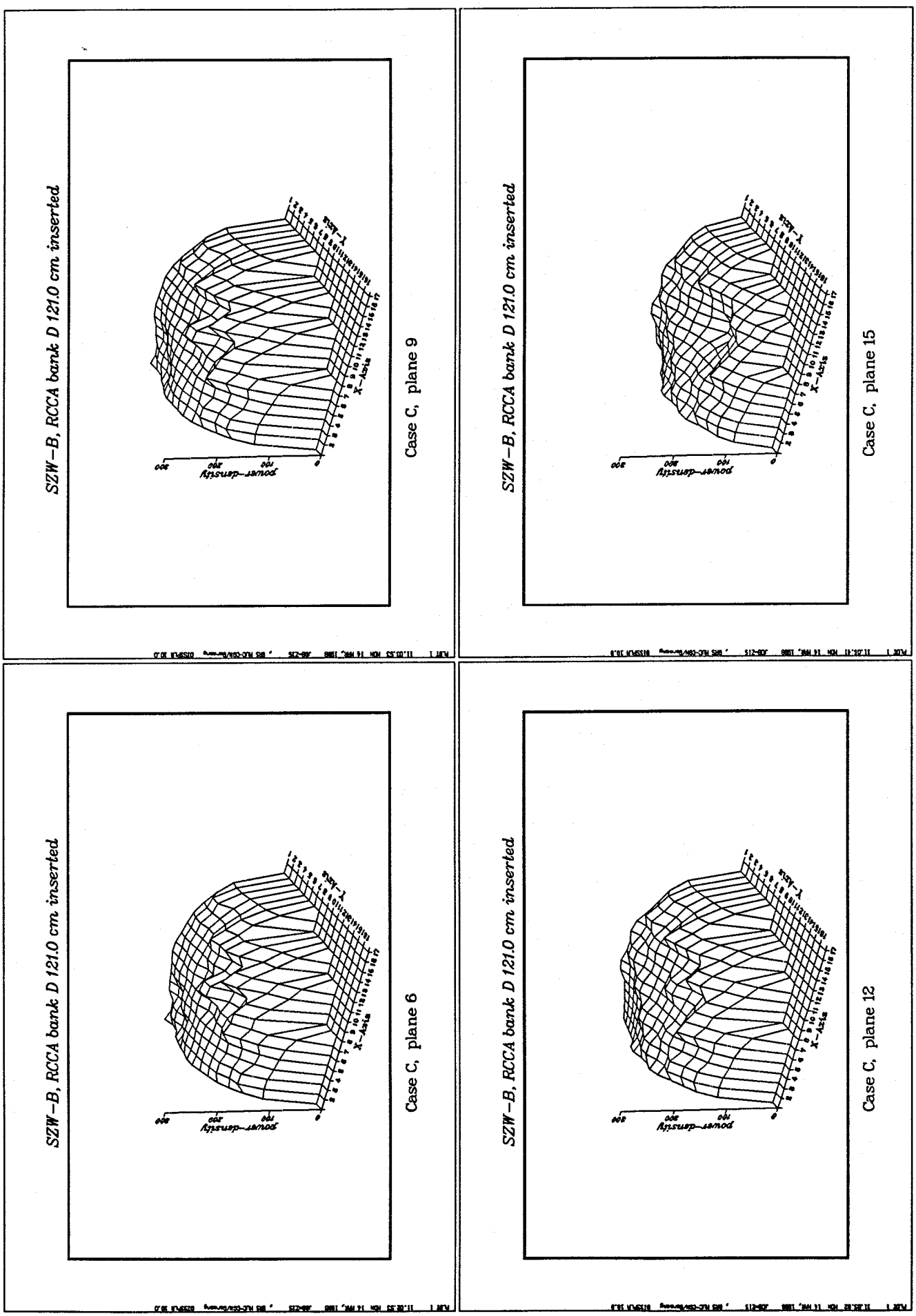

Fig. 5.11 Power density distribution for D-bank insertion

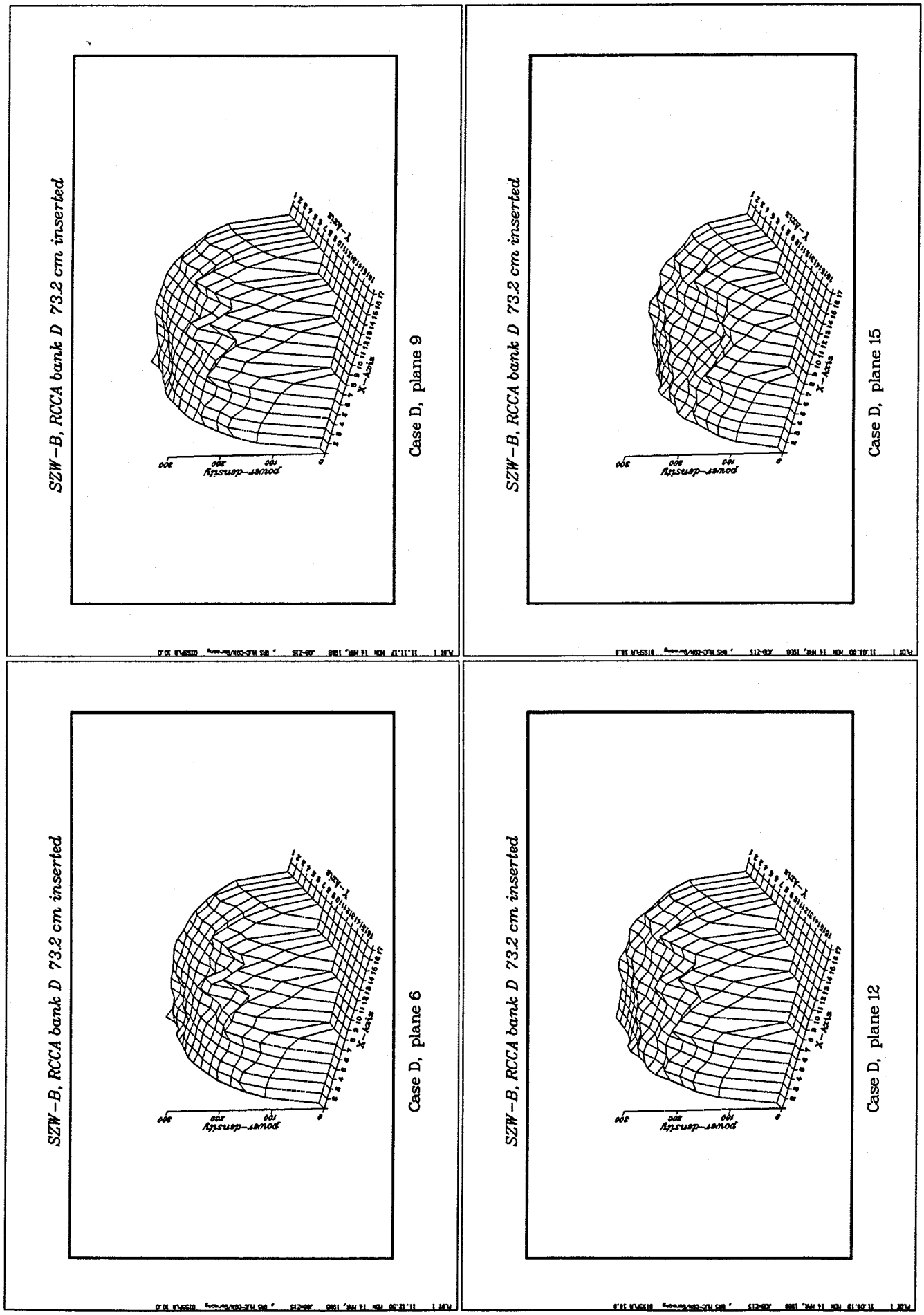

Fig. 5.12 Power density distribution for D-bank insertion

Z15MERGD FIG. 1 03/14/88 14:26:53

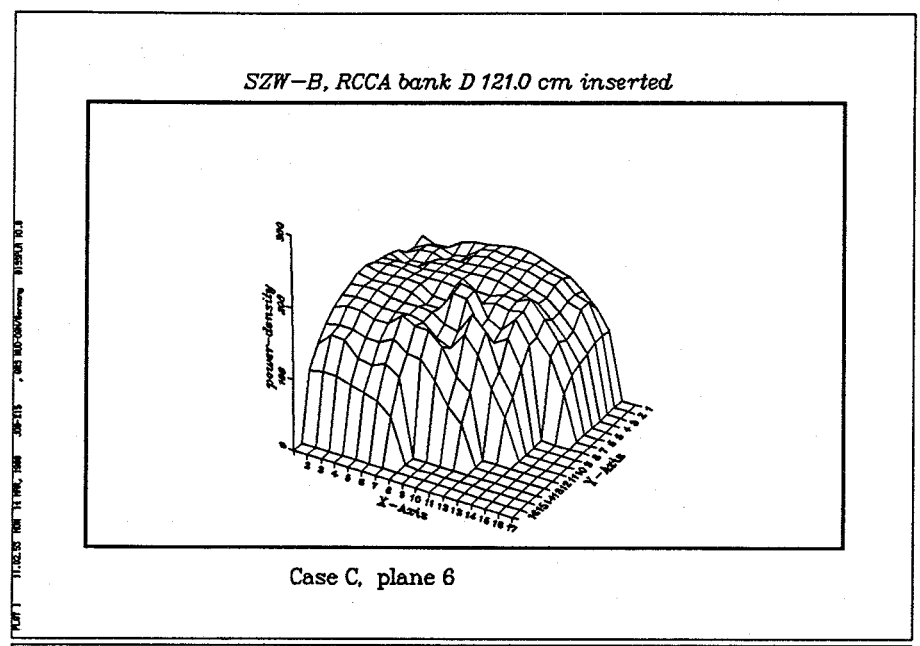

Case C, plane 6

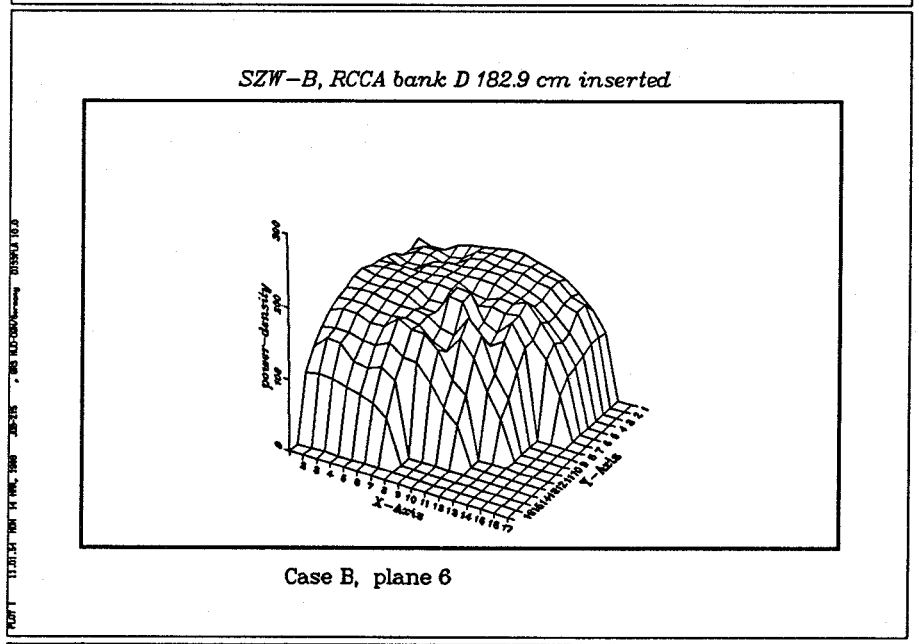

Case B, plane 6

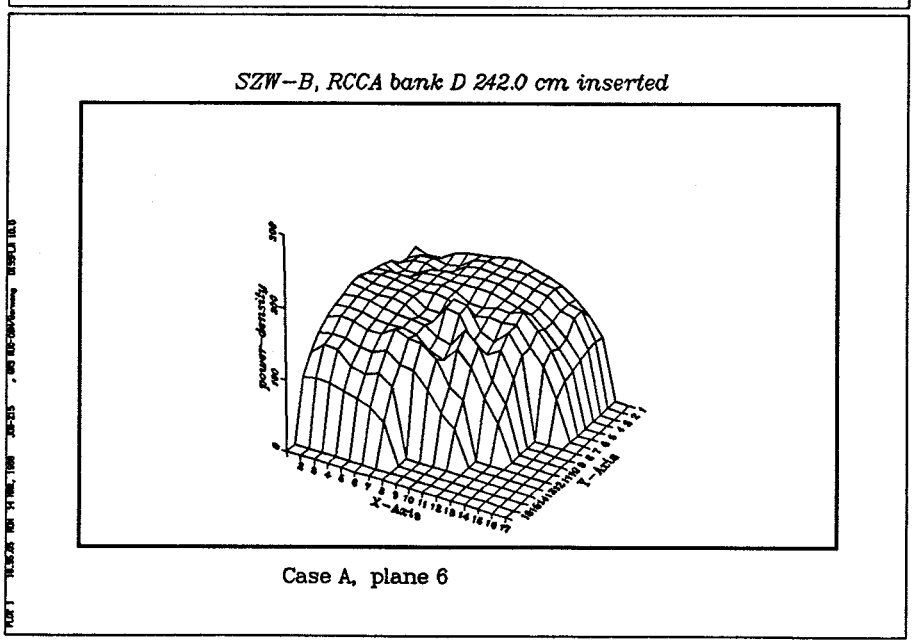

Case A, plane 6

Fig. 5.13 Power density distribution for D-bank insertion

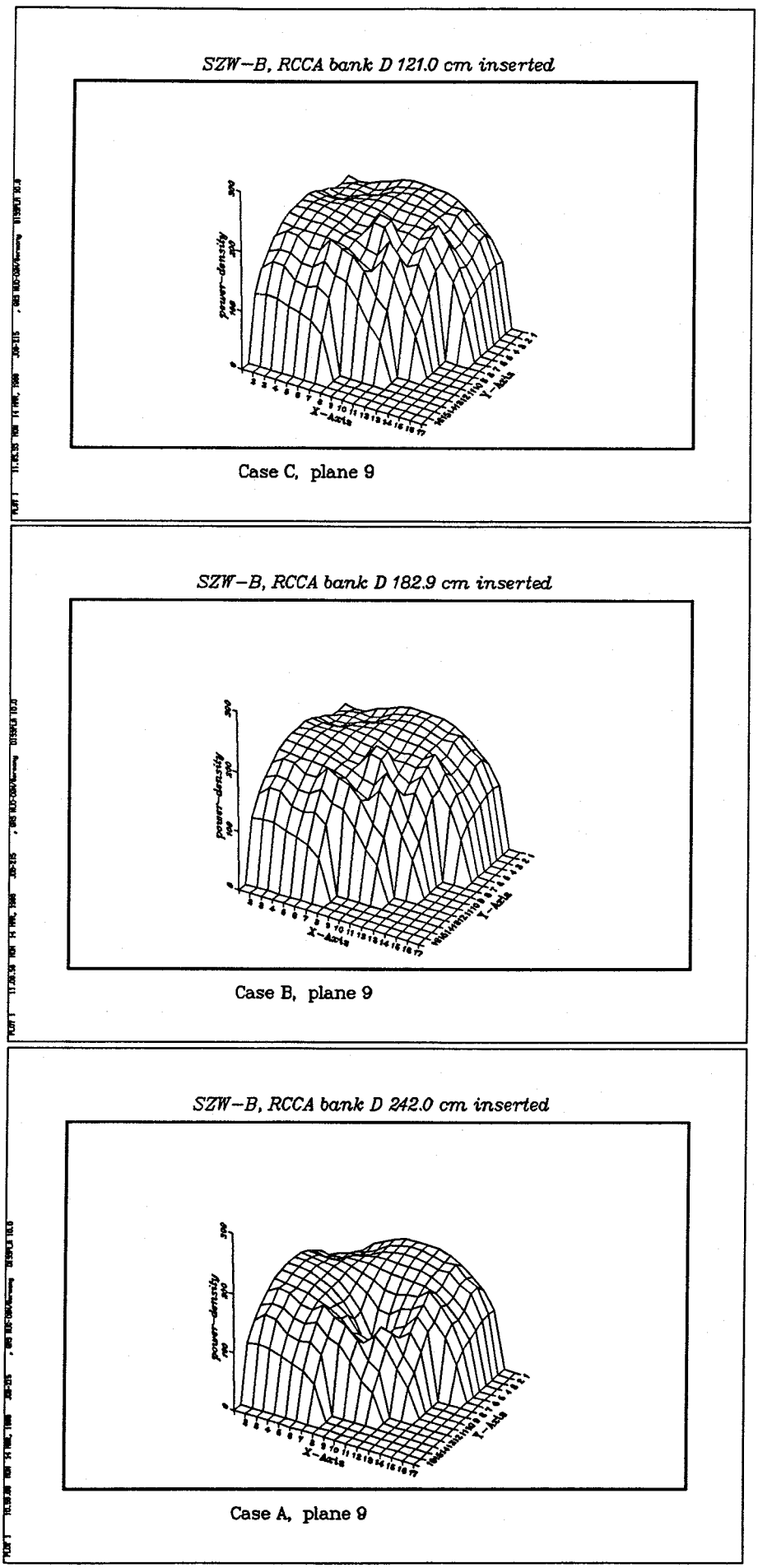

Fig. 5.14 Power density distribution for D-bank insertion

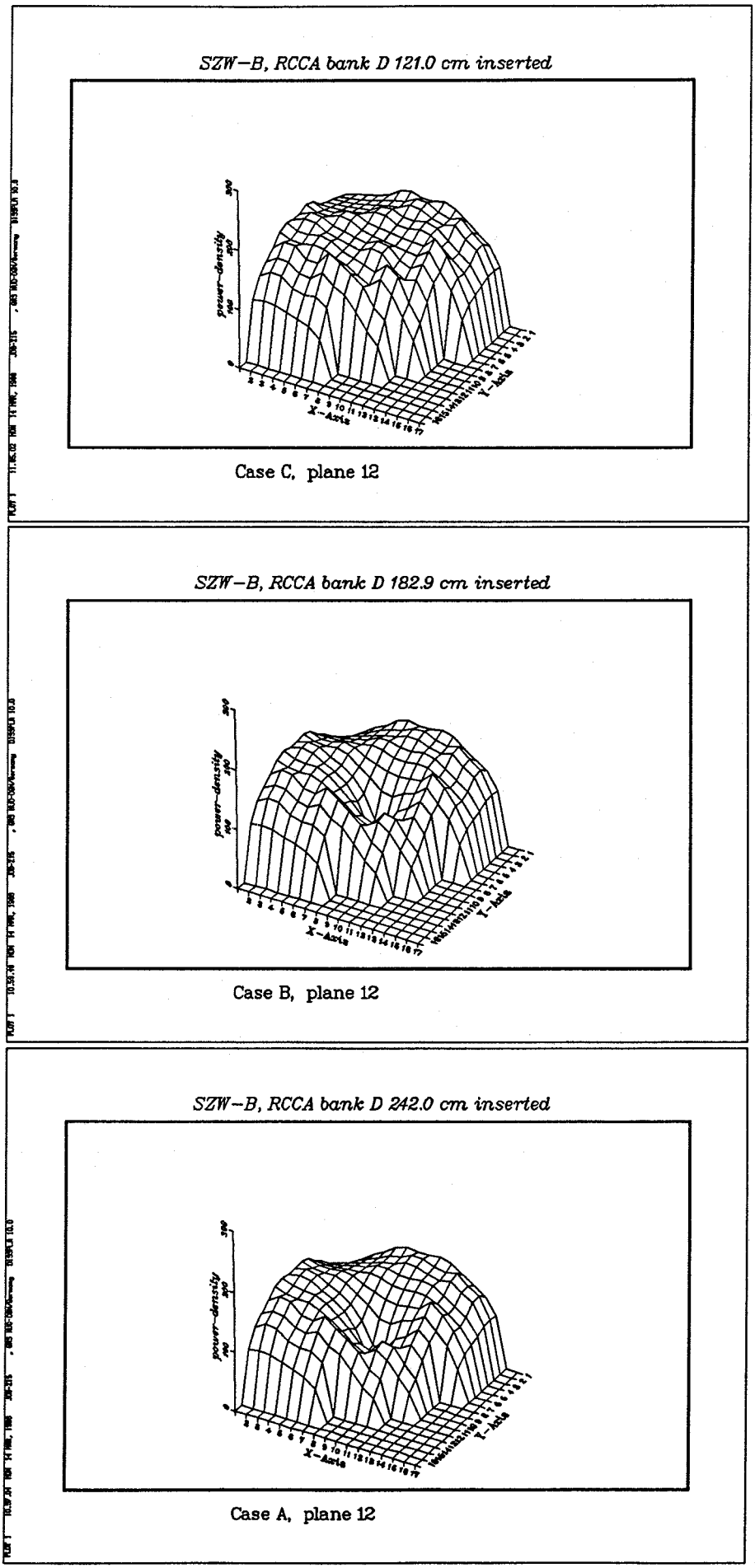

Fig. 5.15 Power density distribution for D-bank insertion

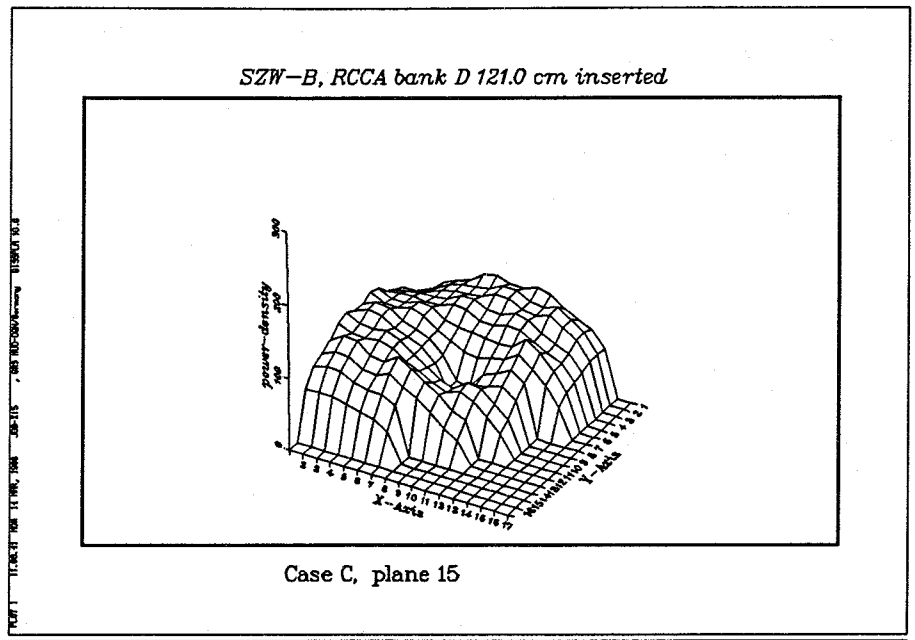

Case C, plane 15

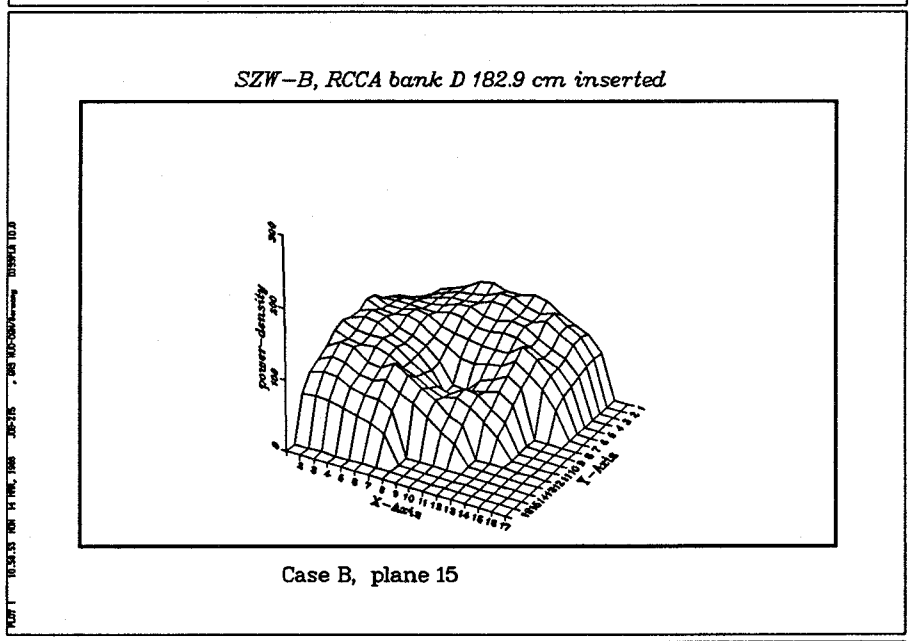

Case B, plane 15

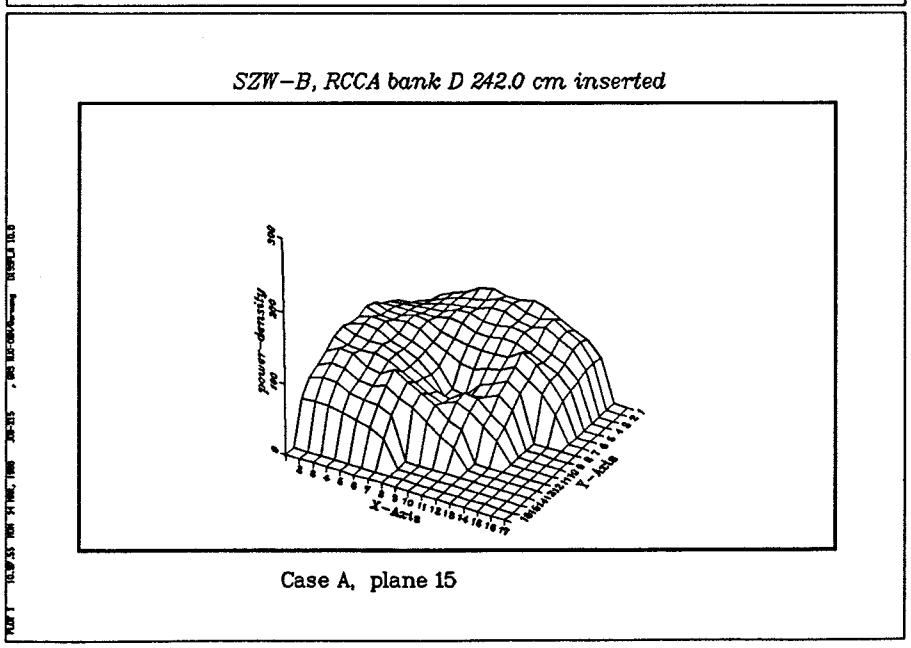

Case A, plane 15

Fig. 5.16 Power density distribition for D-bank insertion

FIGURES

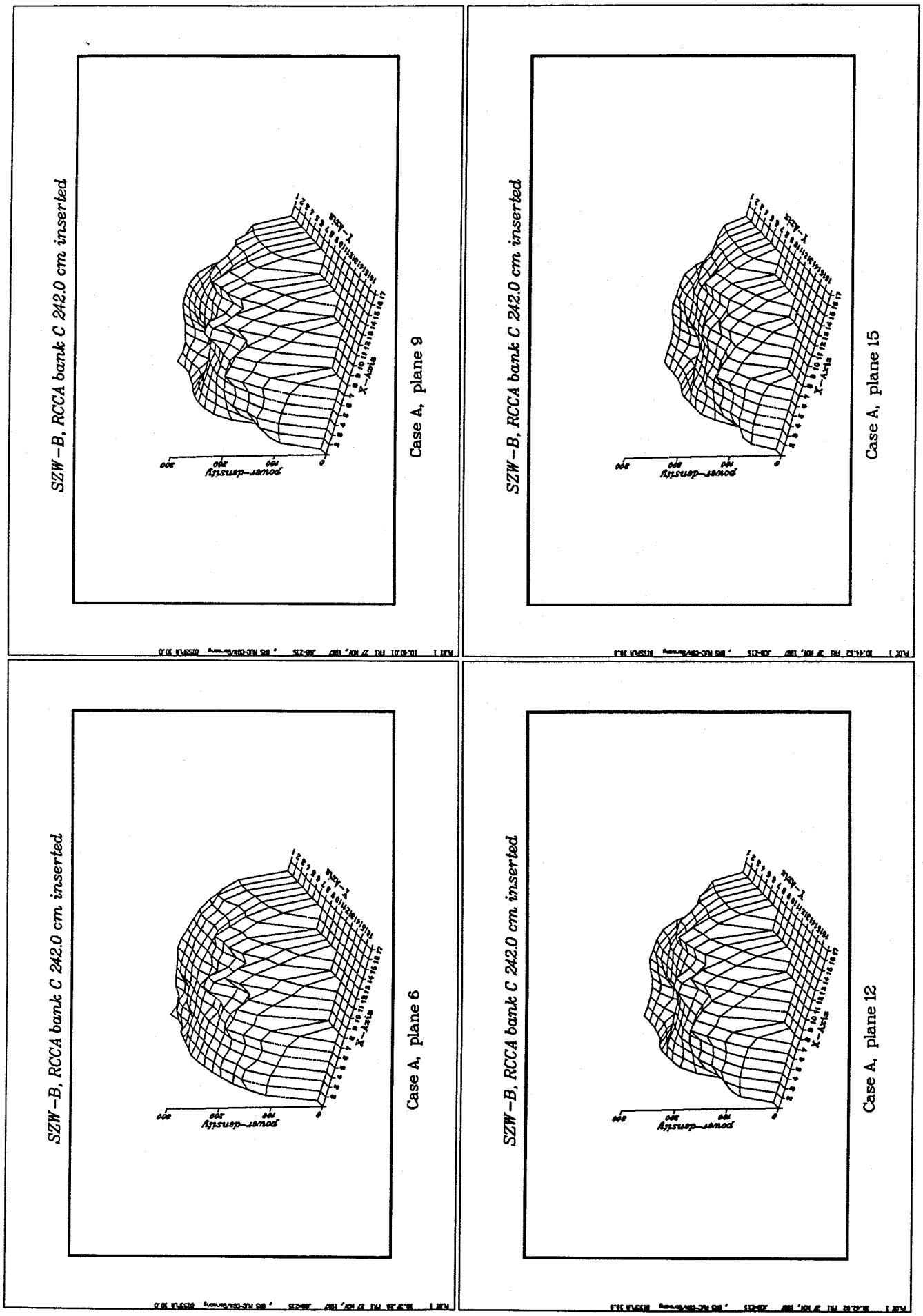

Fig. 5.17 Power density distribution for C-bank insertion

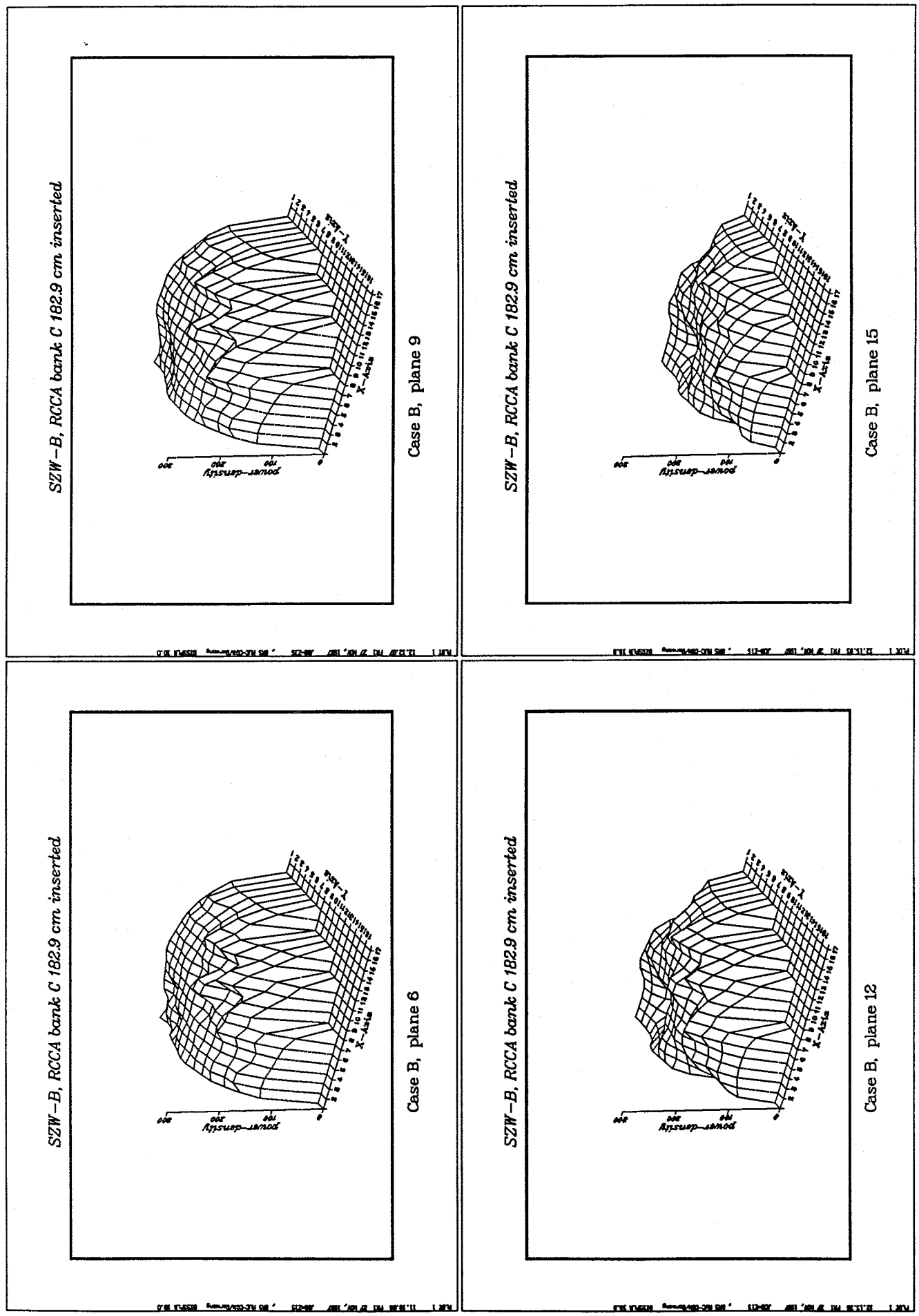

Fig. 5.18 Power density distribution for C-bank insertion

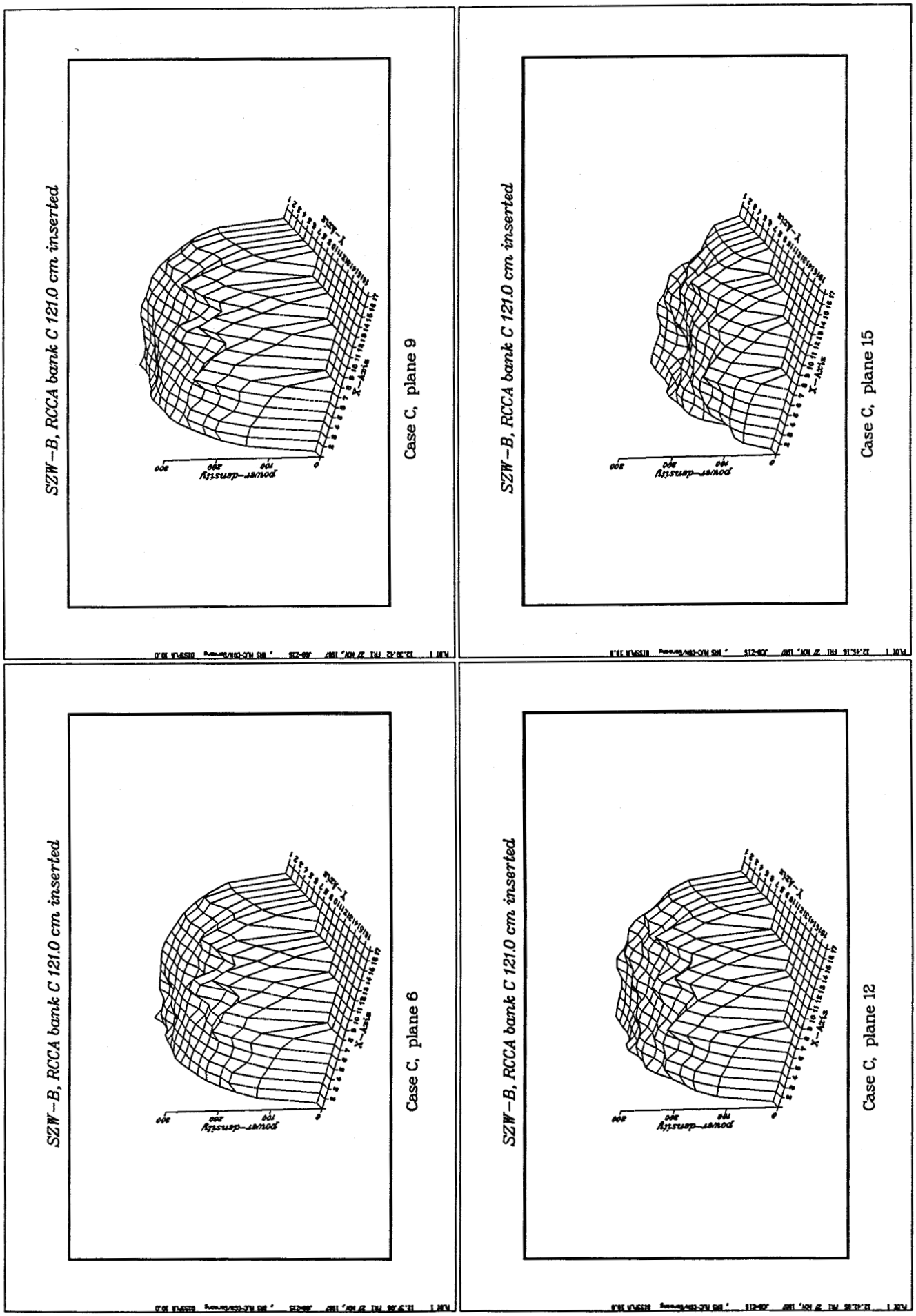

Fig. 5.19 Power density distribution for C-bank insertion

Z15MERCS FIG. 1 11/27/87 14:27:40

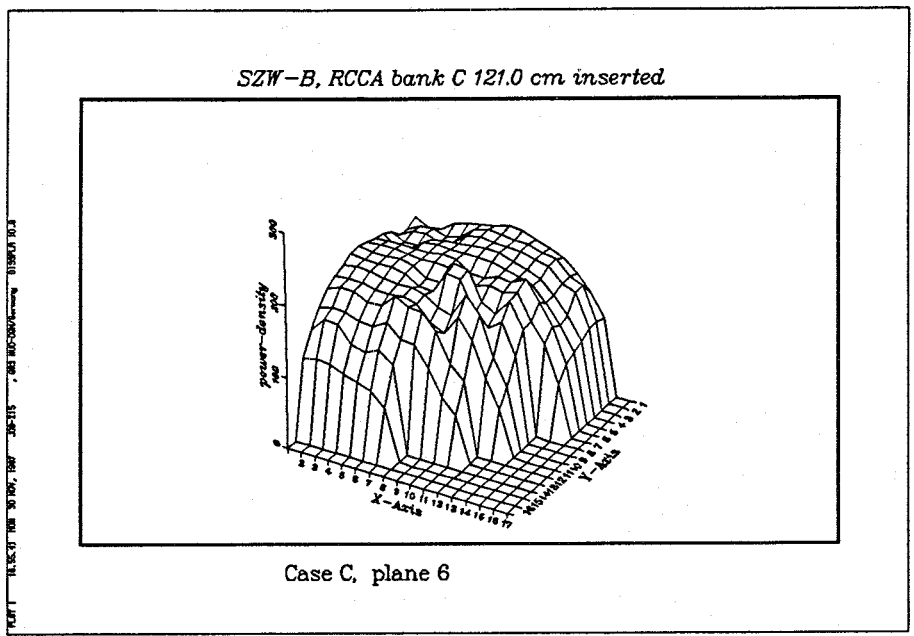

Case C, plane 6

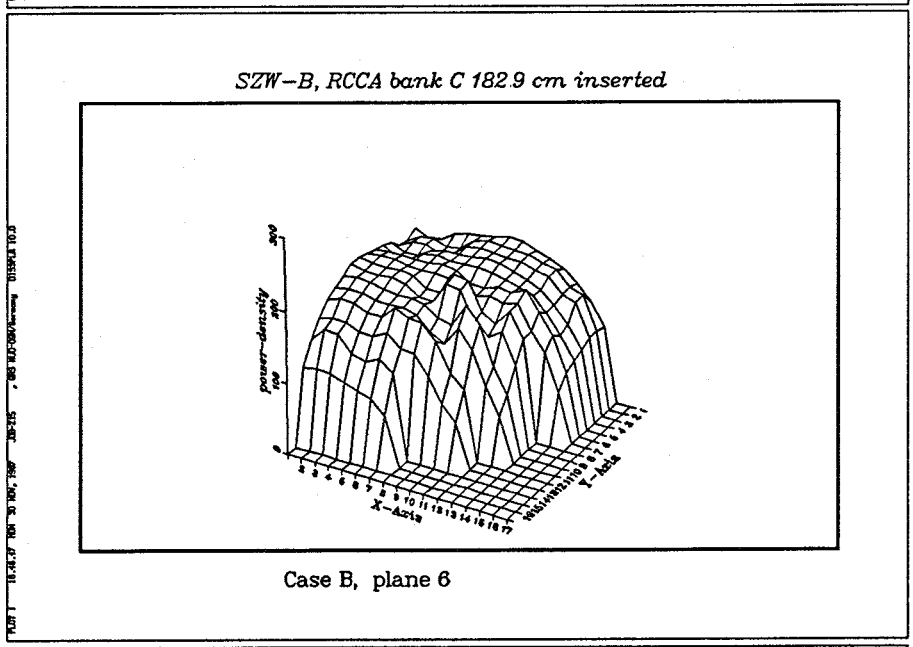

Case B, plane 6

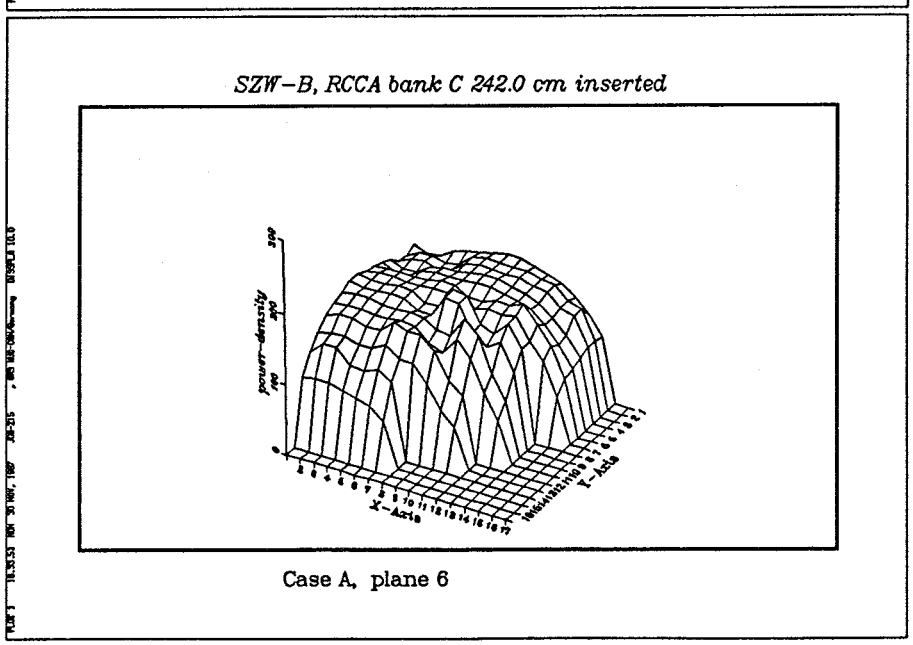

Case A, plane 6

Fig. 5.20 Power density distribution for C-bank insertion

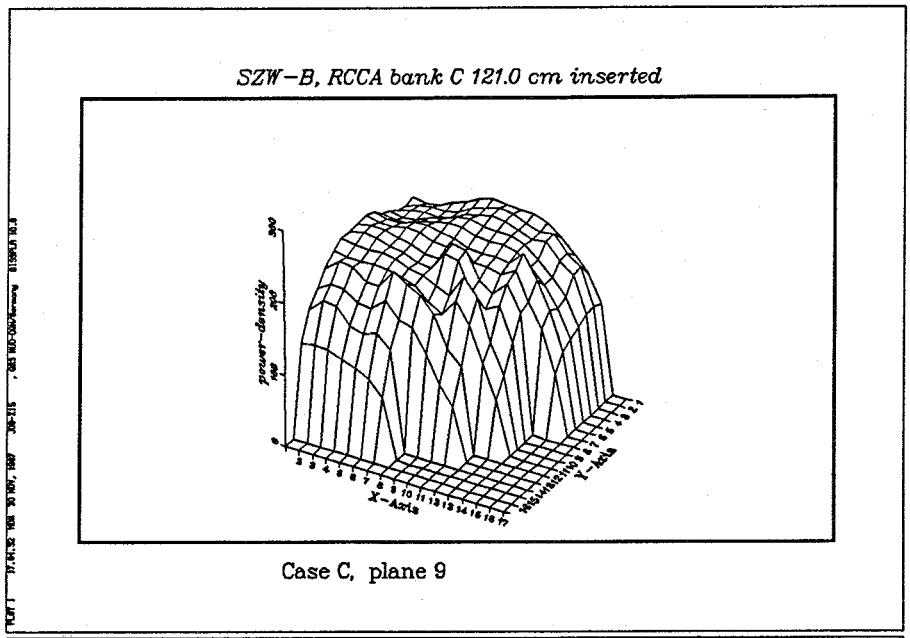

Case C, plane 9

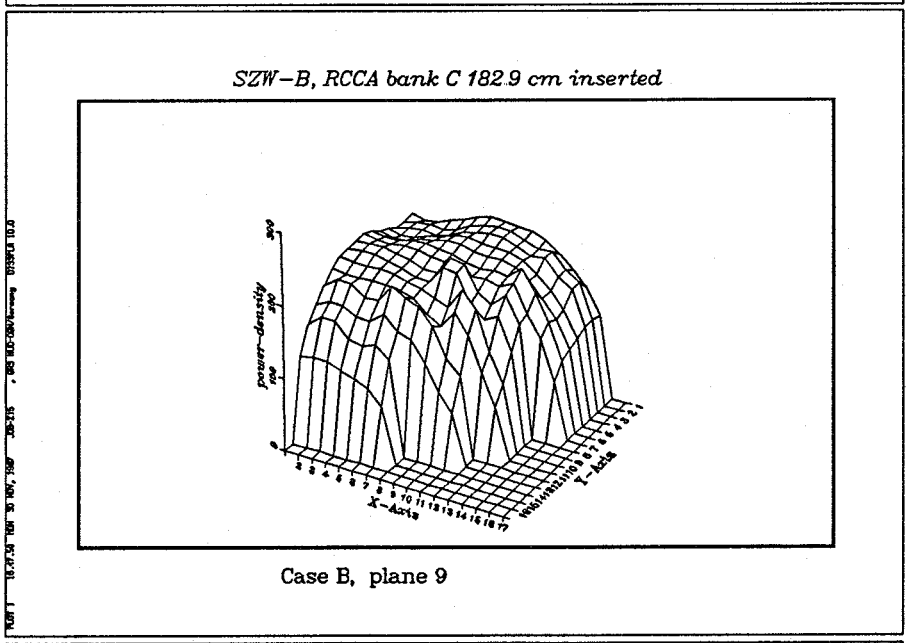

Case B, plane 9

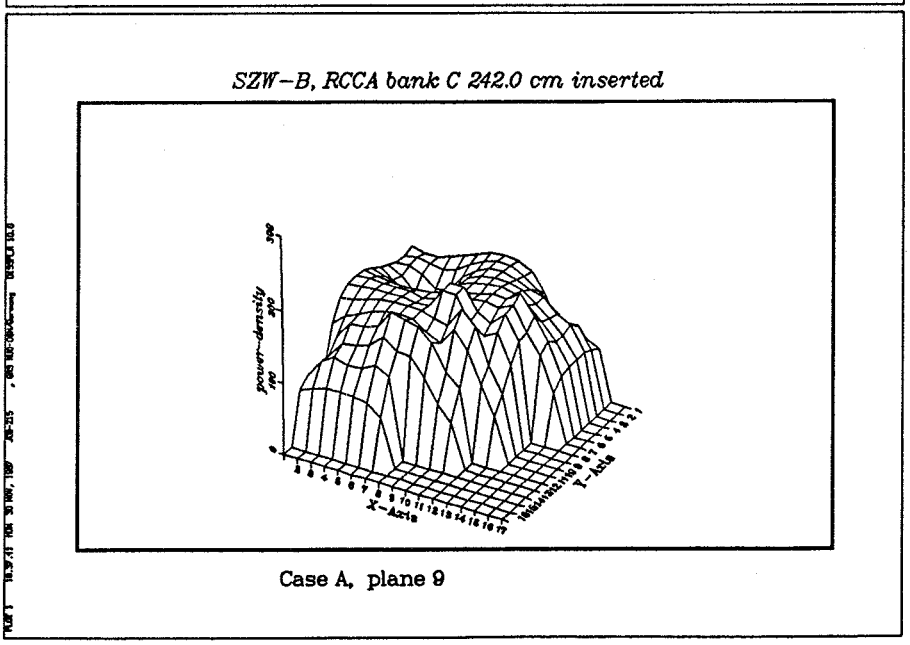

Case A, plane 9

Fig. 5.21 Power density distribution for C-bank insertion

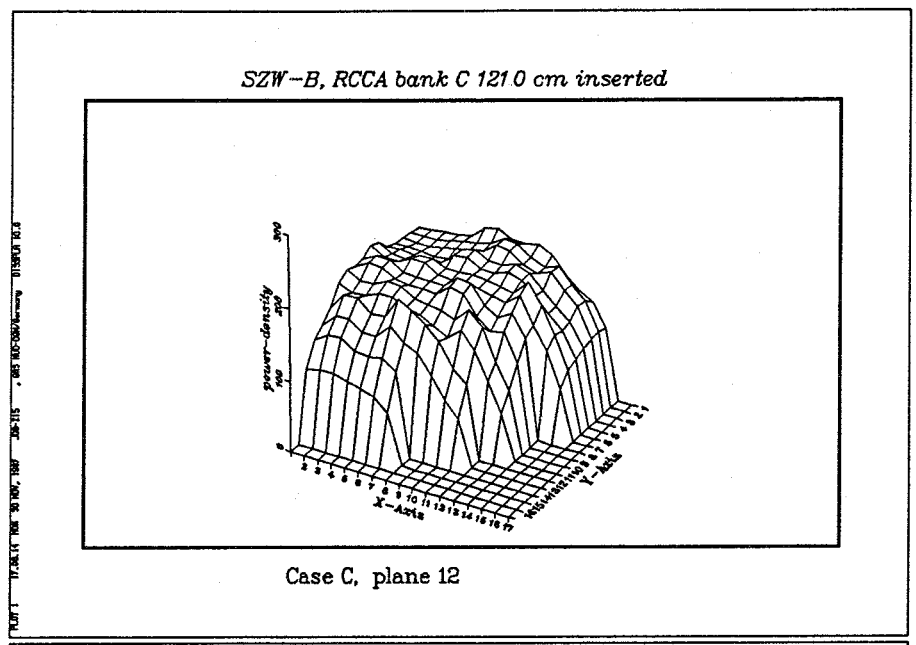

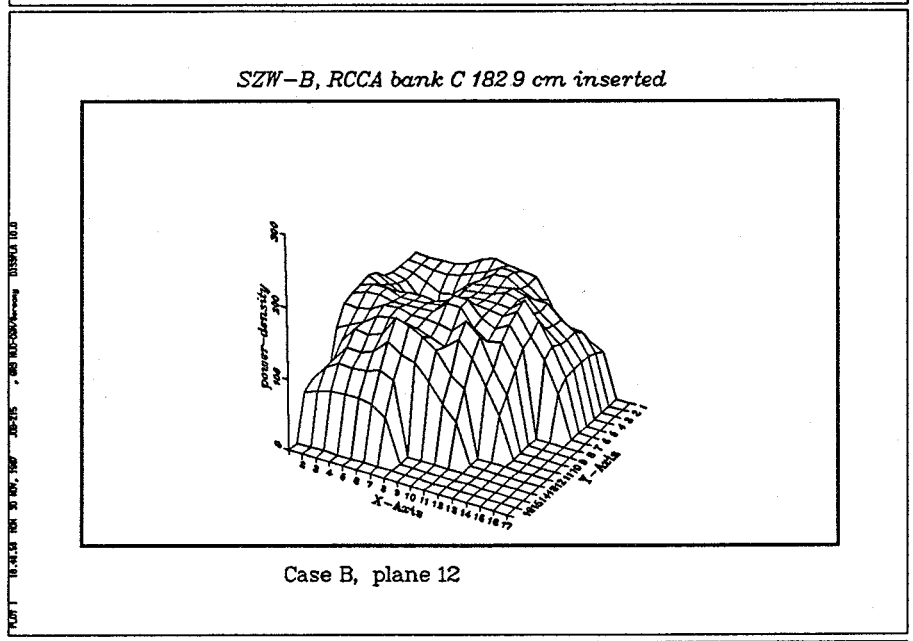

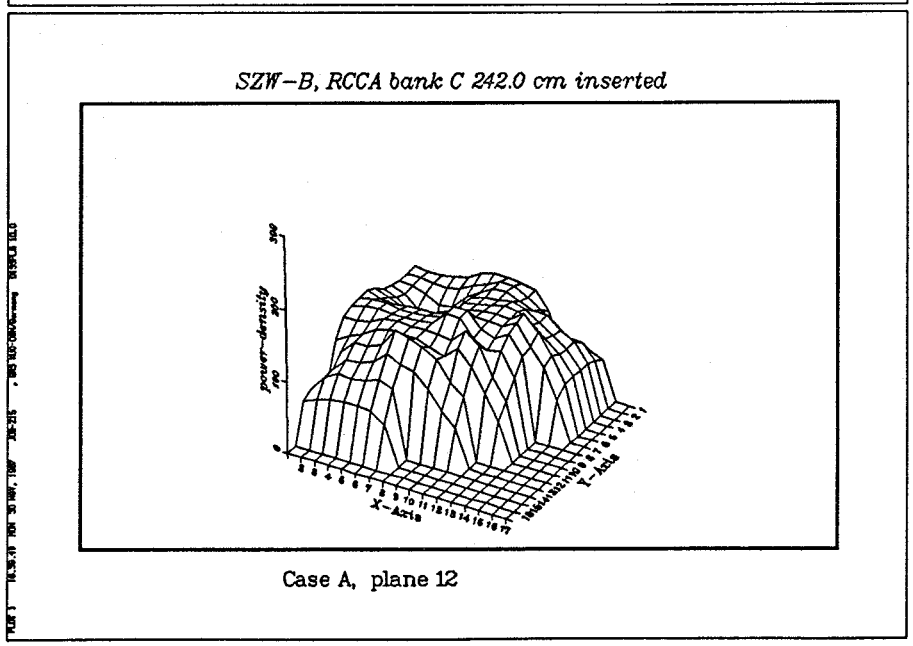

Fig. 5.22 Power density distribution for C-bank insertion

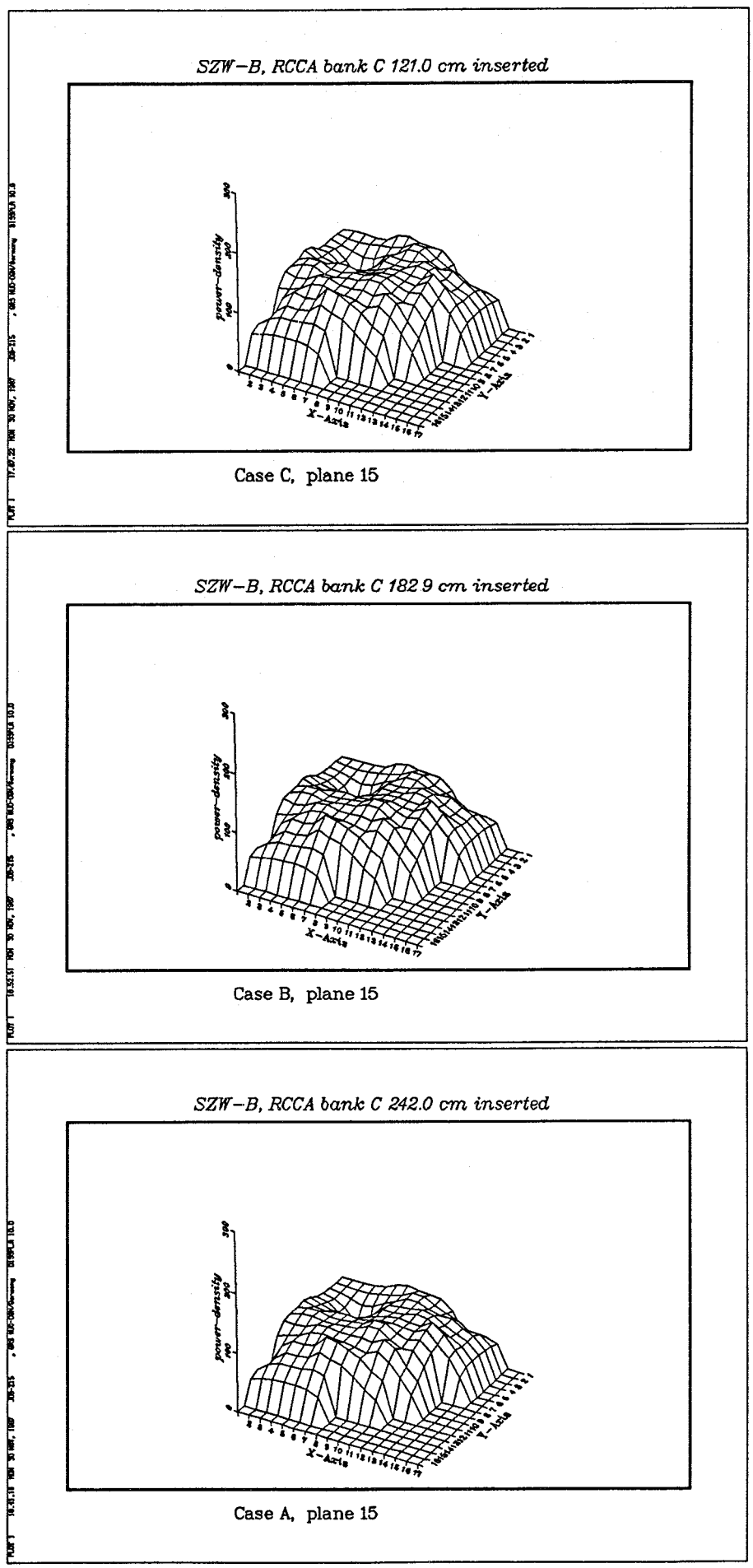

Fig. 5.23 Power density distribution for C-bank insertion

FIGURES

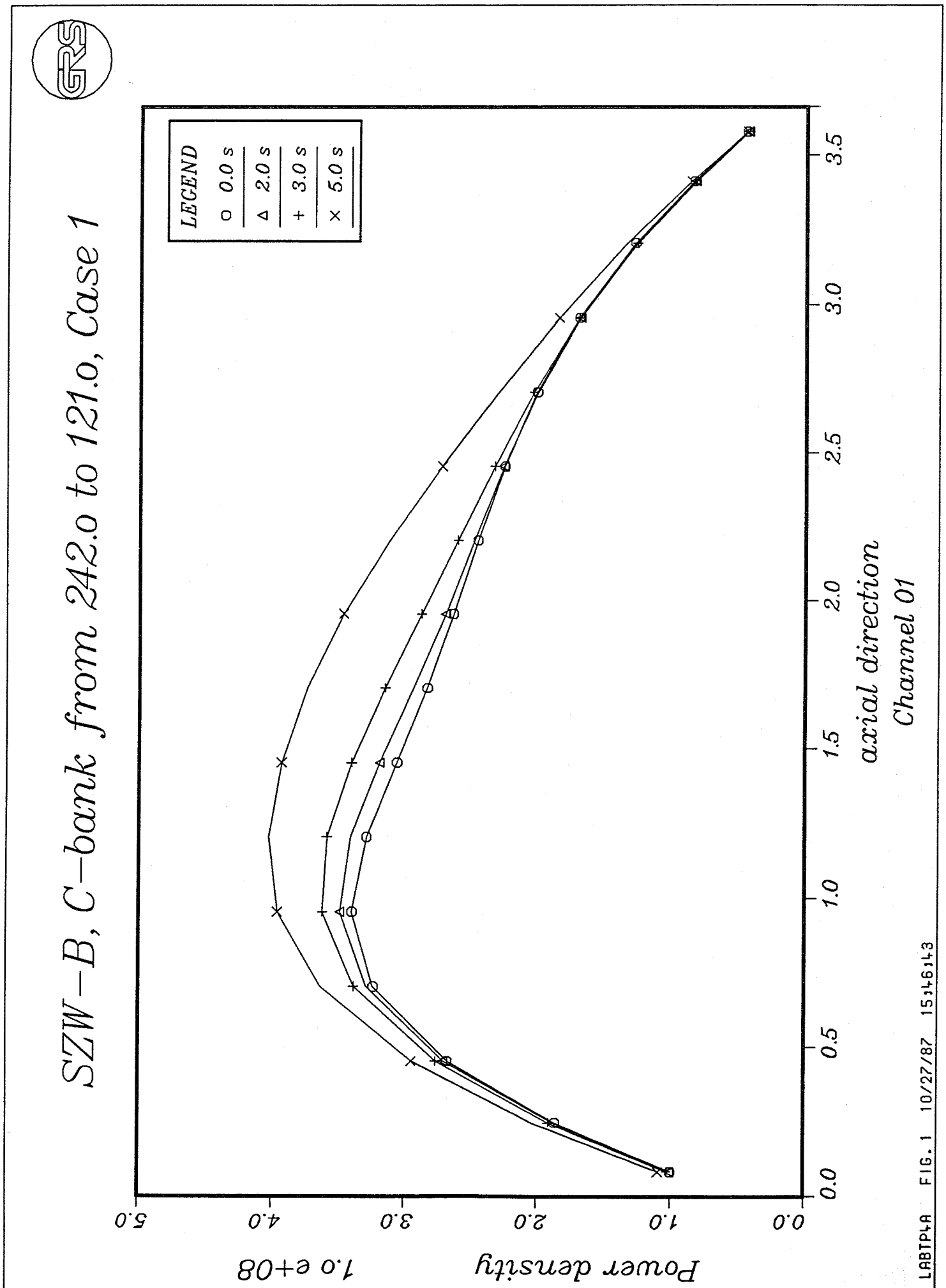
SZW-B, C-bank from 242.0 to 121.0, Case 1
LEGEND
o 0.0 s
Δ 2.0 s
+ 3.0 s
× 5.0 s
Power density
1.0 e+08
0.0
1.0
2.0
3.0
4.0
5.0
axial direction
Channel 01
0.0
0.5
1.0
1.5
2.0
2.5
3.0
3.5
LABTPLA FIG. 1 10/27/87 15:46:43

Fig. 5.24

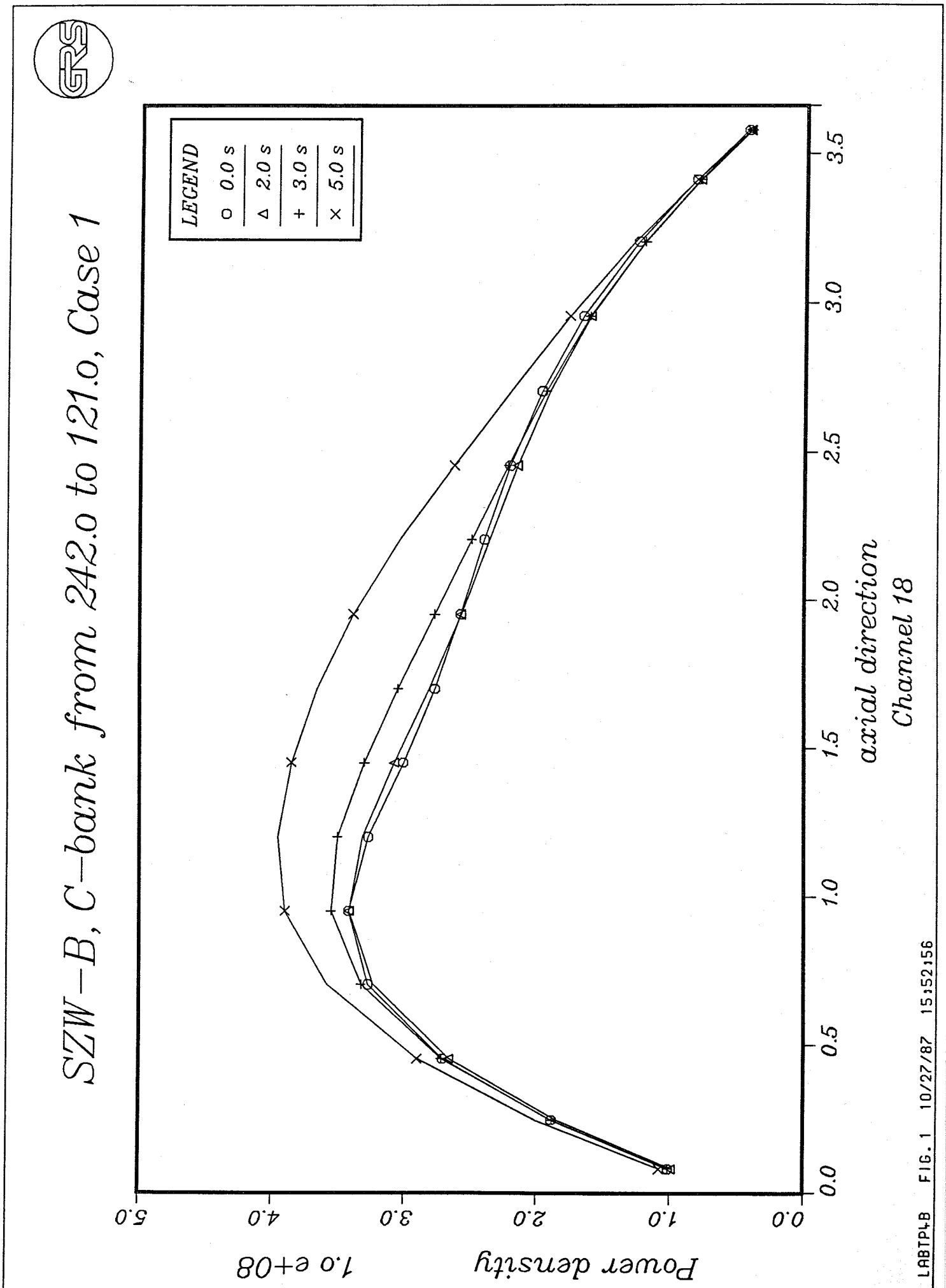
SZW-B, C-bank from 242.0 to 121.0, Case 1
LEGEND
o 0.0 s
Δ 2.0 s
+ 3.0 s
× 5.0 s
Power density
1.0 e+08
0.0
1.0
2.0
3.0
4.0
5.0
axial direction
Channel 18
0.0
0.5
1.0
1.5
2.0
2.5
3.0
3.5
LABTPLB FIG. 1 10/27/87 15:52:56

Fig. 5.25

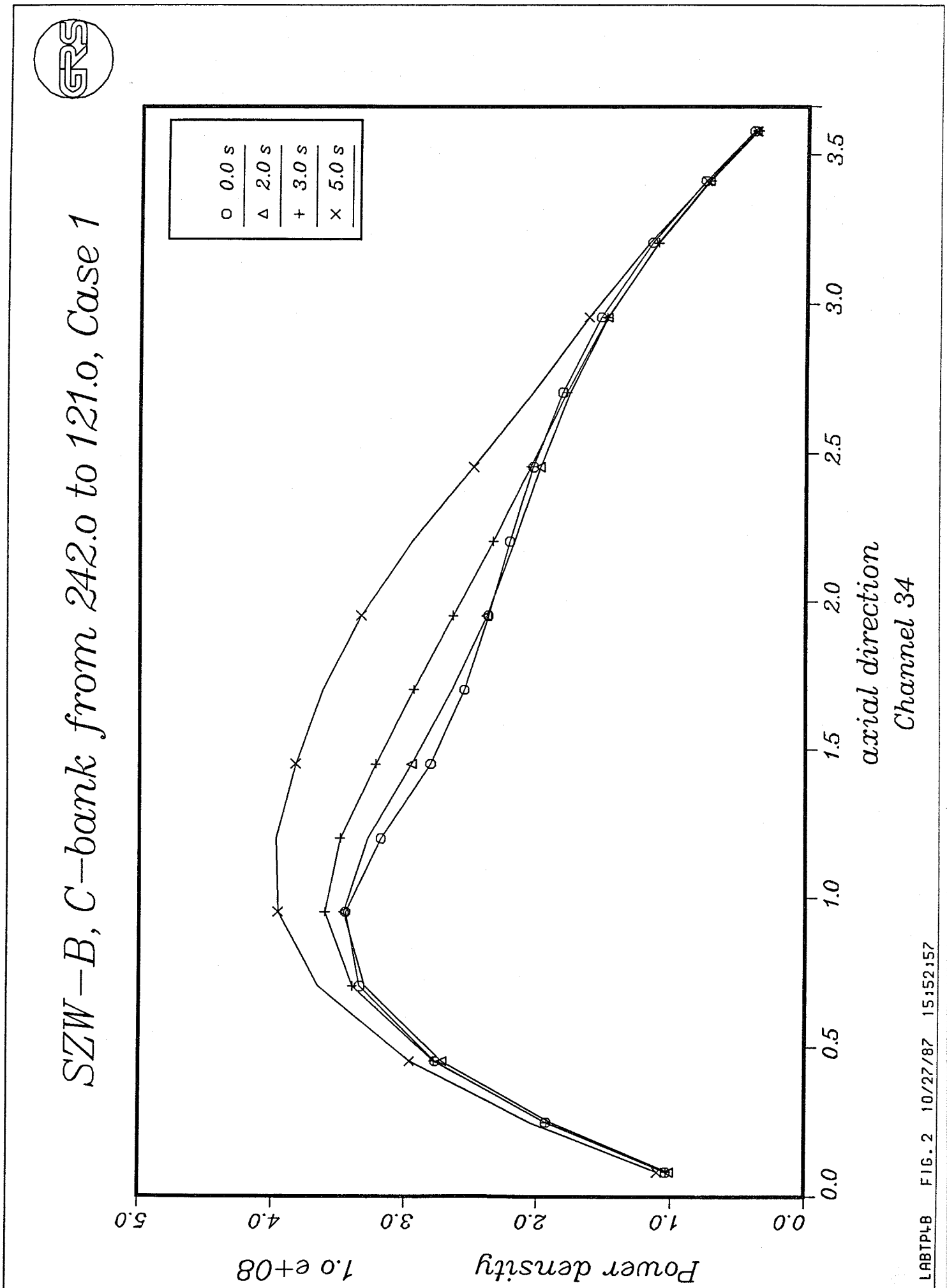
SZW-B, C-bank from 242.0 to 121.0, Case 1
o 0.0 s
Δ 2.0 s
+ 3.0 s
× 5.0 s
Power density
1.0 e+08
0.0
1.0
2.0
3.0
4.0
5.0
0.0
0.5
1.0
1.5
2.0
2.5
3.0
3.5
axial direction
Channel 34
LABTPL4B FIG. 2 10/27/87 15:52:57

Fig. 5.26

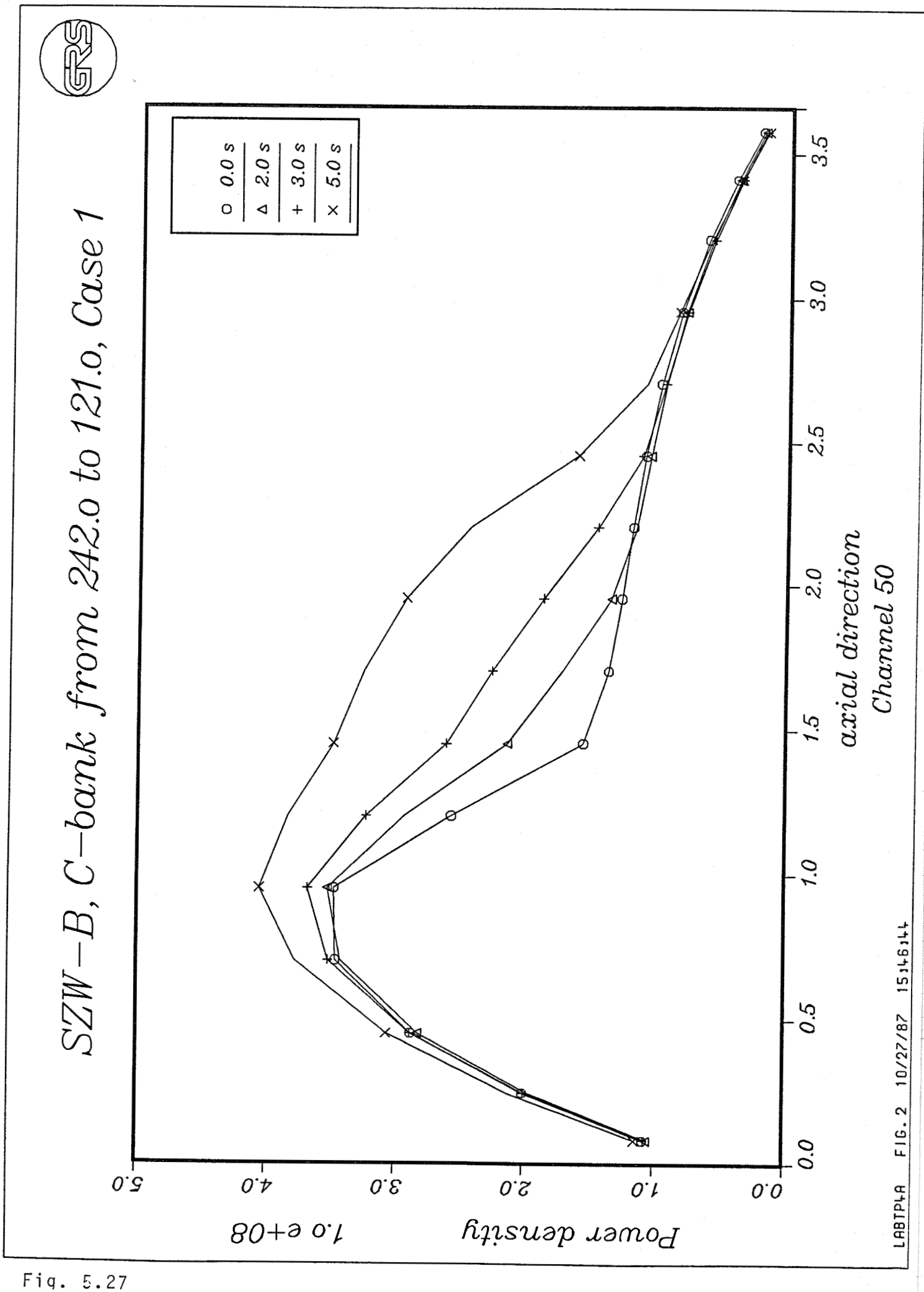
SZW-B, C-bank from 242.0 to 121.0, Case 1
o 0.0 s
Δ 2.0 s
+ 3.0 s
× 5.0 s
Power density
1.0 e+08
0.0
1.0
2.0
3.0
4.0
5.0
axial direction
Channel 50
0.0
0.5
1.0
1.5
2.0
2.5
3.0
3.5
LABTP1A FIG. 2 10/27/87 1514144

Fig. 5.27

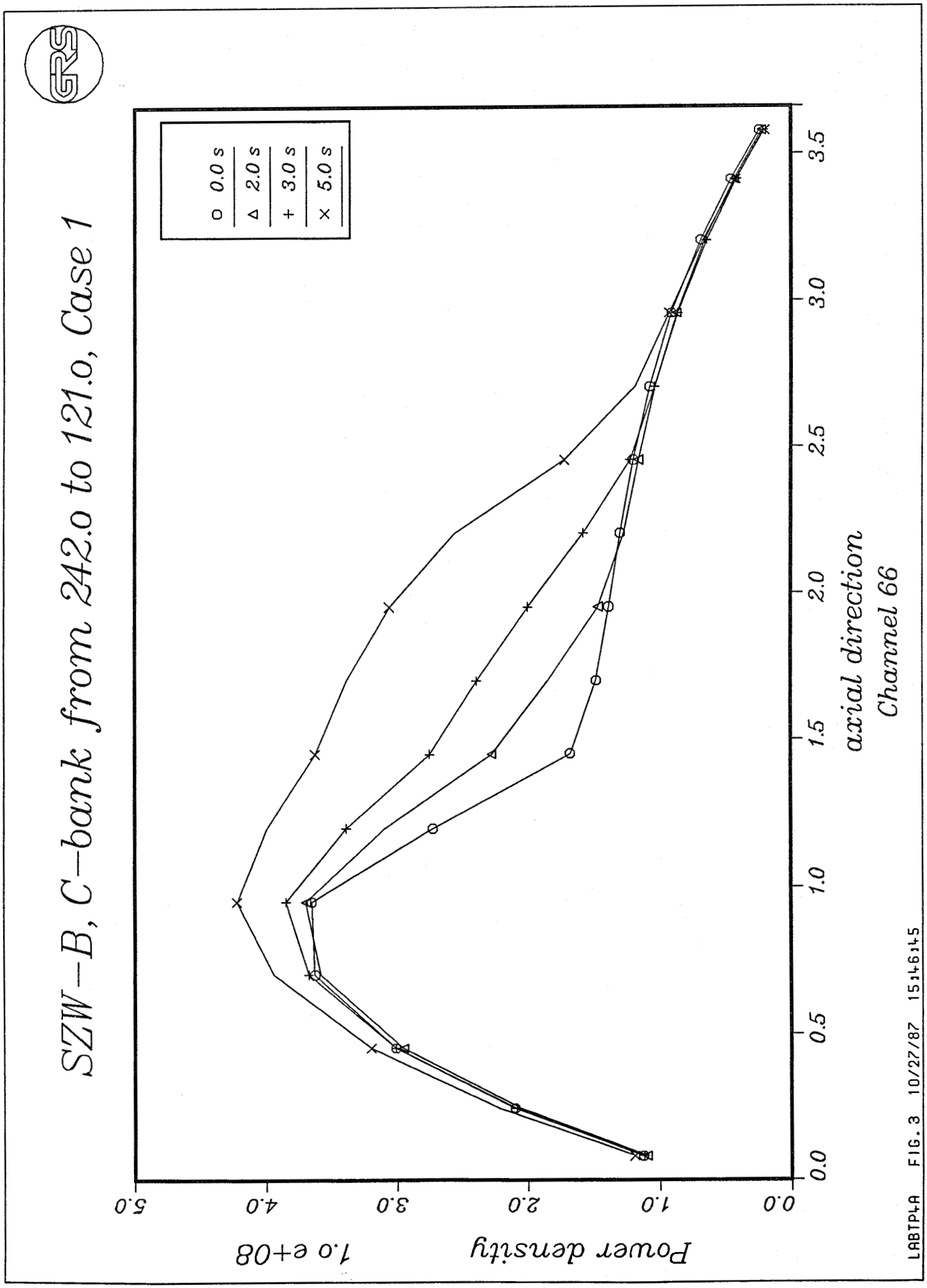
SZW-B, C-bank from 242.o to 121.o, Case 1
o 0.0 s
Δ 2.0 s
+ 3.0 s
× 5.0 s
Power density
1.o e+08
0.0
1.0
2.0
3.0
4.0
5.0
0.0
0.5
1.0
1.5
2.0
2.5
3.0
3.5
axial direction
Channel 66
LABTP4A FIG.3 10/27/87 15:46:45

Fig. 5.28

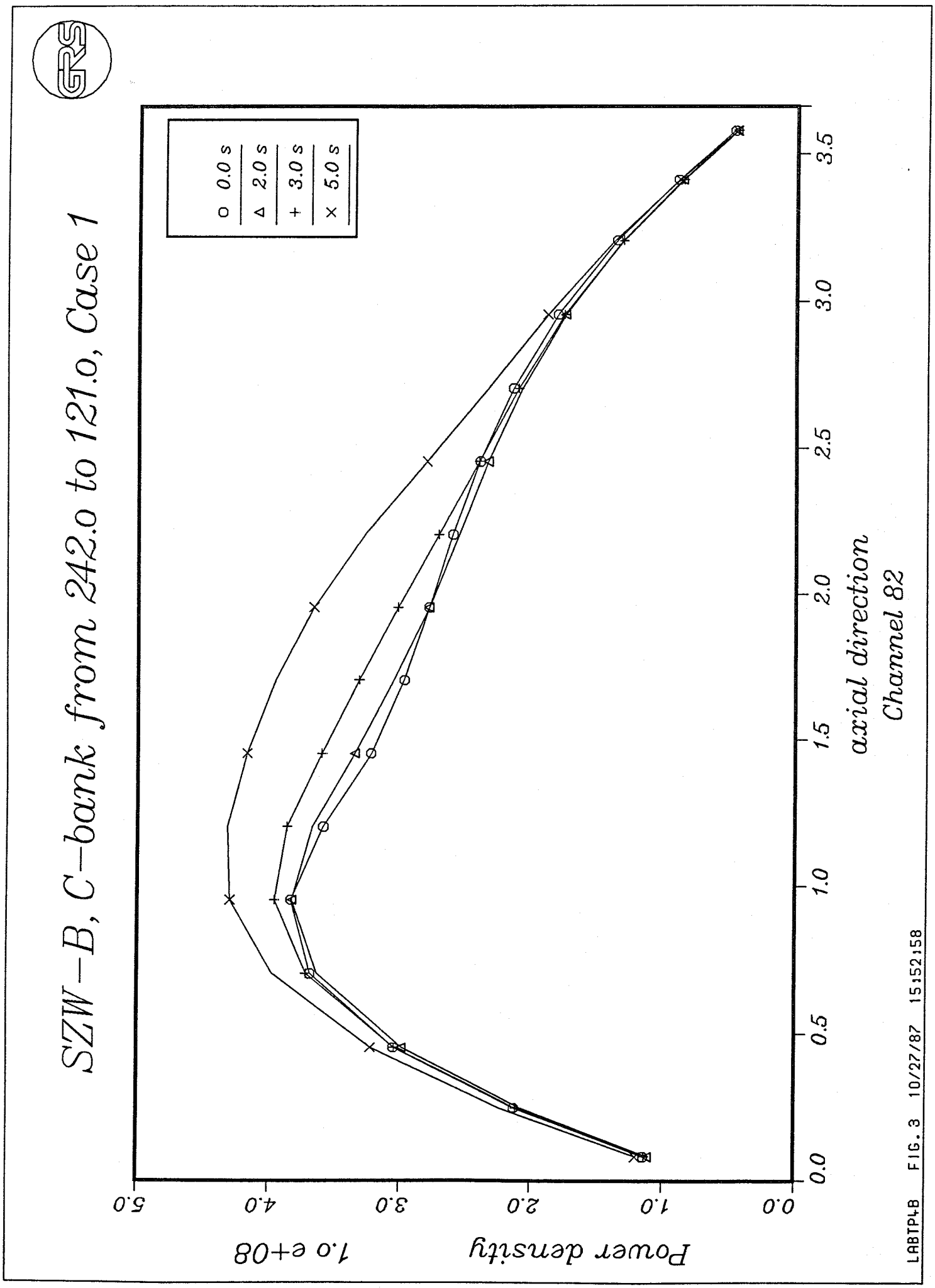
SZW-B, C-bank from 242.o to 121.o, Case 1
o 0.0 s
Δ 2.0 s
+ 3.0 s
× 5.0 s
Power density
1.o e+08
0.0
1.0
2.0
3.0
4.0
5.0
0.0
0.5
1.0
1.5
2.0
2.5
3.0
3.5
axial direction
Channel 82
LABTPLB FIG.3 10/27/87 15:52:58

Fig. 5.29

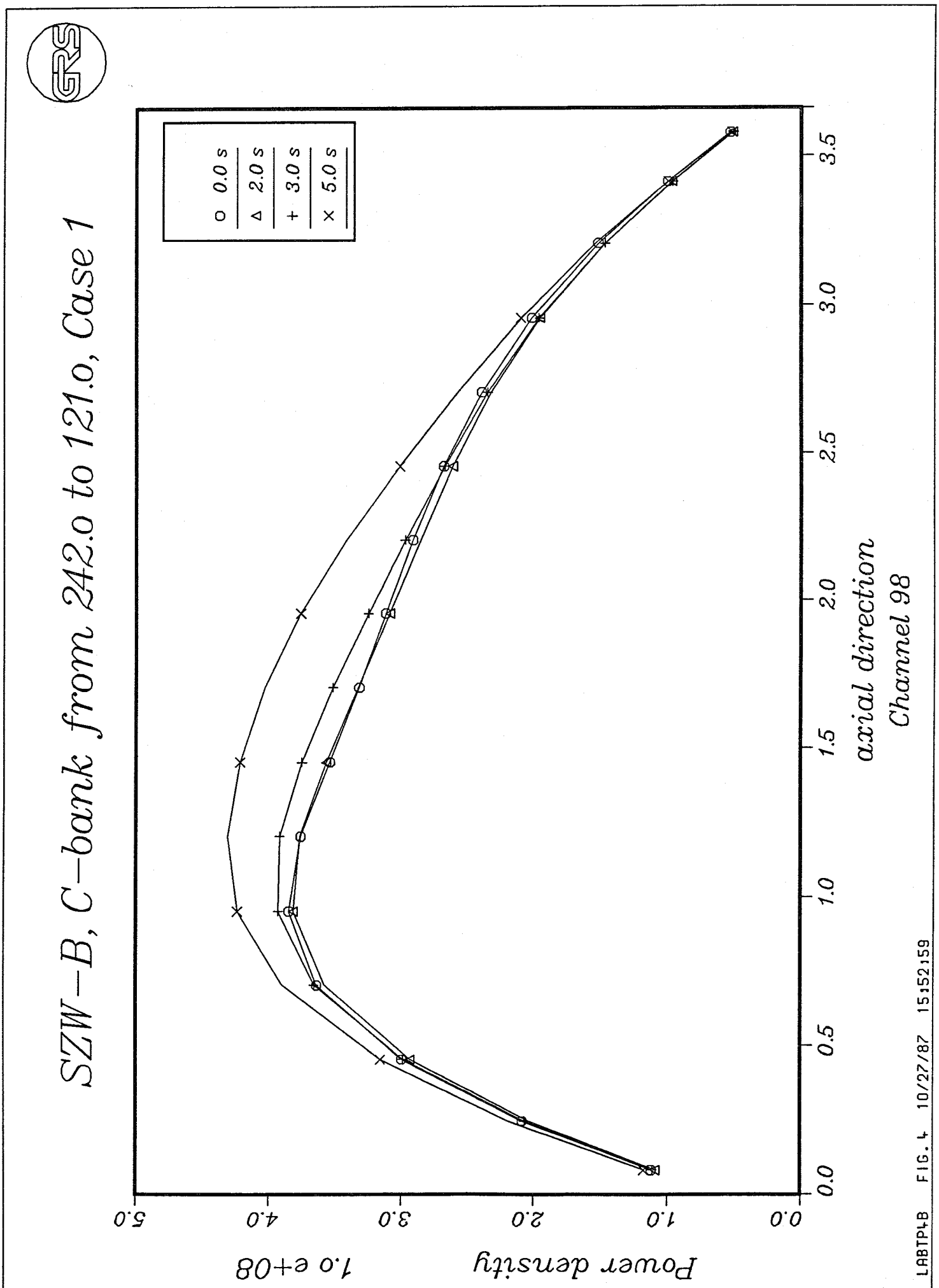
SZW-B, C-bank from 242.0 to 121.0, Case 1
o 0.0 s
Δ 2.0 s
+ 3.0 s
× 5.0 s
Power density
1.0 e+08
0.0
1.0
2.0
3.0
4.0
5.0
0.0
0.5
1.0
1.5
2.0
2.5
3.0
3.5
axial direction
Channel 98
LABTPLB FIG.4 10/27/87 15:52:59

Fig. 5.30

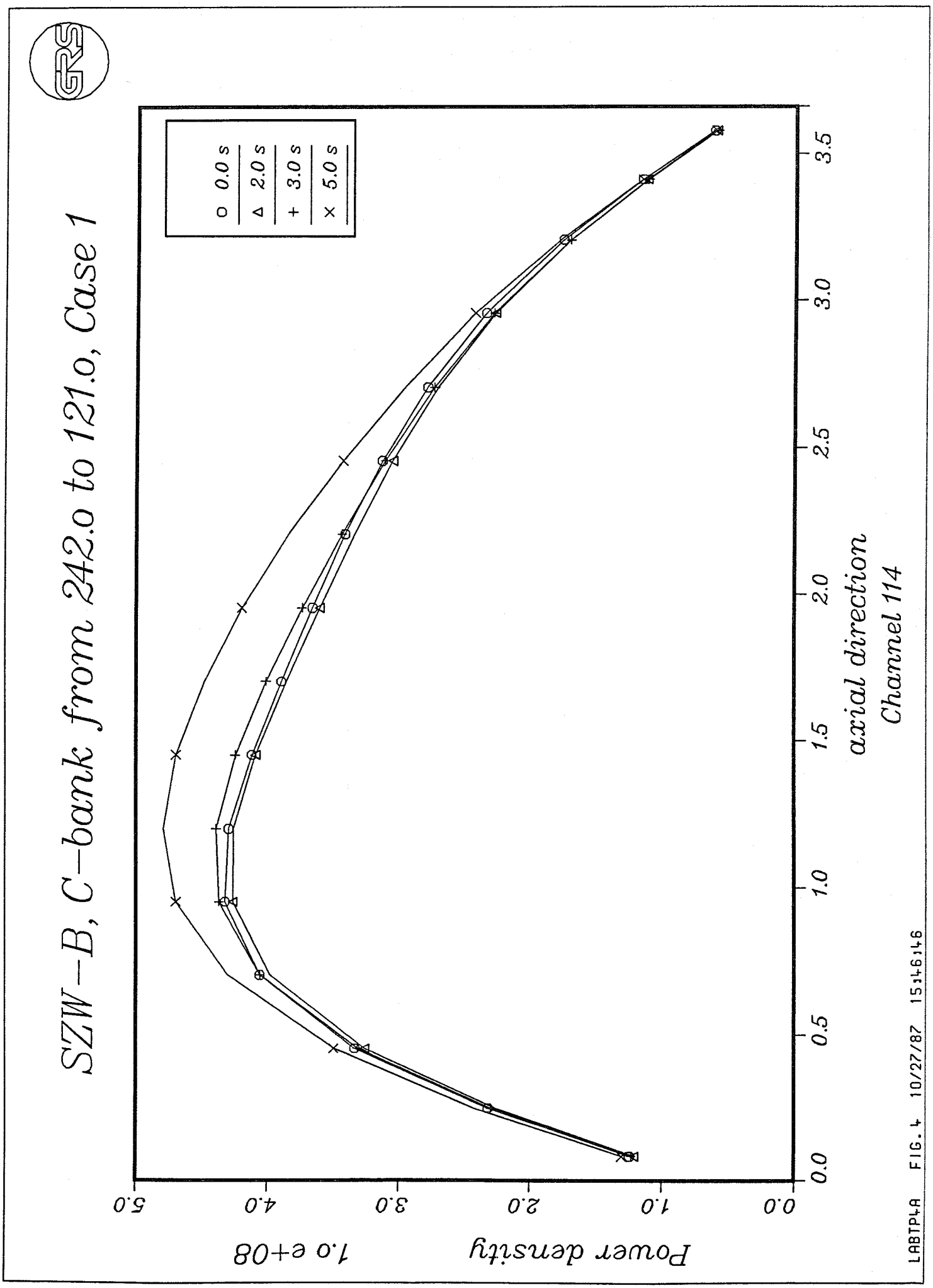
SZW-B, C-bank from 242.0 to 121.0, Case 1
o 0.0 s
Δ 2.0 s
+ 3.0 s
× 5.0 s
Power density
1.0 e+08
0.0
1.0
2.0
3.0
4.0
5.0
0.0
0.5
1.0
1.5
2.0
2.5
3.0
3.5
axial direction
Channel 114
LABTPLA FIG. 4 10/27/87 15:46:46

Fig. 5.31

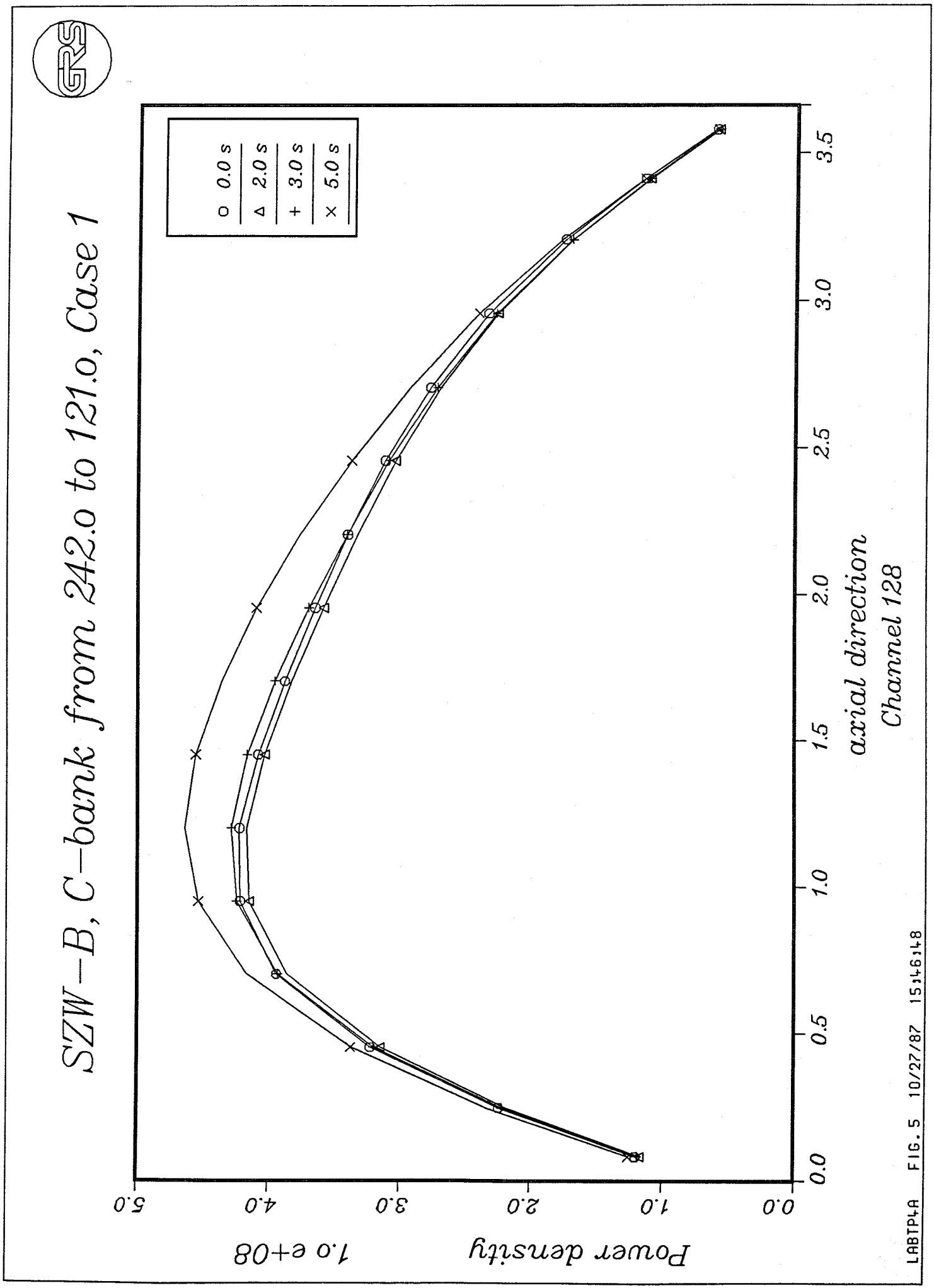
SZW-B, C-bank from 242.0 to 121.0, Case 1
o 0.0 s
Δ 2.0 s
+ 3.0 s
× 5.0 s
Power density
1.0 e+08
0.0
1.0
2.0
3.0
4.0
5.0
axial direction
Channel 128
0.0
0.5
1.0
1.5
2.0
2.5
3.0
3.5
LABTP4A FIG. 5 10/27/87 15:46:48

Fig. 5.32

FIGURES

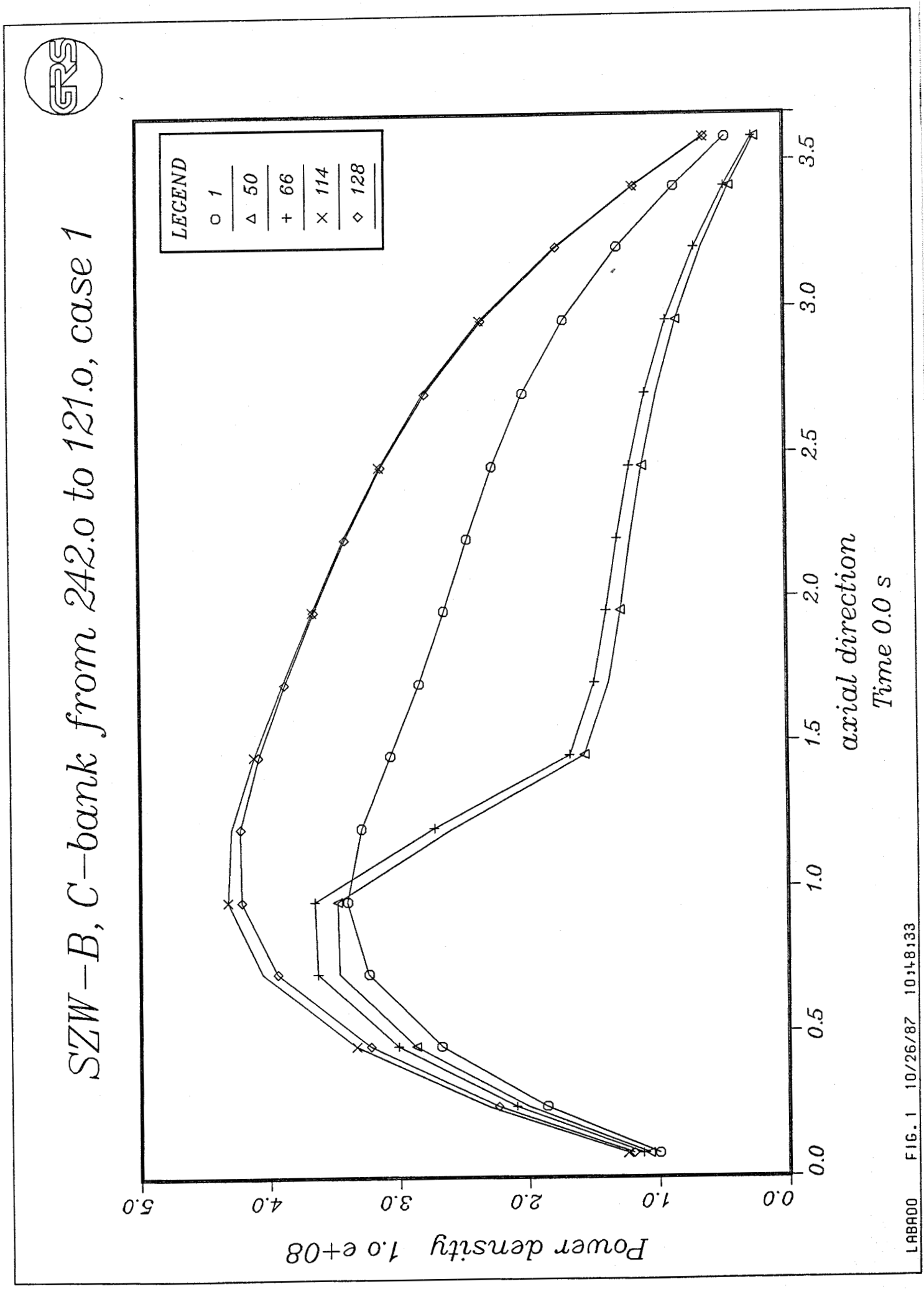
SZW–B, C–bank from 242.0 to 121.0, case 1
LEGEND
○ 1
△ 50
+ 66
× 114
◇ 128
Power density 1.0 e+08
5.0
4.0
3.0
2.0
1.0
0.0
0.0
0.5
1.0
1.5
2.0
2.5
3.0
3.5
axial direction
Time 0.0 s
LABADO FIG. 1 10/26/87 10:48:33

Fig. 5.33

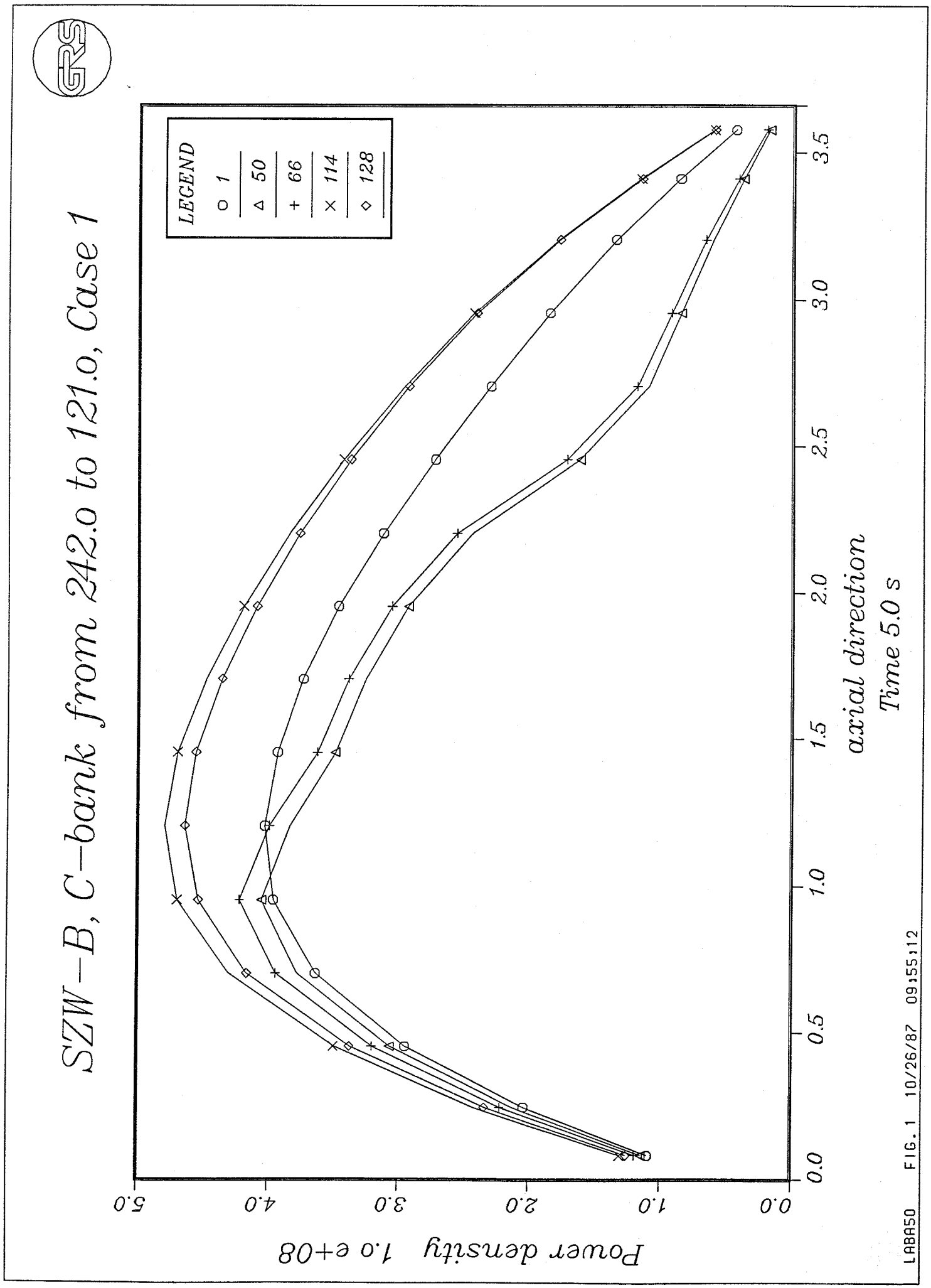
SZW-B, C-bank from 242.0 to 121.0, Case 1
LEGEND
○ 1
△ 50
+ 66
× 114
◇ 128
Power density 1.0 e+08
0.0
1.0
2.0
3.0
4.0
5.0
0.0
0.5
1.0
1.5
2.0
2.5
3.0
3.5
axial direction
Time 5.0 s
LABASO FIG. 1 10/26/87 09:55:12

Fig. 5.34

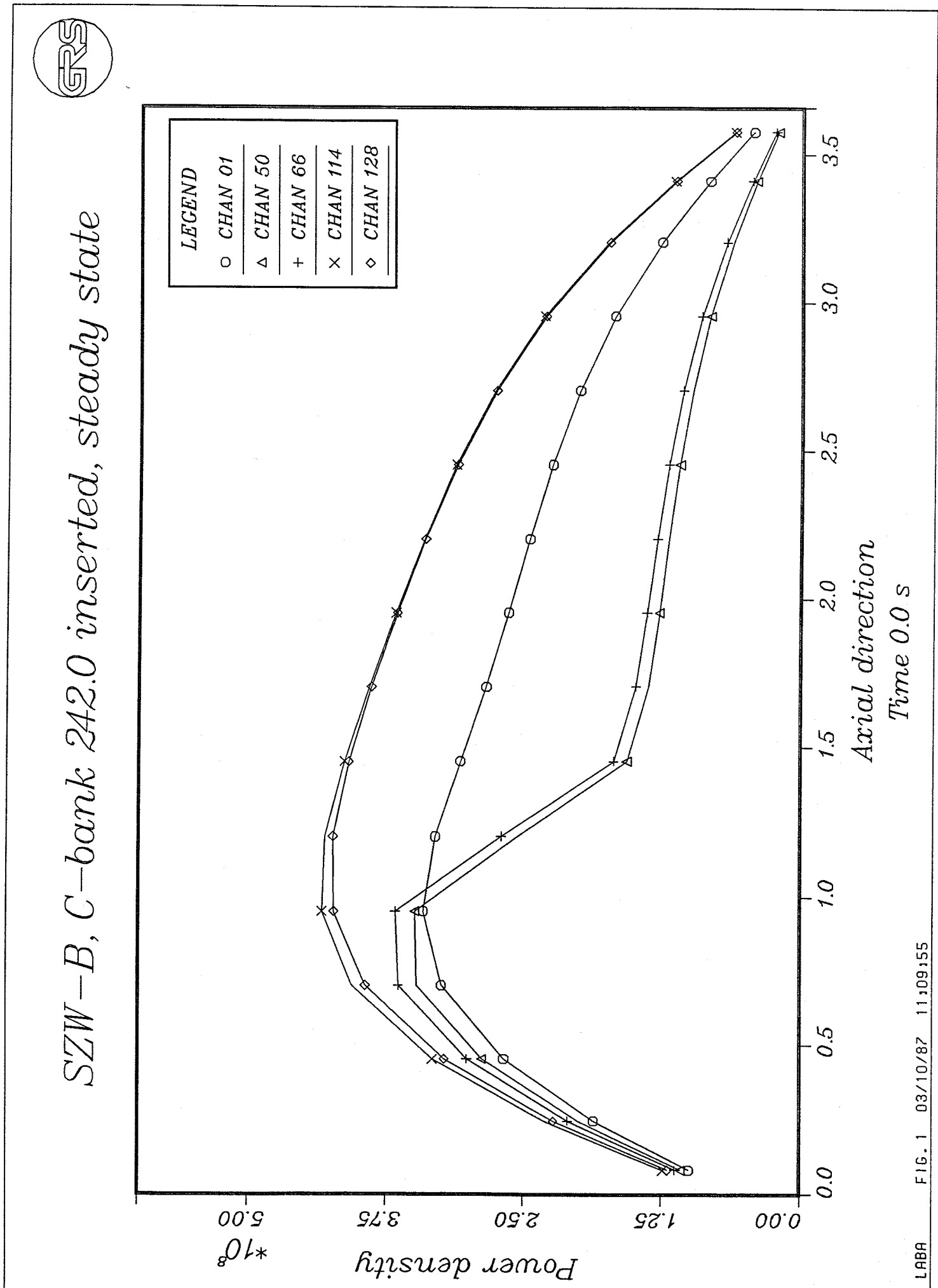
SZW-B, C-bank 242.0 inserted, steady state
LEGEND
CHAN 01
CHAN 50
CHAN 66
CHAN 114
CHAN 128
Power density
*10^8
0.00
1.25
2.50
3.75
5.00
Axial direction
Time 0.0 s
0.0
0.5
1.0
1.5
2.0
2.5
3.0
3.5
LABA FIG. 1 03/10/87 11:09:55

Fig. 5.35

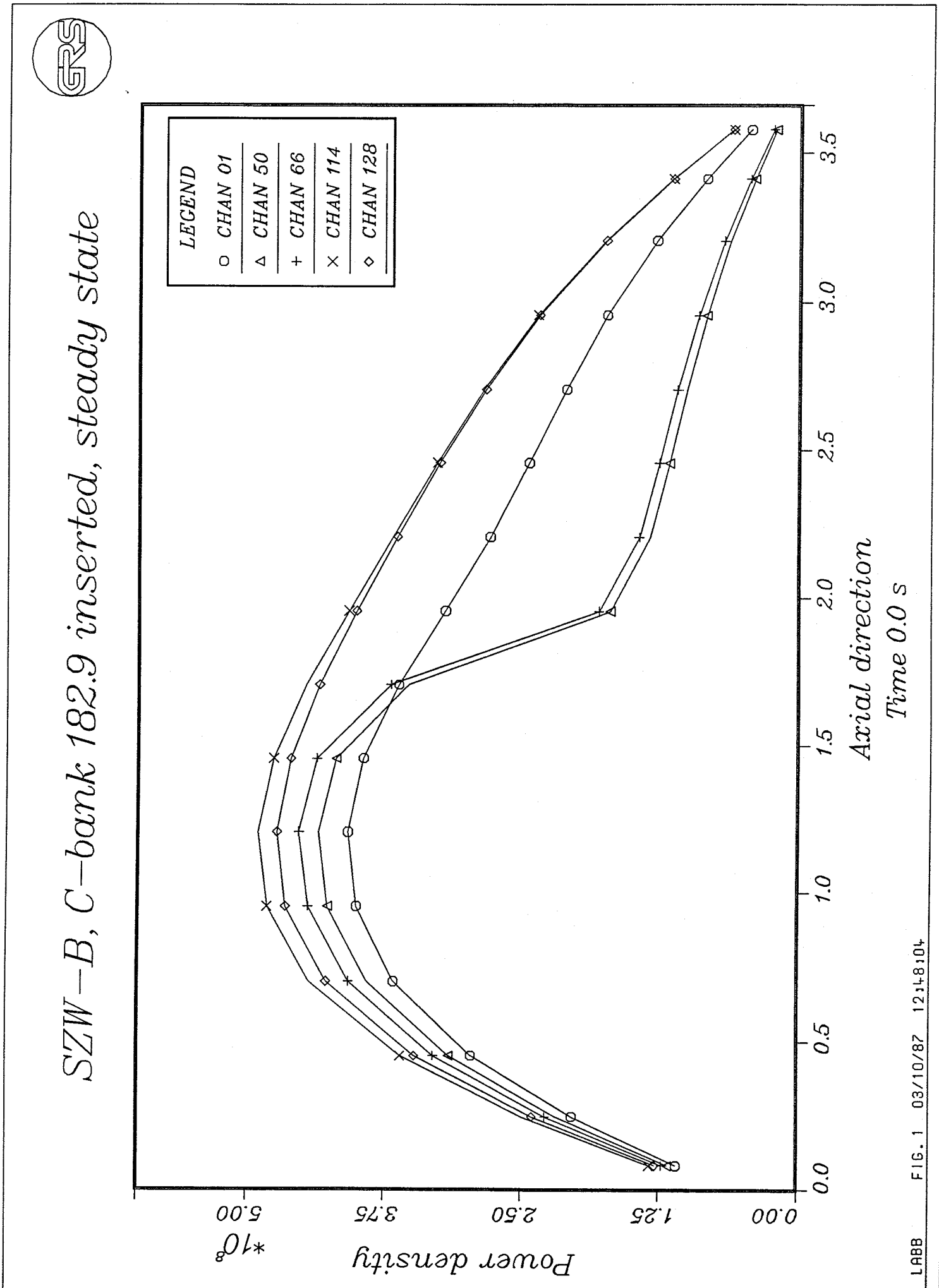
SZW-B, C-bank 182.9 inserted, steady state
LEGEND
CHAN 01
CHAN 50
CHAN 66
CHAN 114
CHAN 128
Power density
*10^8
0.00
1.25
2.50
3.75
5.00
Axial direction
Time 0.0 s
0.0
0.5
1.0
1.5
2.0
2.5
3.0
3.5
LABB
FIG. 1 03/10/87 12:48:04

Fig. 5.36

SZW–B, C–bank 121.0 inserted, steady state

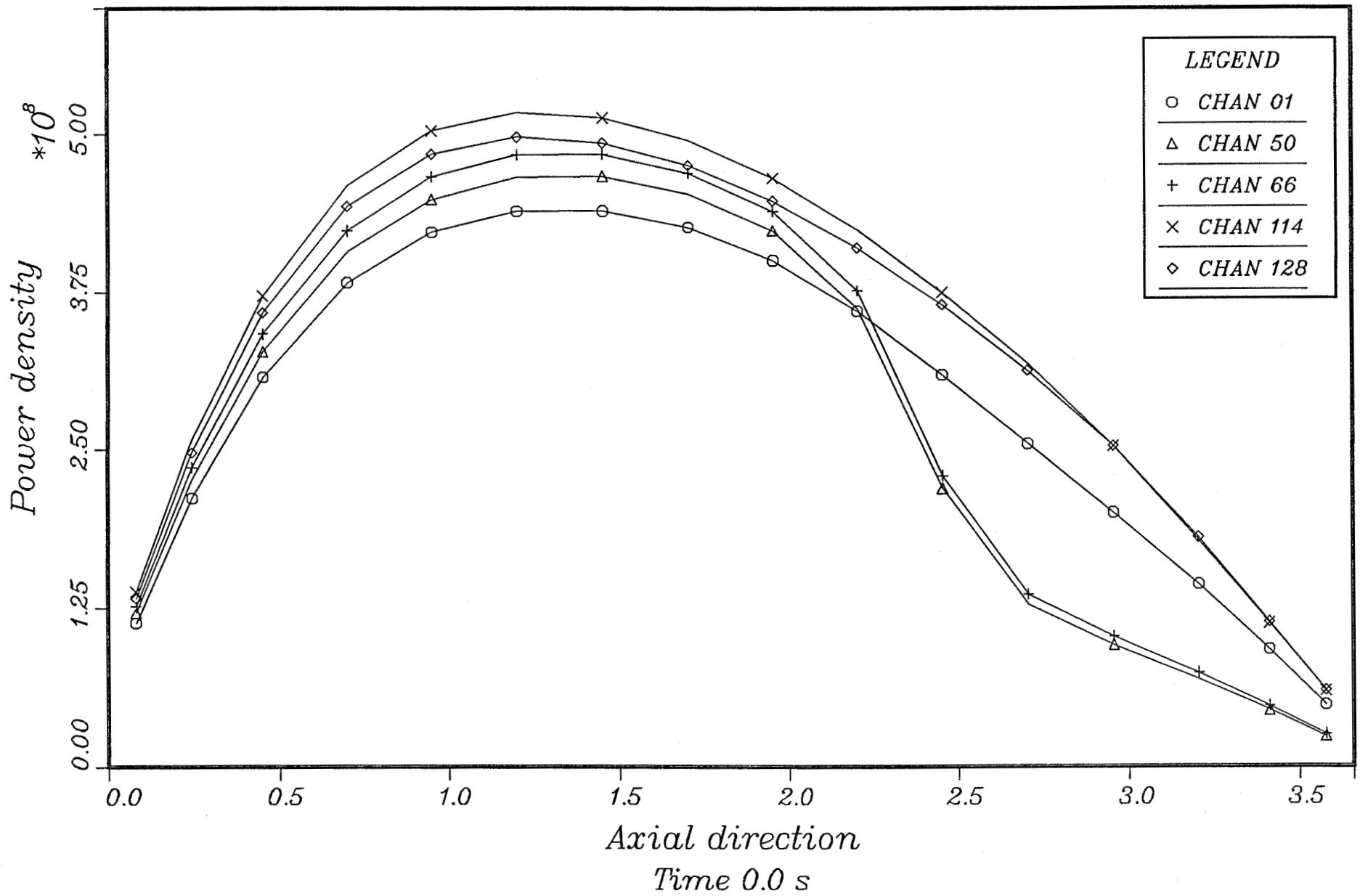

LABC FIG. 1 03/10/87 12:44:08

FIGURES

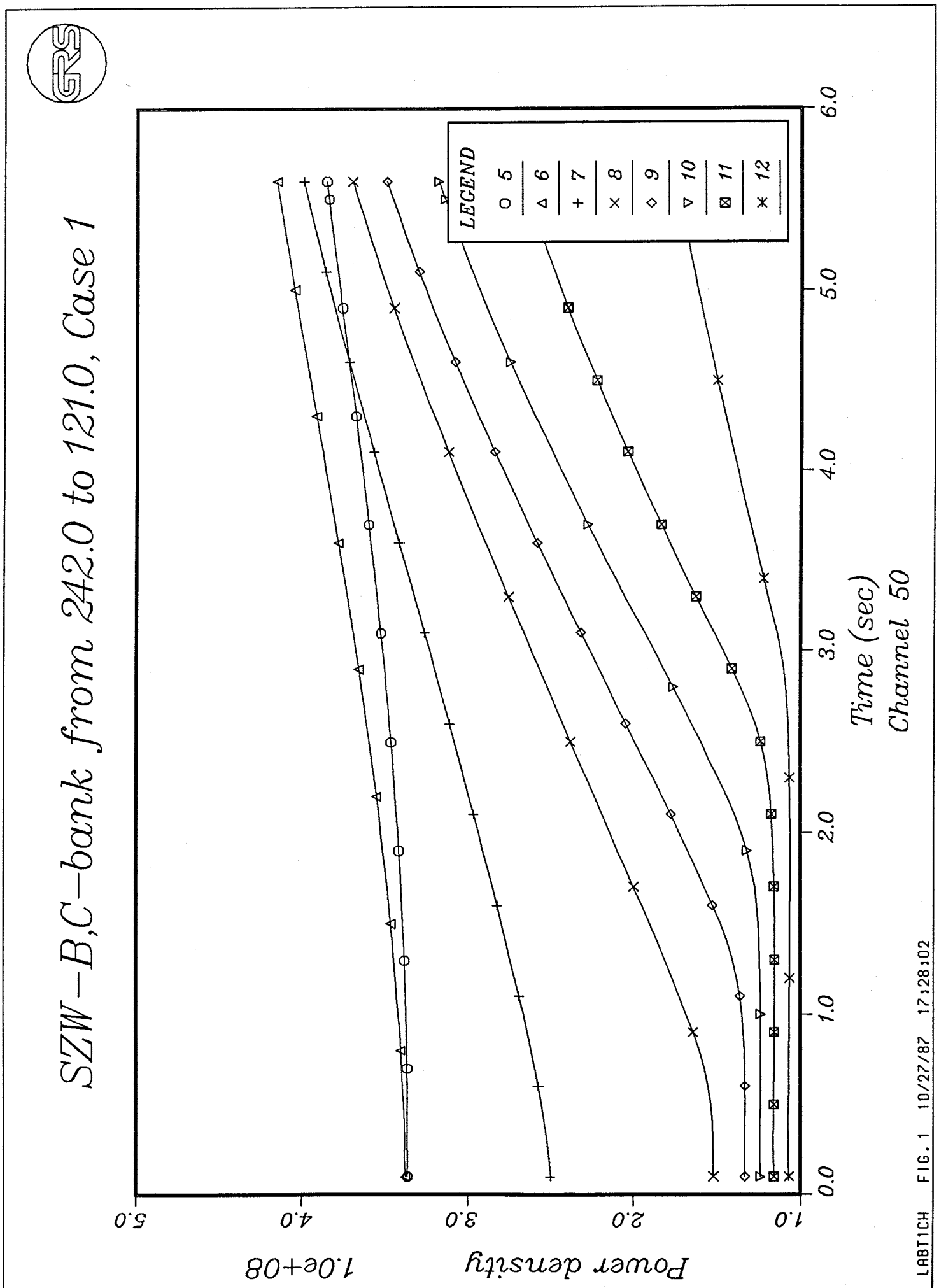
SZW-B,C-bank from 242.0 to 121.0, Case 1
LEGEND
o 5
Δ 6
+ 7
× 8
◇ 9
▽ 10
⊠ 11
* 12
Power density
1.0e+08
Time (sec)
Channel 50
LABTICH FIG. 1 10/27/87 17:28:02

Fig. 5.38

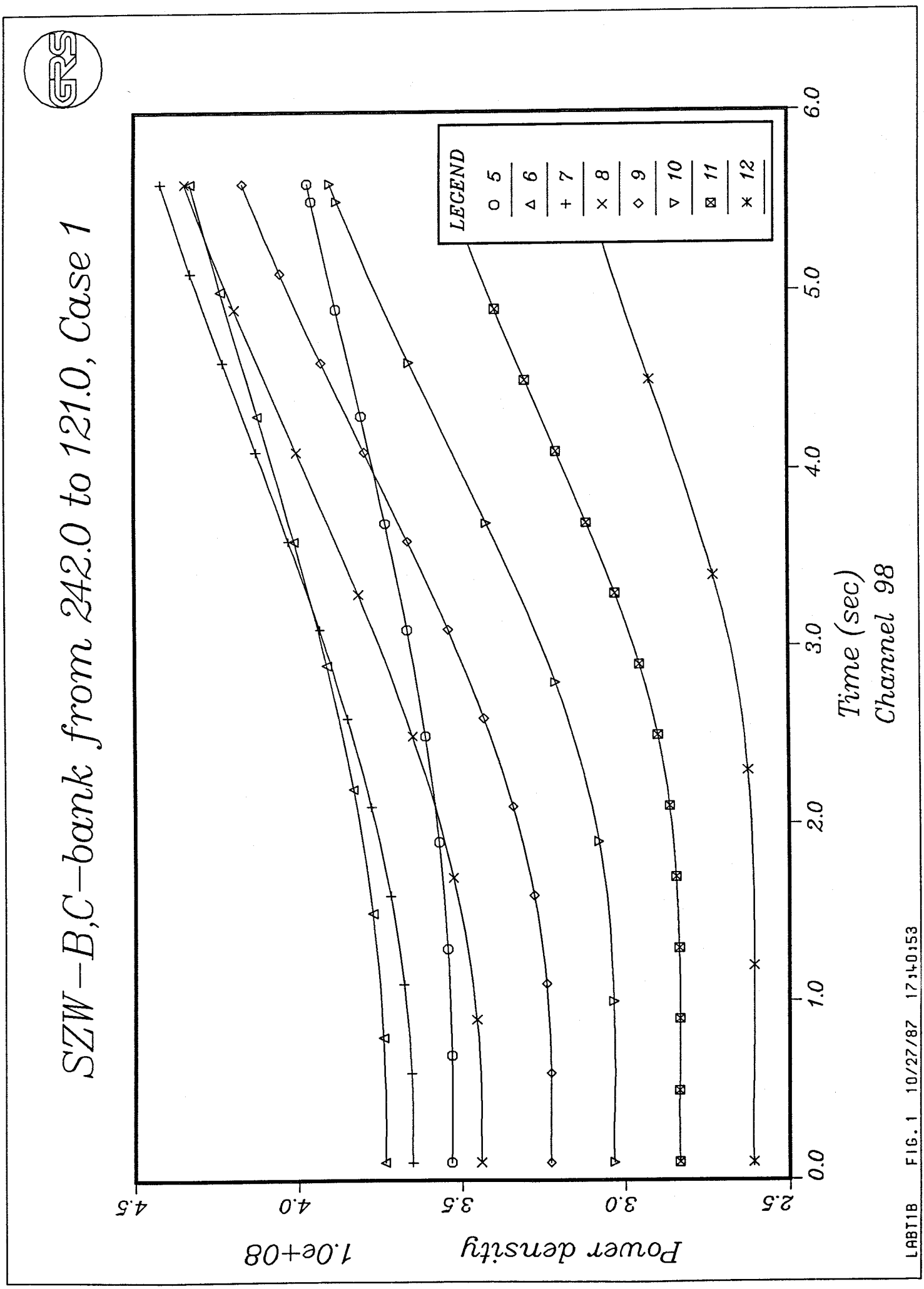
SZW-B,C-bank from 242.0 to 121.0, Case 1
LEGEND
5
6
7
8
9
10
11
12
Power density
1.0e+08
4.5
4.0
3.5
3.0
2.5
0.0
1.0
2.0
3.0
4.0
5.0
6.0
Time (sec)
Channel 98
LABT1B FIG. 1 10/27/87 17:40:53

Fig. 5.39

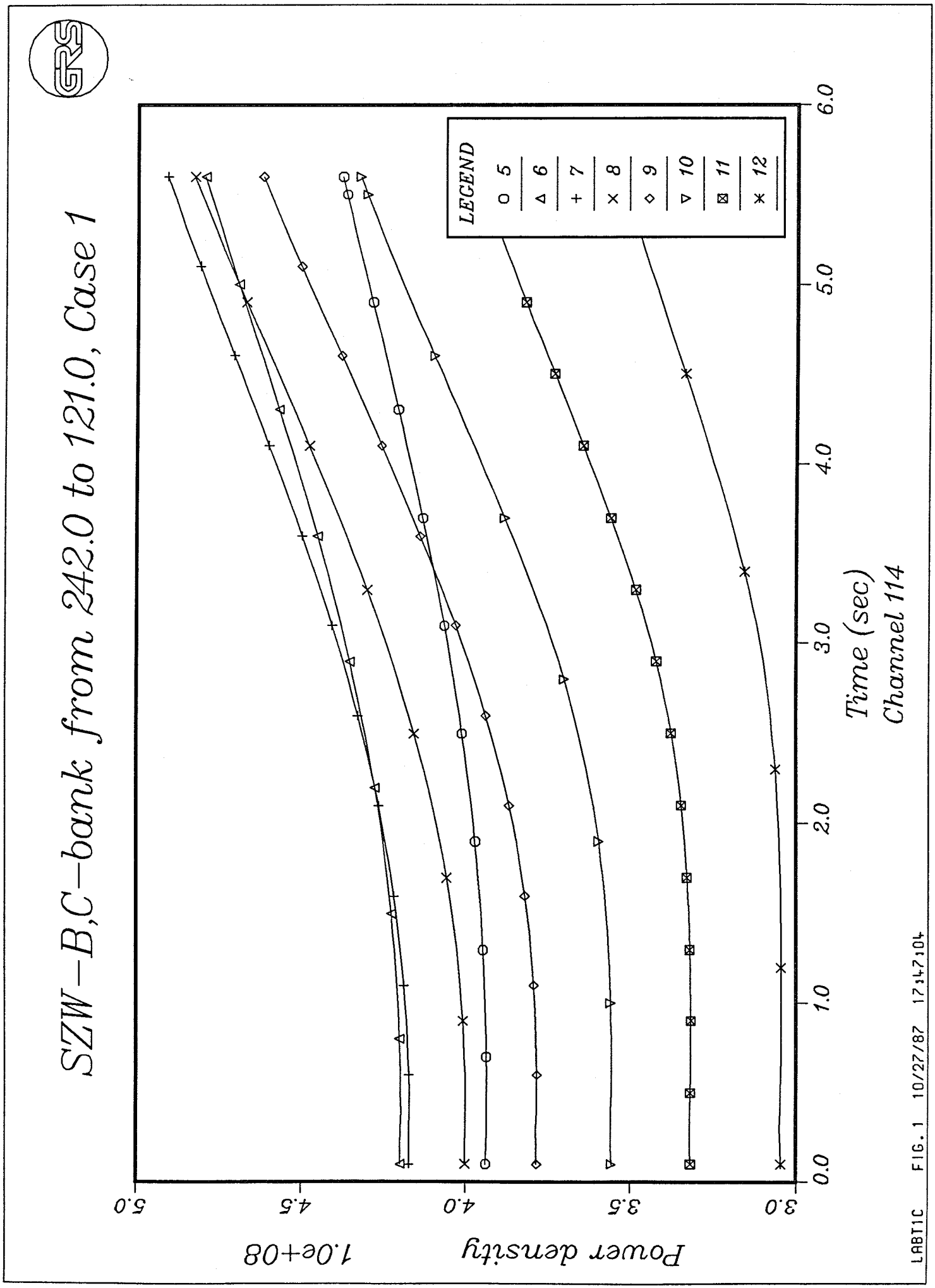
SZW-B,C-bank from 242.0 to 121.0, Case 1
LEGEND
5
6
7
8
9
10
11
12
Power density
1.0e+08
3.0
3.5
4.0
4.5
5.0
0.0
1.0
2.0
3.0
4.0
5.0
6.0
Time (sec)
Channel 114
LABT1C FIG. 1 10/27/87 17:47:04

Fig. 5.40

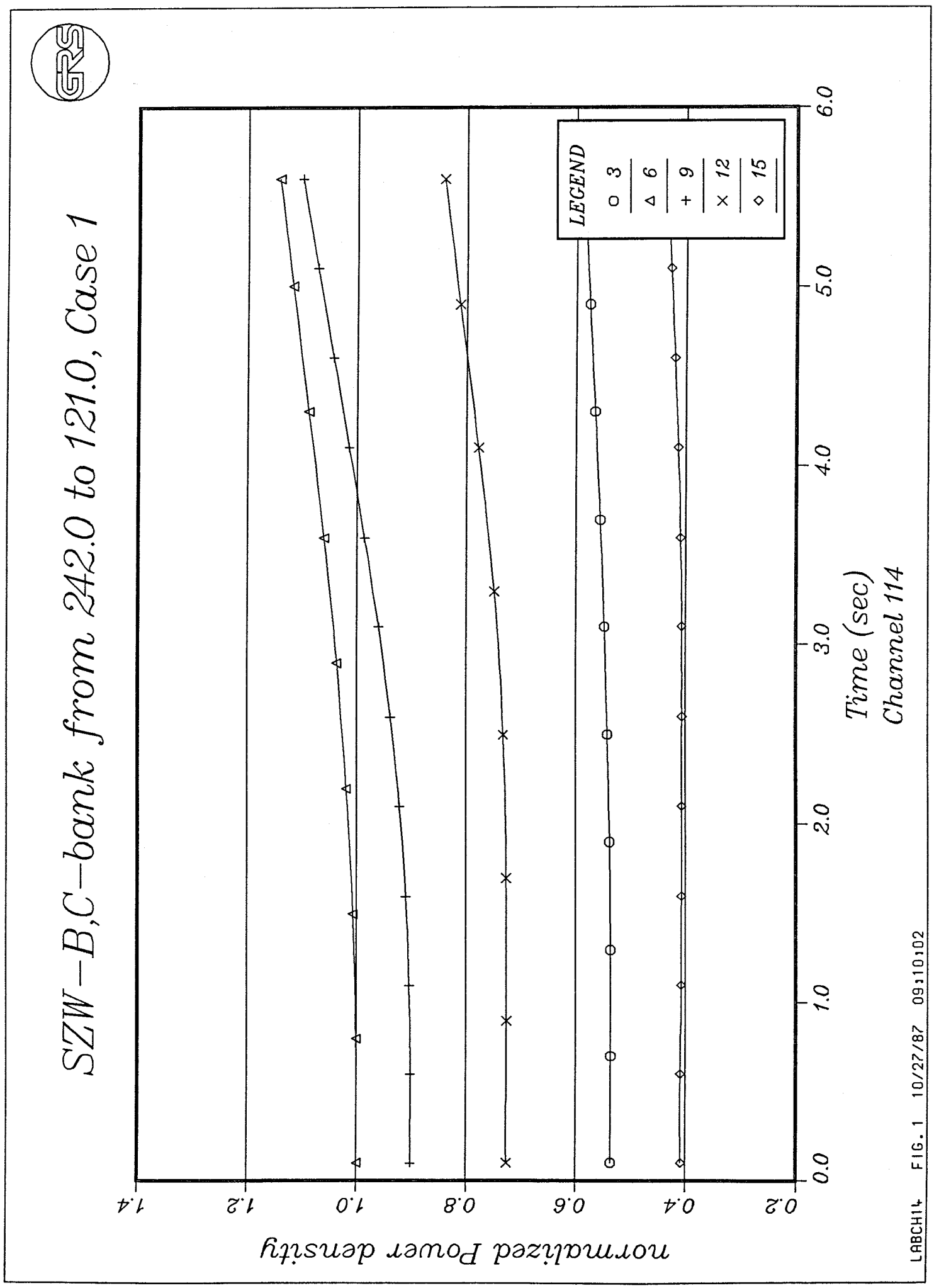
SZW-B,C-bank from 242.0 to 121.0, Case 1
normalized Power density
Time (sec)
Channel 114
LEGEND
3
6
9
12
15
0.0
1.0
2.0
3.0
4.0
5.0
6.0
0.2
0.4
0.6
0.8
1.0
1.2
1.4
LABCH14 FIG. 1 10/27/87 09:10:02

Fig. 5.41

FIGURES

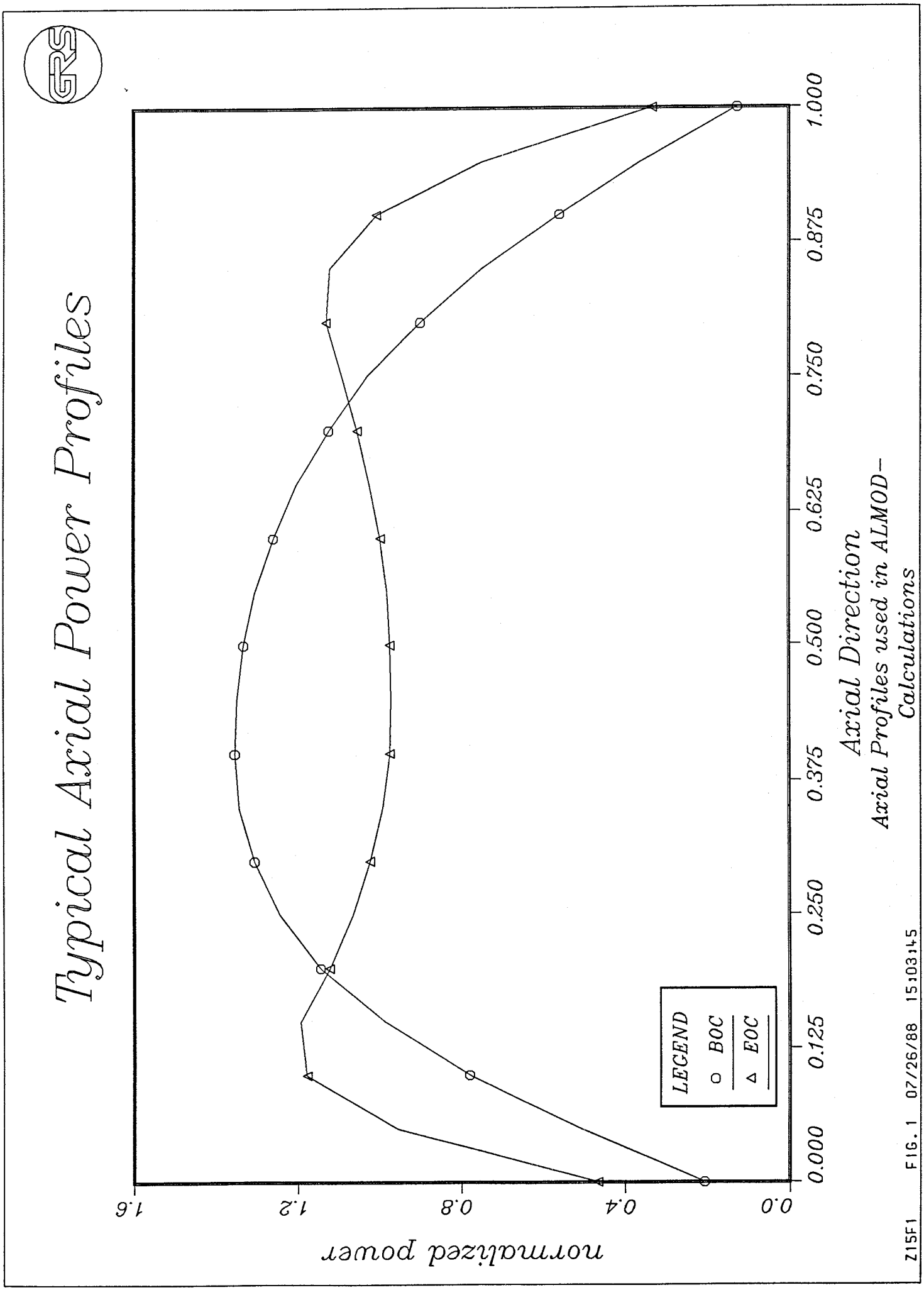
Typical Axial Power Profiles
normalized power
0.0
0.4
0.8
1.2
1.6
0.000
0.125
0.250
0.375
0.500
0.625
0.750
0.875
1.000
Axial Direction
Axial Profiles used in ALMOD-
Calculations
LEGEND
BOC
EOC
Z15F1 FIG. 1 07/26/88 15:03:45

Fig. 5.42

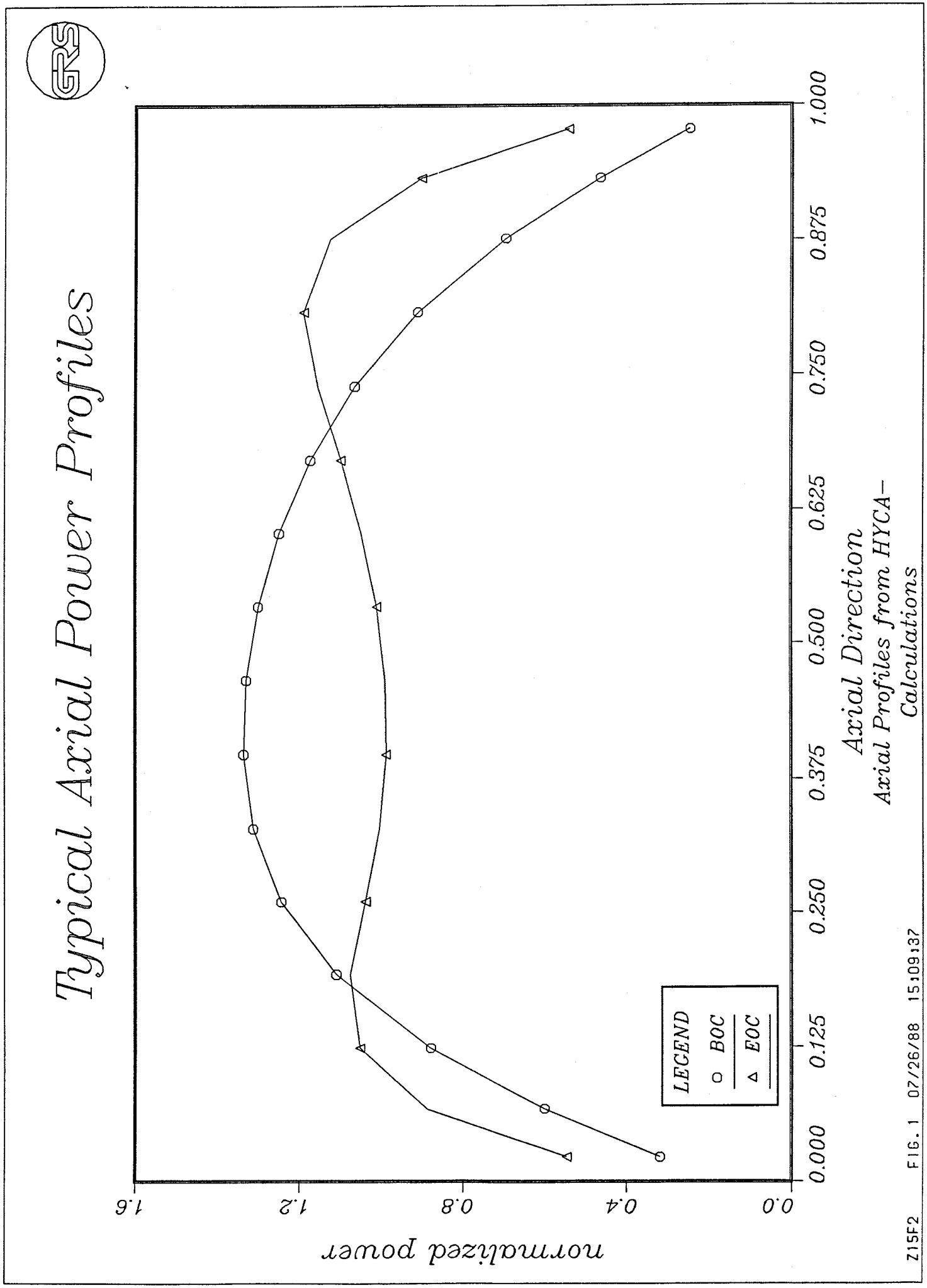
Typical Axial Power Profiles
normalized power
0.0
0.4
0.8
1.2
1.6
0.000
0.125
0.250
0.375
0.500
0.625
0.750
0.875
1.000
Axial Direction
Axial Profiles from HYCA-Calculations
LEGEND
BOC
EOC
Z15F2 FIG. 1 07/26/88 15:09:37

Fig. 5.43

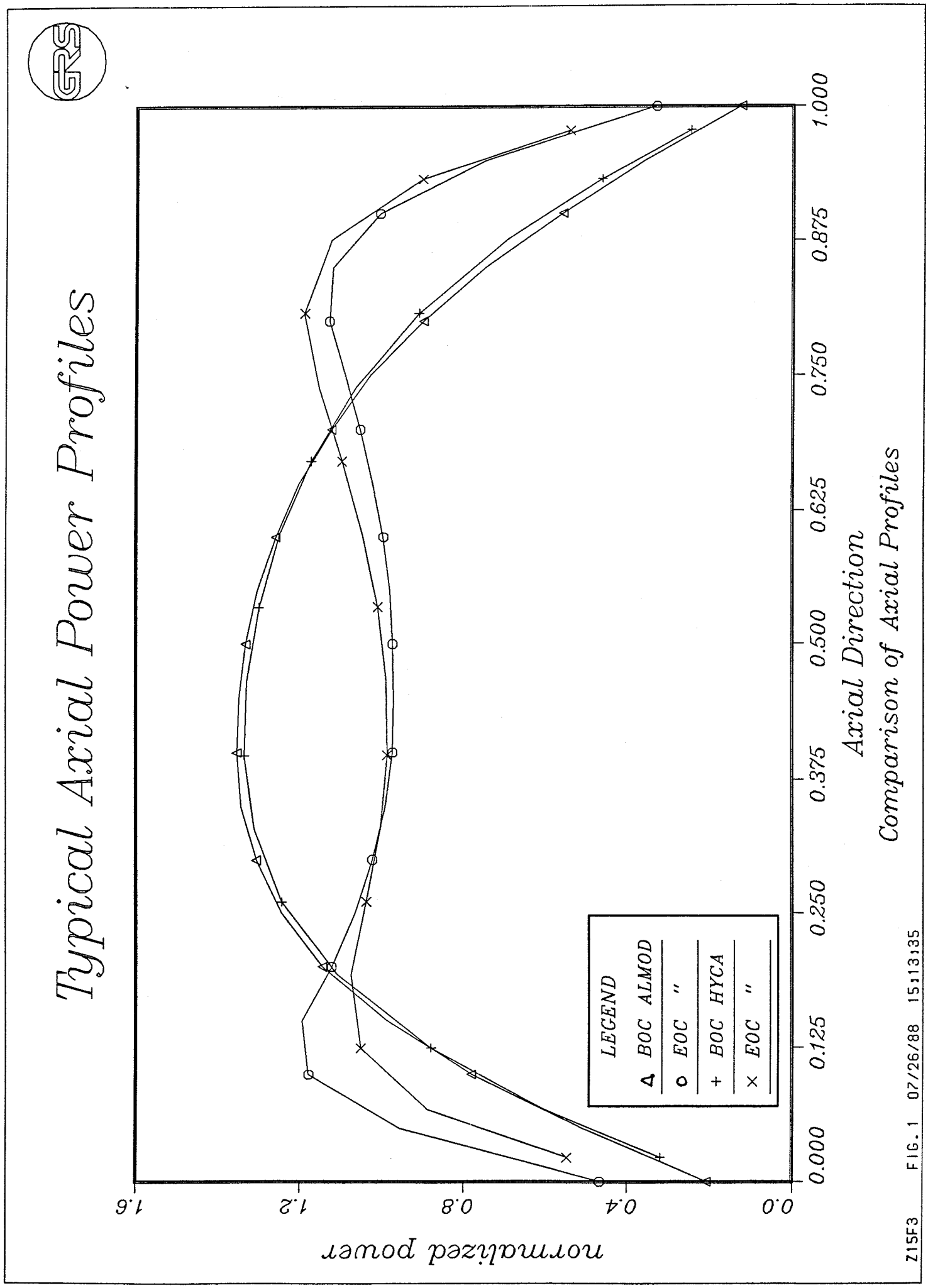
Typical Axial Power Profiles
normalized power
Axial Direction
Comparison of Axial Profiles
LEGEND
Δ BOC ALMOD
o EOC "
+ BOC HYCA
× EOC "
0.0
0.4
0.8
1.2
1.6
0.000
0.125
0.250
0.375
0.500
0.625
0.750
0.875
1.000
Z15F3 FIG. 1 07/26/88 15:13:35

Fig. 5.44